DISSERTATION

Titel der Dissertation

„The structural and dynamic basis for co-operative ligand binding in the KIX domain of CBP "

Verfasser

Mag. rer. nat. Sven Brüschweiler

angestrebter akademischer Grad

Doktor der Naturwissenschaft (Dr. rer. nat.)

Wien, 2011

Studienkennzahl lt. Studienblatt:	A 091 419
Dissertationsgebiet lt. Studienblatt:	Dr. Studium der Naturwissenschaften Chemie
Betreuer:	Univ.-Prof. Dr. Robert Konrat

Acknowledgements

List of Publications

      This thesis is based on the compilation of the following two peer-reviewed publications and one publication manuscript in preparation, which will be submitted to peer-review.

Article I   **Brüschweiler S**, Schanda P, Kloiber K, Brutscher B, Kontaxis G, Konrat R, Tollinger M (2009) Direct Observation of the Dynamic Process Underlying Allosteric Signal Transmission. *J Am Chem Soc* **131:** 3063-3068

Article II   Breuker K, **Brüschweiler S**, Tollinger M (2010) Electrostatic Stabilization of a Native Protein Structure in the Gas Phase. *Angew Chem, Inter Ed* 50: 873-877

Article III   **Brüschweiler S**, Ribarics R, Konrat R, Tollinger M (2011) Allosteric communication in the KIX domain proceeds through re-packing of the hydrophobic core. (in preparation)

List of Abbreviations

B_0	static magnetic field
CBP	CREB binding protein
CPMG	Carr-Purcell-Meiboom-Gill
CREB	cAMP response element-binding protein
CSA	chemical shift anisotropy
ECD	electron capture dissociation
ESI	electrospray ionization
FAT	factor acetyltransferase
FT	Fourier transform
γ	gyromagnetic ratio
HAT	histone acetyltransferase
hnNOE	heteronuclear NOE
ITC	isothermal titration calorimetry
$J(\omega)$	spectral density
MLL	mixed-lineage leukemia
MS	mass spectrometry
NMR	nuclear magnetic resonance
NOE	nuclear Overhauser effect
NOESY	nuclear Overhauser effect spectroscopy
pKID	phosphorylated kinase inducible domain
PRE	paramagnetic relaxation-enhancement
RDC	residual dipolar coupling
R1	longitudinal relaxation rate
R2	transverse relaxation rate
S^2	order parameter
TF	transcription factor

Table of Contents

Preface

During my PhD studies I was investigating two fundamental processes of CBPs KIX domain: 1) allosteric signal transmission and 2) helical stability.

Allosteric activation of protein function is a common and effective regulation mechanism in biological processes (Hardy and Wells 2004). Allostery requires that information about the binding of a ligand is communicated to additional remote binding sites within a protein or protein complex. This is mainly achieved through conformational rearrangements. Traditionally, allosteric binding mechanisms have been studied in a rather static manner, using X-ray crystallography that enables the characterization of the final states of these structural rearrangements that need to occur for signal transmission. Allosteric communication is, however, fundamentally dynamic in nature, and can therefore be characterized in a quantitative manner and at atomic resolution by nuclear magnetic resonance (NMR) relaxation techniques (Tzeng and Kalodimos 2011). An outline of the basic theory of these NMR relaxation methods will be given in Chapter 2.

KIX mediates cooperativity between pairs of transcription factors through binding to two distinct interaction surfaces in an allosteric manner (see Chapter 1.2.1). Using NMR relaxation dispersion measurements, we characterized the conformational rearrangements by which the KIX domain communicates information about the presence of the transcription factor (TF) MLL (mixed-lineage leukemia) to a remote second transcription factor binding site that binds TFs c-Myb and pKID (phosphorylated kinase inducible domain of CREB). These CPMG experiments established that the binary KIX.MLL complex interconverts between a highly populated ground state (93%) and a low populated exited state (7%) that binds the second ligand with higher affinity than the ground state (Article I). We elucidated the structural basis of the allosteric communication mechanism by determining the solution structures of apo-KIX, the binary KIX.MLL complex and the ternary KIX.MLL.pKID complex. KIX undergoes very subtle structural rearrangements, with exception of loop L12, in the presence of MLL. Binding of pKID to the binary KIX.MLL complex results in a loss of compactness in the hydrophobic core of KIX (Article III). The isoleucine side chain (methyl group δ1) relaxation dispersion data already indicated conformational changes in the hydrophobic core upon MLL binding. It is known that sub-nanosecond dynamics can be related to conformational entropy. Thus, entropy changes of a protein upon ligand binding can be obtained from probing this motional time-

scale (Stone 2001). We therefore determined the changes in picosecond to nanosecond dynamics of the ^{15}N backbone amides of KIX as a function of different ligand-bound states. In all cases we observed a rigidification of KIX on this motional time-scale that is in accordance with our thermodynamic data obtained for the binding of pKID from isothermal titration calorimetry (Article III).

Traditionally, it was assumed that small proteins (< 100 amino acids) fold to their native three-dimensional structure in a cooperative two-step transition (Jackson 1998). However, over the past years, there is clear evidence that even small proteins can fold via intermediate states (Brockwell and Radford 2007). One of these proteins is the KIX domain of CBP. Tollinger and coworkers were able to show that the fully folded ground state of KIX exists in equilibrium with a low populated exited state that is partially unfolded (Tollinger et al. 2006, Schanda et al. 2008). These studies further showed that the least stable helix in solution is α_1 whereas α_3 is the most stable one (Schanda et al. 2008).

Mass Spectrometry (MS) is known to retain the noncovalent bonding interactions of proteins in the gas phase in cases where a "soft" ionization method such as electrospray ionization (ESI) is used (Breuker and McLafferty 2008). Bearing this in mind, we analyzed if the helix stability of KIX is altered due to the removal of its solvation shell. Using electron capture dissociation (ECD) experiments we investigated if parts of the solution structure of KIX are retained in the gas phase. Our data showed that the relative helix stability in the gas phase is in agreement with the solution data determined by Schanda *et al.* (2008). Detailed results are given in Article II and the theoretical basis of the used MS experiment is given in Chapter 4.

Chapter 1

Gene Transcription

1.1 Introduction

The process of protein production is divided into several steps. The first step is RNA synthesis, called transcription. In the next step the synthesized RNA gets processed and transported to the ribosomes where it is used as a template for protein synthesis. Protein production is a highly regulated process, as different cell types need different sets of proteins, and cells need to adjust to environmental changes and to the stage of development (Courey 2008).

The most efficient way to regulate gene expression is at the level of transcription, this avoids the costly synthesis of RNA. Eukaryotic organisms are using an immense set of transcription factors in a combinatorial way for transcriptional regulation (Reményi et al. 2004). The so-called regulatory machinery controls the rate at which the basal transcription machinery expresses a gene by using transcription factors that either activate or repress transcription. Activators and repressors are gene-specific, i.e. their DNA binding domains recognize a specific DNA sequence, which allows the cell to determine which gene is expressed at a particular moment. The binding sites of transcription factors are usually clustered within a cis-regulatory module, which can be defined in terms of enhancers, repressors and insulators. These regulatory elements can spread up to 1Mb upstream or downstream of the initiation site of a gene (De-Leon and Davidson 2007, Kleinjan and van Heyningen 2005). The intricate patterns of gene regulation in eukaryotes require additional regulatory factors such as coactivators and corepressors, which interact with transcription factors and the RNA polymerase II and thereby regulate the rate of transcription. They do not posses a DNA binding domain themselves, however, they do posses protein domains that catalyze covalent or non-covalent changes in the structure of chromatin thereby providing an additional mechanism of transcription regulation (Courey 2008).

1.2 Transcriptional Synergy

The assembly of the so-called preinitiation complex, which contains RNA polymerase II and five or six general transcription factors at the promoter site, requires the assistance of coregulators (Kornberg 2007). In eukaryotes coactivators like CBP, its paralog p300 (Goodman and Smolik 2000) or the so-called Mediater complex (Kornberg 2005) transduce signals between activators and the basal transcription machinery (Figure 1.1), this leads the RNA polymerase to the promoter site and stimulates later steps in the transcription process.
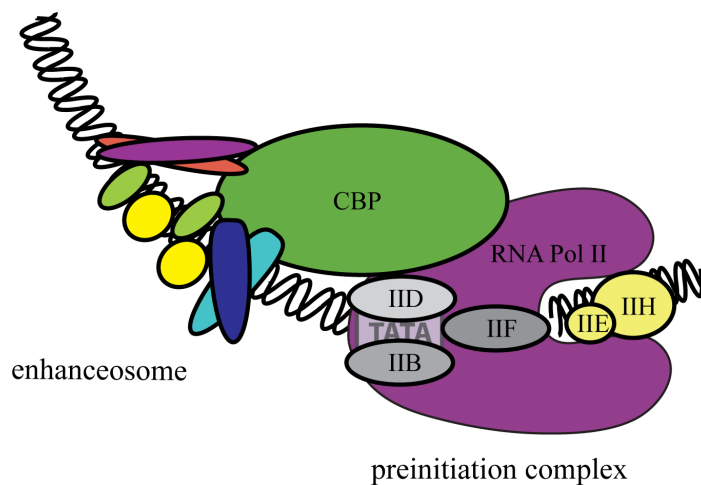

Figure 1.1. *Representation of the complex formed by the IFN-β enhanceosome, CBP and the basal transcription machinery at a TATA-box containing promoter.* The promoter is recognized by a subunit of TFIID the TATA-binding protein (TBP)

How do these contacts enhance transcription? They can either lead to an increase in the closed transcriptional complex formation through an increase in affinity for RNA polymerase or by increasing the rate of interconversion between the closed and open transcriptional complex (Courey 2008). On a molecular level, transcriptional synergy is achieved by two effects: 1) cooperative binding within the protein-DNA complex and 2) chromatin remodeling. These effects are used in a combinatorial manner so that a relatively small number of different transcription factors (~2000-3000) (Brivanlou and Darnell 2002) compared to the number of genes (~ 40000 in human) is sufficient for the regulation of the complex patterns of gene expression (Tjian and Maniatis 1992).

In molecular terms, cooperative binding can either result from direct protein-protein interaction within the transcriptional complex, or from a conformational rearrangement of the cis-regulatory DNA that facilitates the binding of transcription factors. The latter effect is seen for the transcription factors PU.1 and IRF-4, which bind to Ets-IRF DNA (EICE) elements and regulate gene expression in the immune system. Cooperativity is achieved by the overlap of the DNA binding sequence of both TF on the IgL λ enhancer element, the binding of the first TF leads to a configuration of the enhancer DNA so that the second TF can bind with higher affinity to the cis-regulatory module (Escalante et al. 2002).

Protein-protein interactions can occur between adjacent transcription factors that bind closely to each other on the enhancer site. This is the case for cooperative binding of the transcription factors NFAT, c-Jun and c-Fos to the ARRE2 DNA sequence of the interleukin (IL)-2 enhancer region. Cooperativity results from a tight complex between the DNA-binding domain of c-Jun and c-Fos (AP1) and the DNA-binding domain of NFAT (Figure 1.2a). These interactions lead to a ~ 10-fold increase in DNA binding affinity of Ap1 (Chen et al. 1998).
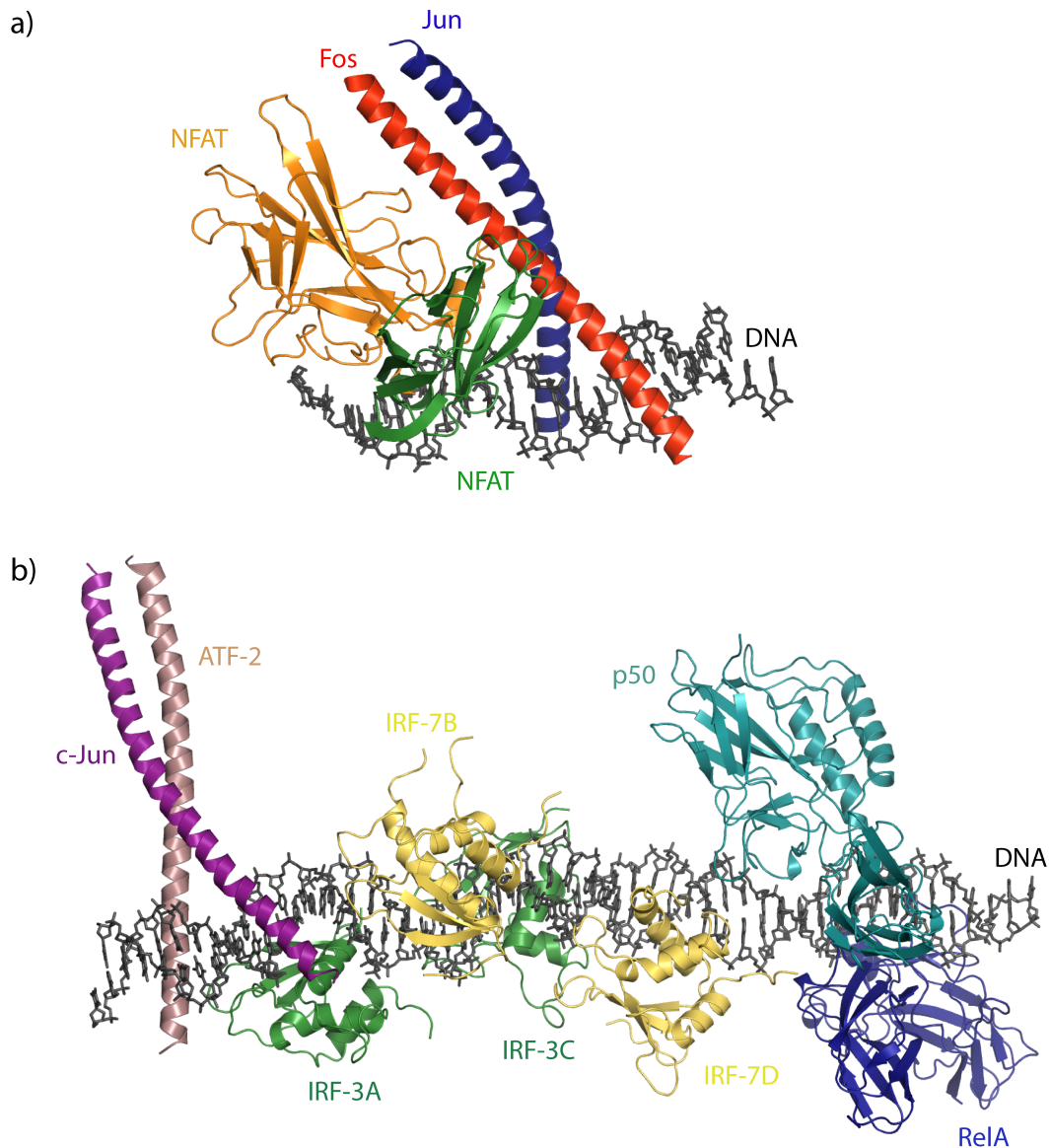
Figure 1.2. a) *Structure of the NFAT-AP-1-DNA complex* (PDB code 1A02). The N- and C-terminal domain of NFAT are shown in yellow and green, respectively. Fos is shown in red and Jun in blue. The DNA is colored grey. **b)** *Model of the IFN-β enhanceosome* (for PDB file see Panne *et al.* (2007)). IRF-3B and IRF-7D are in yellow and IRF-3A and IRF-3C are in green. C-Jun and AFT-2 are shown in violet and pink, respectively. RelA is colored blue and p50 is in cyan.

For the interferon (IFN)-β enhancer region, tight contacts between the eight transcription factors known as the enhanceosome, c-Jun, AFT-2, IRF-3A, IRF-3C, IRF-7B, IRF-7C, p50 and RelA, are absent (Figure 1.2b). Panne *et al.* (2007) hypothesized that the strong in vivo synergy of IFN-β gene regulation most likely results from the interactions between the enhanceosome and the coactivator CBP/p300. CBP is present in many eukaryotic cells such as mice, flies, plants and humans but not in yeast. It is a modular protein that contains a N- and a C-terminal activation domain (AD) that interact with the general TFs TATA-binding protein (TBP) and TFIIB (Kalkhoven 2004). CBP further binds a large number of

transcription factors through its CH-1, CH-3, KIX and SID domains (Figure 1.3). Next to its bridging function, CBP acts as a histone acetyltransferase (HAT) and thereby acetylates the N-terminal lysines of histones H2A, H2B, H3 and H4. In addition, it acts as a factor acetyltransferase (FAT), acetylating TFs and coactivators (Sterner and Berger 2000). The contribution of bridging between TFs and transcription machinery, HAT- and FAT-function to transcriptional synergy is often unknown (Vo and Goodman 2001, Kalkhoven 2004).
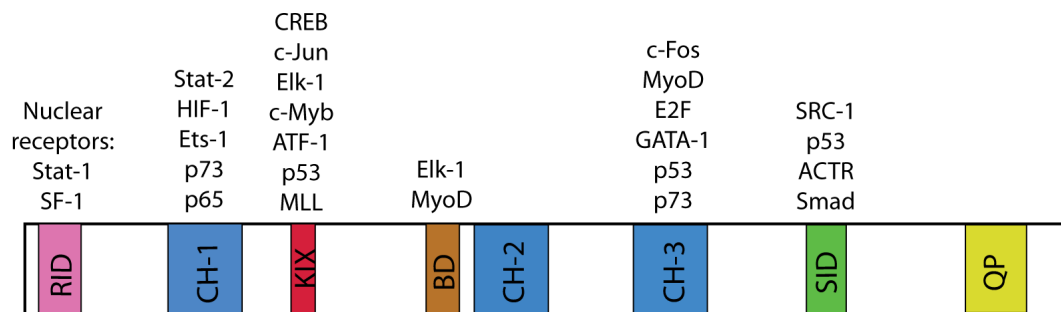

Figure 1.3. *Schematic representation of functional domains of CBP.* Interacting proteins are shown at the top of the figure. BD, bromodomain; CH1-3, cysteine and histidine-rich regions 1-3; QP, glutamine- and proline-rich domain; RID, receptor-interacting domain; SID, steroid-receptor co-activator-1 interaction domain. Figure adapted from Karamouzis *et al.* (2007).

1.2.1 The role of KIX in transcriptional synergy

The KIX domain is the only TF-binding domain of CBP that has two binding sites. This allows for direct mediation of interactions between bound transcription factors (De Guzman et al. 2006). KIX binds several TF factors such as MLL, c-Myb and pKID in a cooperative manner, which might be essential for transcriptional activation.

The transcriptional activators mixed-lineage leukemia (MLL) and c-Myb, which appear to be critical for normal blood cell development, are expressed at the same developmental stage in hematopoietic precursor cells (Graf 1992) and might act in concert to accomplish their biological tasks.

CBP binds CREB upon phosphorylation of its transactivation domain KID at serine 133, resulting in the rapid induction of gene expression (Montminy 1997). However, there are instances were the phosphorylation of CREB does not result in the recruitment of CBP or the induction of CREB regulated genes (Brindle et al. 1995). This suggests that at least one additional compound is needed for the induction of some CREB regulated genes. Korsmeyer and coworkers identified MLL as a binding partner of the binary KIX.pKID complex in a yeast genetic screen suggesting that the cooperative interaction of MLL and CREB with CBP most likely play a role in gene regulation (Ernst et al. 2001).

The three-dimensional structure of KIX (residue 586-672) consists of a three helical bundle (α_1, residue 597-611; α_2, residue 623-642; α_3, residue 646-669), an unstructured N-terminus (residues 586-596) that contains a short 3_{10}-helix G_1 (residues 591-593), helix α_1 and α_2 are linked by a flexible loop L12 (residues 612-622) that contains another short 3_{10}-helix G_2 (residues 617-620) (Article III). The packing of the secondary structure elements leads to the formation of two adjacent hydrophobic cores. The first core, constituted by the N-terminal residues of α_1 and α_3 (residues Leu599, Leu603, Tyr649, Tyr650, Leu653) and the C-terminal Met639 of helix α_2 is followed by a second hydrophobic core, formed by residues of all three helices, namely Leu607, Ala610, Ile611, Leu628, Tyr631, Ala632, Ile657 and Ile660. The binding sites for the TFs, which are spatially separated from each other, consist of two isolated hydrophobic binding surfaces (De Guzman et al. 2006, Article III). Thus the KIX domain of CBP bridges between varies transcription factors, through simultaneous binding and it can do so in a cooperative manner (Ernst et al. 2001). Goto *et al.* (2002) showed that in vitro binding of the MLL activation domain to KIX cooperatively enhances the interaction with the activation domain of the transcription factors c-Myb and pKID and vice versa. The binary KIX.MLL complex binds c-Myb and pKID with a ~2-fold higher affinity than apo-KIX (Goto et al. 2002). These cooperative effects provide a potential mechanism of transcription synergy through the scaffolding function of CBP.

This discovery raises a number of fundamental questions about the mechanism of cooperative binding of the KIX domain. How does the binding of MLL affect the structural and dynamic properties of KIX? How do these changes lead to an increase in binding affinity? Wright and coworkers used isothermal titration calorimetry (ITC) to characterize the thermodynamic basis of the cooperative binding process. They showed that the increase in binding affinity of c-Myb upon MLL binding to KIX is based on a decrease in binding enthalpy. pKID, however, binds entropically less unfavorably to the binary KIX.MLL complex than to apo-KIX. The different thermodynamic driving forces, for c-Myb enthalpy and for pKID entropy indicates a different mechanism of cooperative binding for these two ligands. In atomistic terms this means that, despite showing approximately the same increase in affinity, cooperative binding of c-Myb in the presence of MLL is on the one hand likely due to the formation of additional polar interactions that are absent in the binary complex. One the other hand cooperative binding of pKID could either arise from the stabilization of a conformation of KIX upon MLL binding that binds pKID more favorably or MLL binding leads to an increase of hydrophobic interactions between pKID and KIX (Goto et al. 2002). In a later study De Guzman *et al.* (2006) argued that the length of α_3 in the ternary KIX.MLL.c-Myb complex is stabilized and extends to residue R669 upon

binding of MLL, compared to the binary KIX.c-Myb complex where α_3 is unstructured past R665 (Zor et al. 2004).

In contrast to the study of De Guzman *et al.*, we were able to unambiguously identify, that α_3 of apo-KIX already consists of residues 646-669, the effect of MLL binding is rather a decrease in picosecond to nanosecond flexibility of the C-terminal end of α_3 helix than a helix extension. This finding is based on RDC measurements and order parameter data (Article III). Furthermore we were able to show that the binding of MLL to KIX induces only subtle structural changes if any at all, with the exception of its binding site that consists of the G_2 helix and the L12 loop, which are both translocated toward MLL. This movement is necessary for the formation of electrostatic interactions between the KIX residues Thr614 and Glu616 with the MLL residue Asn2856, as well as for the formation of a hydrophobic core between KIX and MLL. In addition, KIX shows an overall rigidification of its motions on the picosecond to nanoseconds time-scale (Article III). It is known that changes of these motions have a strong influence on the conformational entropy of proteins (Frederick et al. 2007), thus our findings are consistent with the reduced entropy penalty, derived from ITC measurements, for pKID binding to the binary complex. Proteins are not only sampling conformations that are very similar in free energy, they also frequently interconvert between conformations that are separated by a kinetic barrier of several k_BT (Baldwin and Kay 2009). The resulting slow motions on the microsecond to millisecond time-scale are important for allosteric signal transmission (Tzeng and Kalodimos 2011). Our CPMG relaxation dispersion data on the binary KIX.MLL complex unequivocally established that in the binary KIX.MLL complex KIX spontaneously interconverts between a major (lower energy) state and a minor (higher energy) state, which adopts a conformation similar to that of the ternary complex and binds c-Myb/pKID with higher affinity. Our data enabled us to measure the rate at which allosteric communication between binding sites occurs, and to directly map the pathway through which allosteric information is transmitted. The data further indicates conformational rearrangements of the upper hydrophobic core that connects the ligand binding surfaces of KIX and this most likely is the path of signal transmission between the two binding sites (Article I, del Sol et al. 2009).

Mutational studies showed that the I611V and I657V mutants of KIX are still able to bind pKID cooperatively, whereas for the I660V mutant MLL binding did not result in an increase in binding affinity for pKID. However, apo-KIX I660V already binds pKID with approximately the same affinity as the wild-type KIX.MLL complex does. Comparison of the solution structures of KIX.MLL and KIX.MLL.pKID indicates that the binding of pKID changes the χ_1 angle of Ile657 ~ -110°, with the result that the δ_1-methyl group is no longer

part of the hydrophobic core of KIX. Instead it forms hydrophobic contacts with Ile137 and Leu141 of pKID. Furthermore Ile660 translocates away from helix α_1 so that no NOEs between Leu607 and Ile660 can be measured. These conformational rearrangements of Ile657 and Ile660 lead to a loss of compactness in the upper hydrophobic core of KIX in the ternary complex (Article III).

Cooperativity has also been reported for binding of MLL to KIX in complex with c-Myb or pKID (Goto et al. 2002). To study allosteric communication in this direction we performed relaxation dispersion experiments on a binary KIX.c-Myb/pKID complex. Flat dispersion profiles were obtained so that the allosteric communication process cannot be monitored by this technique (Article II). However, our order parameter data indicates that binding of pKID gives rise not only to a local rigidification at the c-Myb/pKID binding site it also leads to a decrease in picoescond to nanosecond dynamics at the remote MLL binding site which is in accordance with the thermodynamic measurements for MLL binding (Article III).

Chapter 2

Protein Structure Determination utilizing Liquid State NMR Spectroscopy

2.1 Introduction

In the pioneering work on NMR structure determination of Wüthrich *et al.* and Clore *et al.* NOE (nuclear overhauser effect) inter-proton distances were used as the sole experimental constraints for protein structure calculations (Braun et al. 19981, Clore et al. 1986). Over the following years additional experimental restraints were introduced, including protein backbone torsional angles from chemical shifts (Wishart et al. 1992, Cornilescu et al. 1999), bond orientations from residual dipolar couplings (RDCs) (Tjandra and Bax 1997) and long-range distances from paramagnetic relaxation enhancement (PRE) (Battiste and Wagner 2000), which are now routinely used for NMR structure determination.

These additional structural restraints made the protein structure determination of systems with the molecular weight of ~80kDa possible (Tugarinov et al. 2005, Gautier et al. 2010). Determining restraints for such high molecular weight systems has become practicable due to significant progress in the area of 1) isotope labeling methodologies (Tugarinov and Kay 2003, Nietlispach et al. 1996), 2) NMR pulse-sequences (Pervushin et al. 1997) and 3) Spectrometer probe design. However, because these restraints are not sufficient for an ab initio protein structure determination, the experimental information needs to be combined with non-experimental constraints such as 1) bond length, 2) bond angles, 3) torsional angles and 4) non-bonding interactions. Experimental and non-experimental constrains are combined to a so-called hybrid energy function (Eq. 1), which is then minimized in the process of a structure calculation (Brünger and Nilges 1993).

$$E_{hybrid} = E_{phys} + \omega_{data} E_{data} \tag{1}$$

where ω_{data} is a weighting constant.

In the following Chapter I will briefly introduce the physical basis for NOE and RDC restraints.

2.2 Dipole-Dipole Coupling

The magnetic fields of nuclear spins can interact through space with each other. In the case of two interacting spins the strength of the dipolar coupling depends on the size of the magnetic field generated by one spin and the strength of the magnetic moment of the influenced spin (Figure 2.1, Eq. 2). Dipolar couplings can yield inter-nuclei distances, and in anisotropic systems the orientation of inter-atomic vectors relative to the static magnetic field B_0 (Levitt 2001, Rule and Hitchens 2006).
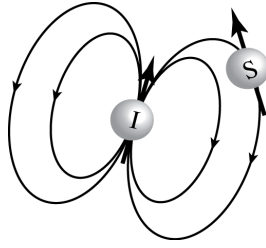
Figure 2.1. *Dipolar coupling between two spins.* The magnetic field generated by spin I is shown. Figure adapted from Levitt (2001).

The quantum mechanical spin Hamiltonian for the dipole-dipole interactions is given by (Rule and Hitchens 2006):

$$H^{DD} = \frac{\gamma_I \gamma_S}{r_{IS}^{3}} \left(I \cdot S - 3 \left(I \cdot e_{IS} \right) \left(S \cdot e_{IS} \right) \right) \tag{2}$$

where γ_I and γ_s are the gyromagentic ratio of spins I and S, respectively; r_{IS} is the distance between spins I and S; e_{IS} is the unit vector parallel to the vector between spins I and S; I and S are the vector operators for the spin angular momentum of nuclei I and S.

Substituting the spin angular momentum operators of nuclei I and S with the raising and lowering operators, I^+, I^- and S^+, S^- gives rise to the following form of the spin Hamiltonian (Rule and Hitchens 2006):

$$H^{DD} = \frac{\gamma_I \gamma_S}{r_{IS}^3} \left(F_Z + F_0 + F_1^+ + F_1^- + F_2^+ + F_2^- \right)$$

$$F_Z = \left(3\cos^2\theta - 1 \right) I_z S_z$$

$$F_0 = -\frac{1}{4} \left(3\cos^2\theta - 1 \right) \left(I^+ S^- + I^- S^+ \right)$$

$$F_1^+ = \frac{3}{2} \sin\theta \cos\theta\, e^{-i\phi} \left(I_z S^+ + I^+ S_z \right)$$

$$F_1^- = \frac{3}{2} \sin\theta \cos\theta\, e^{i\phi} \left(I_z S^- + I^- S_z \right) \qquad (3)$$

$$F_2^+ = \frac{3}{4} \sin^2\theta \cos\theta\, e^{-2i\phi} \left(I^+ S^+ \right)$$

$$F_2^- = \frac{3}{4} \sin^2\theta \cos\theta\, e^{2i\phi} \left(I^- S^- \right)$$

where θ is the angle between the internuclear vector and the external magnetic field B_0. Applying these six terms of the spin Hamiltonian operator to the four basis states of two coupled spins (Eq. 4) will lead to one or more of the transitions indicted in Figure 2.2, as they all contain raising and/or lowering operators, with the exception of the first term F_z, which leads to no transition, because it commutes with I_z and S_z operators (Rule and Hitchens 2006).

$$\phi_1 = |\alpha\alpha\rangle \quad \phi_2 = |\alpha\beta\rangle \quad \phi_3 = |\beta\alpha\rangle \quad \phi_4 = |\beta\beta\rangle \qquad (4)$$

However, it will result in a resonance splitting due to dipolar coupling and if the two spins are scalar coupled, the splitting will be the sum of the dipolar and scalar coupling. Dipolar coupling gives rise to two resonance lines of spin I at the angular frequencies (Rule and Hitchens 2006):

$$\omega = \omega_0 \pm \frac{1}{2} \frac{\gamma_I \gamma_s}{r_{IS}^3} \left(3\cos^2\theta - 1 \right) \qquad (5)$$

where ω_0 is the Larmor frequency of spin I. These splittings are frequently measured between spins that are linked through a covalent bond in weakly aligned systems, thus removing the distance dependence. These so-called residual dipolar interactions (RDCs) give rise to global structural restraints of the orientation of inter-nuclear vectors relative to the static magnetic field B_0 (Bax et al. 2001).
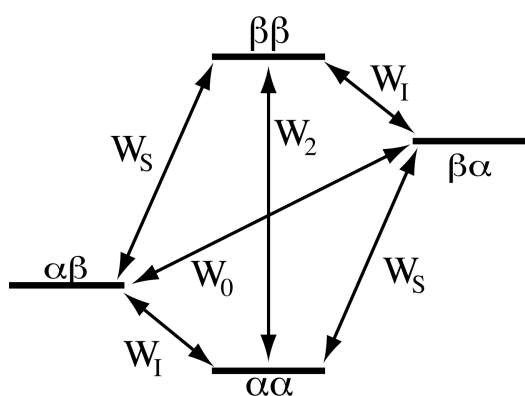
Figure 2.2. *Energy level diagram for a coupled two-spin system.* Transitions and associated rate constants are indicated.

In the case of isotropic rotation in solution the dipolar interaction contribution to the energy of a spin is averaged to zero. However, the tumbling of the molecule gives rise to fluctuating magnetic fields that induce zero-quantum, single-quantum and double-quantum transitions and therefore provides a mechanism for nuclear spin relaxation (Rule Hitchens 2006). This relaxation mechanism induces changes in the population of energy levels of dipolar coupled spins, the so-called nuclear Overhauser effect (NOE) (Overhauser 1953). Thus the relaxation rates contain information about the distance between coupled spins and these distances are usually derived from the crosspeak intensity of NOESY (Nuclear Overhauser Effect Spectroscopy) experiments.

2.2.1 NOE derived distance restraints

The time dependence of the magnetization of dipolar interaction spins can be described in a semi-classical manner using the Solomon equations (Solomon 1955). For a two spin system (Figure 2.2) with the transition rates W_0 (zero-quantum), W_I, W_S (single-quantum) and W_2 (double-quantum) between the four energy states the following differential equations describe the change in magnetization as function of time (Solomon 1955, Cavanagh et al. 2007):

$$\frac{d\Delta I_z(t)}{dt} = \rho_I \Delta I_z(t) - \sigma_{IS} \Delta S_z(t)$$
$$\frac{d\Delta S_z(t)}{dt} = \rho_S \Delta S_z(t) - \sigma_{IS} \Delta I_z(t)$$

$$(6)$$

where $\Delta I_z = I_z(t) - I_z(0)$ and $\Delta S_z = S_z(t) - S_z(0)$; $I_z(0)$ and $S_z(0)$ are the equilibrium magnitude of the I_z and S_z spin operator, respectively, and $\rho_I = W_0 + 2W_I + W_2$ and $\rho_S = W_0 + 2W_S + W_2$ are the autorelaxation rate constants, and $\sigma_{IS} = W_2 - W_0$ is the cross-relaxation constant.

For a rigid body, which means no internal motion, the transition rates of the zero-, single- and double-quantum transition can be calculated from the autocorrelation function Eq. 7 (Neuhaus and Williamson 2000).

$$g(t) = \overline{f(t)f(t+\tau)}$$

$$(7)$$

This describes the correlation between a parameter measured at time t and the same parameter measured at a later time $t+\tau$. For an isotropically tumbling sphere it takes the following exponential form (Neuhaus and Williamson 2000):

$$g(t) \propto \exp(-t/\tau_c)$$

$$(8)$$

As we are interested in the intensity of the magnetic field fluctuations as a function of frequency, as they cause of zero-, single- and double-quantum transition, we need to Fourier transform (FT) Eq. 8 and the resulting Lorentzian function is called spectral density function $J(\omega)$ (Neuhaus and Williamson 2000, Rule and Hitchens 2006):

$$J(w) = \frac{1}{1 + \omega^2 \tau_c^2}$$

$$(9)$$

The transition probabilities W_0, W_I, W_S and W_2 can be calculated from the spectral density function (Solomon 1955, Neuhaus and Williamson 2000) and ρ_I and σ_{IS} can be expressed as:

$$\rho_I = \frac{1}{20}\left(\frac{\mu_0 \hbar \gamma_I \gamma_S}{4\pi r_{IS}^3}\right)^2 \left[J(0) + 3J(\omega_0) + 6J(2\omega_0)\right] \qquad (10)$$

$$\sigma_{IS} = \frac{1}{20}\left(\frac{\mu_0 \hbar \gamma_I \gamma_S}{4\pi r_{IS}^3}\right)^2 \left[6J(2\omega_0) - J(0)\right] \qquad (11)$$

The autorelaxation rate, which is proportional to r^{-6} gives rise to the NOE and can therefore be used to obtain inter-proton distances. For biomolecules inter-proton distances are determined using multidimensional NOESY experiments. During the mixing time of the NOESY sequence magnetization is exchanged between spatially close spins, which gives rise to crosspeaks between nuclei that are not further than ~6 Å apart. The volume of crosspeaks is proportional to the inter-proton distance between the coupled spins (Eq. 12) (Neuhaus and Williamson 2000).

$$V_{IS} = d_{IS}^{-6} f(\tau_c) \qquad (12)$$

The only unknown in Eq. 12 is τ_c, which can be determined. However, in most cases NOE volumes of unknown distances are compared with NOE volumes of known distances and lower and upper bounds of the distances are introduced:

$$d_l = \left(\frac{d_{ref}}{V_{ref}} V_{IS}\right) - \Delta$$

$$d_u = \left(\frac{d_{ref}}{V_{ref}} V_{IS}\right) + \Delta \qquad (13)$$

where Δ is an error estimate and d_{ref} and V_{ref} are the reference distance and volume. These inter-proton distances are then introduced into Eq. 1 using a square-well energy function (Clore et al. 1986):

$$E_{NOE} = \sum_{NOE} \begin{cases} (d_{ij} - d_u)^2 & d_u < d_{ij} \\ 0 & d_l < d_{ij} > d_u \\ (d_l - d_{ij})^2 & d_{ij} < d_l \end{cases} \qquad (14)$$

where the sum is over all NOE-derived distances and d_{ij} is a distance between a particular spin pair.

2.2.2 RDC derived orientational restraints

As mentioned above, the F_z term of the dipolar coupling spin Hamiltonian leads to the splitting of resonance lines of spins that are dipolarly coupled (Eq. 5). However, in liquid samples, the intermolecular vector tumbles isotropically and the line splitting is averaged to zero. In solids, there is no overall tumbling of the molecules and thus the dipole-dipole interactions are not averaged to zero, which gives rise to a backbone amide dipolar coupling of ~ 22 kHz, thereby causing severe signal broadening. Reducing the magnitude of dipolar couplings can be achieved by partially restricting molecular tumbling of liquid samples (De Alba and Tjandra 2004). Alignment of a fraction of the molecules is realized in liquid crystalline media, such as phospholipid bicelles and bacteriophages, or compressed gels. These media give rise to amide protein backbone RDCs ranging from 5-30 Hz (Prestegard et al. 2004).

Both NOE and chemical shift restraints give strictly local information of the protein structure. However, residual dipolar couplings provide global restraints through the orientation of internuclear vectors of the protein with respect to the external magnetic field B_0 (Saupe 1964). Eq. 5 gives the resonance line splitting as a function of angle θ, however, if dipolar couplings are employed as orientational restraints in a protein structure calculation they need to be related to the internal coordinates of the protein (Figure 2.3). The dipolar coupling can be written as a function of angle θ (Bax et al. 2001):

$$D = D_{max} \frac{1}{2}\left(3\cos^2\theta - 1\right) \tag{15}$$

where $D_{max} = \dfrac{\mu_0 \hbar \gamma_I \gamma_s}{4\pi^3 r_{IS}^3}$ is the maximum dipolar coupling and $cos\theta$ is the scalar product between the unit vector of the internuclear vector ($cos\alpha_x$, $cos\alpha_y$, $cos\alpha_z$) and a unit vector parallel to B_0 ($cos\beta_x$, $cos\beta_y$, $cos\beta_z$) (Figure 2.3), therefore Eq. 15 can be rewritten as (Bax et al. 2001, Rule and Hitchens 2006):

$$\begin{aligned} D = D_{max} \Bigg[\frac{3}{2}\Big(&\alpha_x^2\left\langle\beta_x^2\right\rangle + \alpha_y^2\left\langle\beta_y^2\right\rangle + \alpha_z^2\left\langle\beta_z^2\right\rangle \\ &+ 2\alpha_x\alpha_y\left\langle\beta_x\beta_y\right\rangle + 2\alpha_x\alpha_z\left\langle\beta_x\beta_z\right\rangle \\ &+ 2\alpha_y\alpha_z\left\langle\beta_y\beta_z\right\rangle\Big) - \frac{1}{2}\Bigg] \end{aligned} \tag{16}$$

where $\alpha_i = cos\alpha_i$ and $\beta_i = cos\beta_i$ and $\left\langle\ \right\rangle$ represents the average of all the molecules in the ensemble. The $\left\langle\beta_i^2\right\rangle$ terms describe the average orientation of an aligned molecule with

respect to the magnetic field, and they are commonly known as the Saupe order matrix, S. The second-rank tensor S is real and symmetric, in the principal axis frame it becomes a diagonal matrix with trace zero, and its elements are defined as follows (Bax et al. 2001, Rule and Hitchens 2006):

$$S_{ij} = \frac{3}{2}\langle \beta_i \beta_j \rangle - \frac{1}{2}\delta_{ij} \tag{17}$$

where δ_{ij} is the Kronecker delta function. The dipolar coupling D can be rewritten, in the principal axis frame, as:

$$D = D_{max}\left[\alpha_x^2 S_{xx} + \alpha_y^2 S_{yy} + \alpha_z^2 S_{zz}\right] \tag{18}$$

The difference between the anisotropic $\langle \beta_{ii} \rangle^2$ value and its isotropic value ($=1/3$) determines the magnitude of the dipolar coupling D. This difference is referred to as the alignment tensor, A (Rule and Hitchens 2006):

$$A_{ii} = \langle \beta_{ii} \rangle^2 - \frac{1}{3} \tag{19}$$

Rewriting Eq. 18 using Eq. 19 and converting it into polar coordinates of the molecular frame we obtain (Bax et al. 2001):

$$D(\vartheta,\varphi) = D_{max}\frac{3}{2}\left[\frac{1}{2}\left(3\cos^2\vartheta - 1\right)A_{zz} + \frac{1}{2}\sin^2\vartheta\cos2\varphi\left(A_{xx} - A_{yy}\right)\right] \tag{20}$$

where $|A_{zz}| \geq |A_{yy}| \geq |A_{xx}|$. Eq. 20 is frequently rewritten, by defining an axial component of the alignment tensor $A_a = \frac{3}{2}A_{zz}$, and a rhombic component $A_r = A_{xx} - A_{yy}$ (Bax et al. 2001):

$$D(\vartheta,\varphi) = D_a\left[\left(3\cos^2\vartheta - 1\right) + \frac{3}{2}R\sin^2\vartheta\cos2\varphi\right] \tag{21}$$

where $D_a = \frac{1}{2}D_{max}A_a$ is called the magnitude of the residual dipolar coupling tensor and $R = \frac{A_r}{A_a}$ is the rhombicity.

Thus, if a protein structure is available, the elements of the alignment tensor can be determined, usually using singular value decomposition (Losonczi et al. 1999, Zweckstetter 2008).
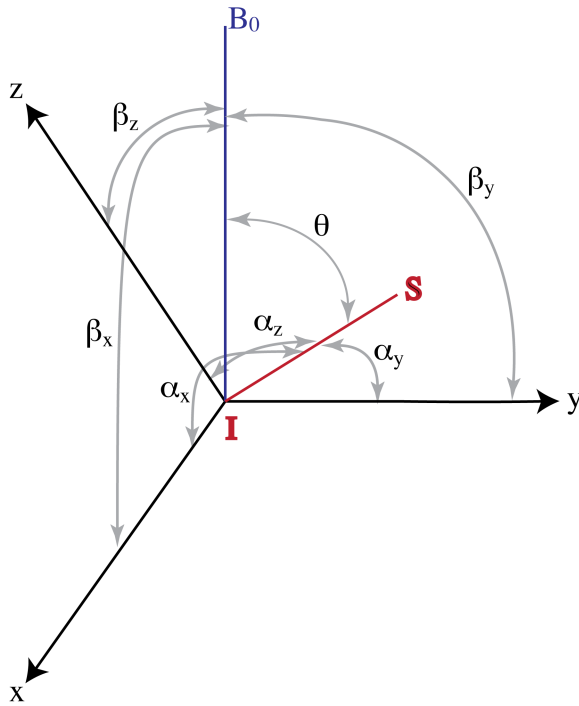
Figure 2.3. *Definition of the angles between the molecular and the laboratory reference frame.* The molecular reference frame is shown in blue. The internuclear vector between spin I and spin S is indicated in red. The time-dependent angles βx, βy and βz define the orientation of the static magnetic field B₀ (blue) relative to the molecular coordinate system. Figure adapted from Bax *et al.* (2001)

Tjandra *et al.* (1997) developed the most commonly used method for the implementation of RDCs into protein structure calculation. RDCs are included to the target function (Eq. 1) as a harmonic energy (Eq. 22).

$$E_{RDC} = \sum_{RDC} K_{RDC}\left(D_{cal} - D_{obs}\right)^2 \tag{22}$$

Where K_{RDC} is the force constant and D_{cal} and D_{obs} are the calculated and measured values of the residual dipolar couplings, respectively.

The alignment tensor is represented as a pseudomolecule that consists of four equidistant atoms (OXYZ). D_{cal} is calculated using Eq. 21 and the alignment tensor (pseudomolecule) is continuously reorientated to minimize E_{RDC} (De Alba and Tjandra 2004). Including RDC restraints in protein structure calculation has a major impact on the precision of protein structures determined by liquid state NMR (Bouvignies et al. 2006).

2.3 Simulated Annealing

The goal of NMR structure determination is to generate an ensemble of three-dimensional structures that are in optimal agreement with the experimental data and the *a priori* chemical knowledge. This can be considered as a global optimization problem of the hybrid energy function (Eq. 1) in Cartesian or torsion angle space (Brünger and Nilges 1993, Güntert 1998). Minimization of E_{hybrid}, using gradient descent minimization algorithms, frequently traps in a local minimum of the energy surface, as these algorithms are only able to move downhill along the gradient of Eq. 1. This problem can be overcome be employing simulation annealing methods, which can move in an uphill direction as well (Kirkpatrick et al. 1983, Brünger and Nilges 1993). These algorithms control the direction of the minimization through the temperature. The higher the kinetic energy of a system, the likelier is the crossing of an energy barrier. Molecular dynamics based simulated annealing methods are commonly used for NMR structure determination and were introduced by Clore *et al.* (1985). In Cartesian coordinates, molecular dynamics consist of the numerical solution of Newton's equation of motion (Allen and Tildesley 1987):

$$m_i \frac{\partial^2 r_i}{\partial t^2} = -\frac{\partial E_{hybrid}}{\partial r_i} \tag{23}$$

where r_i and m_i are the coordinates and mass of atom I, respectively. The equation of motion is numerically integrated using finite difference methods, like the Verlet (Eq. 24) or the leap-frog (Eq. 24) algorithm (Allen and Tildesley 1987).

$$r(t + \delta t) = 2r(t) - r(t - \delta t) + \delta t^2 a(t) \tag{24a}$$

$$v(t) = \frac{r(t + \delta t) - r(t - \delta t)}{2\delta t} \tag{24b}$$

$$r(t + \delta t) = r(t) + \delta t v\left(t + \frac{1}{2}\delta t\right) \tag{25a}$$

$$v\left(t + \frac{1}{2}\delta t\right) = v\left(t - \frac{1}{2}\delta t\right) + \delta t a(t) \tag{25b}$$

where $v(t)$ and $a(t)$ are the velocity and acceleration, respectively. The advantage of the leap-frog algorithm is that it explicitly includes velocities which are functionally dependent to the temperature of the system according to (Leach 2001):

$$\left\langle \sum_{i=1}^{N} m_i v_i^2 \right\rangle = 3Nk_B T \tag{26}$$

18

Thus, a very obvious way to control the temperature of the system is through scaling the velocities.

Chapter 3

Studying Protein Dynamics by NMR

3.1 Analysis of Sub-Nanoseconds and Sub-Milliseconds Dynamics

Traditionally, in structural biology proteins are presented as a single static conformation although it is known that these rigid representations are often not sufficient to fully understand the protein function (Karplus and Kuriyan 2005, Baldwin and Kay 2009). Therefore efforts have been made in NMR spectroscopy as well as in X-ray crystallography to include the conformational flexibility into the structural representation of proteins (Furnham et al. 2006, Markwick et al. 2009). NMR is unique in its ability to probe the structural plasticity of proteins in atomic resolution on a wide range of time-scales.

Conformational heterogeneity of a protein can be described using the concept of a free energy landscape (Figure 3.1). The ground-state of a protein can interconvert between different conformers that are separated from each other by small kinetic barriers that can be overcome by thermal energy, resulting in picosecond to nanosecond dynamics of the protein backbone and side chains (Henzler-Wildman and Kern 2007). Dynamics on the picosecond to nanosecond time-scale forms the basis for conformational entropy that is known to be crucial for protein-ligand binding (Karplus et al. 1987, Stone 2001) and it was shown that these motions can facilitate large-scale conformational rearrangements in proteins (Henzler-Wildman et al. 2007). Wand and coworkers studied the binding entropy of six different petites binding to calmodulin, and determined the conformational entropy ΔS_{conf} of calmodulin in the free and the bound state based on NMR order parameters. They showed that the ΔS_{conf} values linearly correlate with the binding entropy determined by ITC. They conclude that conformational entropy has a major impact on high affinity protein binding and it can be reliably determined utilizing NMR relaxation methods (Frederick et al. 2007).
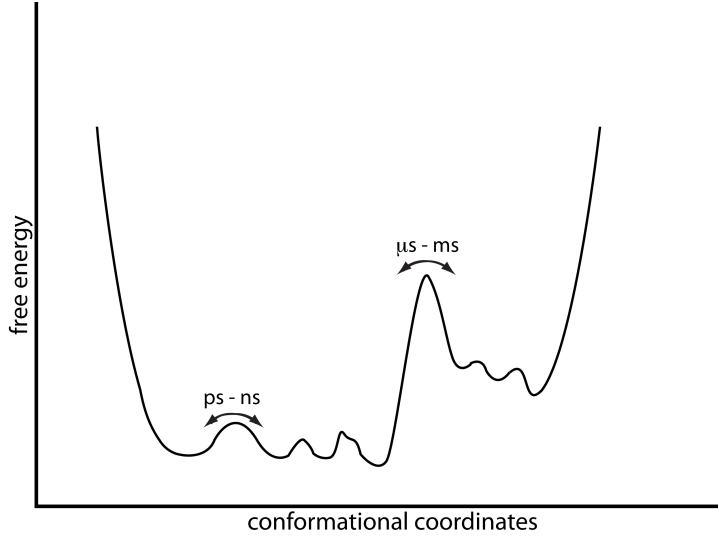
Figure 3.1. *Schematic energy surface.* The time-scale of interconversion between different conformations is indicated. Figure adapted from Henzler-Wildman and Kern (2007).

The picosecond to nanosecond time-scale is directly accessible by NMR spin relaxation properties through the measurement of R_1 (longitudinal relaxation rate), R_2 (transverse relaxation rate) and *hnNOE* (heteronuclear NOE) (Farrow et al. 1994). Relaxation of ^{13}C and ^{15}N atoms is dominated by dipolar interaction to the attached protons and their own chemical shift anisotropy (CSA). Random rotational motion and/or internal motion of the protein leads to oscillating electromagnetic fields which cause relaxation if they occur with a frequency of $\sim 10^9$ Hz. As already mentioned in Chapter 2.1.1 the connection between the relaxation rates and molecular motion can be made by the spectral density function $J(\omega)$. The effect of the relaxation mechanisms on the relaxation rates and the NOE can be calculated as outlined in Chapter 2.1 and Chapter 2.1.1. By taking CSA and dipolar interaction into account R_1, R_2 and *hnNOE* can be calculated as follows (Abragam 1961, Palmer 2004):

$$R_1 = \frac{1}{4}\left(\frac{\mu_0 h \gamma_H \gamma_N}{8\pi r_{HN}^3}\right)^2 \left[J(\omega_H - \omega_N) + 3J(\omega_N) + 6J(2\omega_H + \omega_N)\right]$$

$$+ \frac{1}{3}\omega_N^2 \Delta\sigma^2 J(\omega_N) \tag{27}$$

$$R_2 = \frac{1}{8}\left(\frac{\mu_0 h \gamma_H \gamma_N}{8\pi r_{HN}^3}\right)^2 \left[4J(0) + J(\omega_H - \omega_N) + 3J(\omega_N) + 6J(\omega_H) + 6J(2\omega_H + \omega_N)\right]$$

$$+ \frac{1}{18}\omega_N^2 \Delta\sigma^2 \left[4J(0) + J(\omega_N)\right] + R_{ex} \tag{28}$$

$$hnNOE = 1 + \frac{1}{4R_1^N}\frac{\gamma_H}{\gamma_N}\left(\frac{\mu_0 h \gamma_H \gamma_N}{8\pi r_{HN}^3}\right)^2 \left[6J(\omega_H + \omega_N) - J(\omega_H - \omega_N)\right] \tag{29}$$

where $\Delta\sigma$ is the CSA, ω_H and ω_N are the Larmor frequency of ^{1}H and ^{15}N, respectively; R_{ex} is the relaxation rate constant due to chemical exchange. The CSA for the amide backbone ^{15}N-atom is $\sim$ -157 ppm (Fushman et al. 1998).

A commonly used method for analyzing relaxation rates and *hnNOE* data is the model-free approach (Lipari and Szabo 1982a, Lipari and Szabo 1982b). Libari and Szabo showed that the contribution of internal motion to the relaxation rates can be quantified using two model-independent parameters: 1) the generalized order parameter, S^2, which is a measure of the amplitude of motion and 2) a time constant for internal motion, the effective correlation time τ_e. The model assumes that the internal motion is much faster than the rotational tumbling and thus both can be treated separable in the autocorrelation function (Lipari and Szabo 1982a):

$$g(t) = \frac{1}{5}S^2 e^{-t/\tau_c} + \frac{1}{5}\left(1 - S^2\right)e^{-t/\tau} \tag{30}$$

where $1/\tau = 1/\tau_c + 1/\tau_e$. For isotropic molecular tumbling the corresponding spectral density becomes (Lipari and Szabo 1982a):

$$J(\omega) = \frac{2}{5}\left(\frac{S^2\tau_c}{1 + \left(\omega\tau_c\right)^2} + \frac{\left(1 - S^2\right)\tau}{1 + \left(\omega\tau\right)^2}\right) \tag{31}$$

The order parameter values range between 1 (fully spatially restricted) and 0 (complete unrestricted motion). Clore *et al.* (1990) extended this simple model by introducing two distinct correlation times for the description of the internal motion (Eq. 33) because they found that the relaxation data of the proteins SNase and IL-1β could not be accounted for by the simple two-parameter model-free approach.

$$J(\omega) = \frac{S^2\tau_c}{1 + \left(\omega\tau_c\right)^2} + \frac{\left(1 - S_f^2\right)\tau_f^{'}}{1 + \left(\omega\tau_f^{'}\right)^2} + \frac{\left(S_f^2 - S^2\right)\tau_s^{'}}{1 + \left(\omega\tau_s^{'}\right)^2} \tag{32}$$

with $\tau_i^{'} = \tau_i\tau_c/(\tau_c + \tau_i)$, $i = f,s$; and $S^2 = S_f^2 S_s^2$, S_f^2 S_s^2 are the generalized order parameters for fast and slow motion, respectively. τ_s and τ_f are the correlation time for slow and fast internal motion, respectively.

Assuming that chemical exchange contributions, certain order parameters and correlation times are statistically significant, five model-free models are generally used (Table 2.1). Model selection is based on the partial F-test, which allows to verify if the improvement of the fit to a more complex model is not only due to the introduction of an additional parameter (Mandel et al. 1995).

Model	Parameters
1	S^2
2	S^2, τ_e
3	S^2, R_{ex}
4	S^2, τ_e, R_{ex}
5	S_f^2, S^2, τ_e

Table 2.1. *Model-free models.*

The correlation time of the overall protein tumbling τ_c and the correlation time(s) of internal motion are treated separately in Eq. 31 and Eq. 32, although they are fitted to the same relaxation data (Eq. 27, Eq. 28 and Eq. 29). Thus, an exact model of rotational diffusion must be used otherwise systematic errors will occur in the determination of the order parameter and the internal correlation time(s) (Schurr et al. 1994). Therefore, τ_c or in case of anisotropic diffusion the diffusion tensor is determined using residues that do not undergo extensive internal dynamics (Brüschweiler et al. 1995, Tjandra et al. 1995).

Proteins are not only sampling conformations that are very similar in thermodynamic energy they frequently interconvert between conformations that are separated by a kinetic barrier of several k_BT (Figure 3) (Henzler-Wildman and Kern 2007) (Figure 3.1). Interconversion between a ground and a so-called excited state occurs on the microsecond to millisecond time-scale. These transitions have been extensively studied the last ten years, NMR spectroscopy played a vital role in these studies (Henzler-Wildman and Kern 2007, Baldwin and Kay 2009). The broad interest in such slow motions arose from the fact that these mainly large-amplitude collective rearrangements are essential for many biological processes such as limiting the rate of enzyme catalysis and product release (Bhabha et al. 2011), protein folding (Korzhnev et al. 2010) as well as allosteric regulation (Tzeng and Kalodimos 2011).

Conformational exchange can be studied by NMR, because the exchange of a nucleus between two magnetically inequivalent sites on a time-scale similar to the chemical shift difference between these sites results in an increase in the transversal relaxation rate R_2 (Palmer 2004). The kinetics of chemical exchange is defined by the following equilibrium (Eq. 33) between two states, A and B, with the rate constants k_{12} and k_{21}.

$$A \underset{k_{21}}{\overset{k_{12}}{\rightleftharpoons}} B \tag{33}$$

The time-scale of conformational exchange can be classified into different regimes based on the relationship between the chemical shift difference of the interconverting states, $\Delta\omega$, and the sum of the rate constants k_{ex} (Millet et al. 2000):

$$0 \leq \alpha < 1 \qquad k_{ex} < \Delta\omega \qquad \text{slow exchange}$$
$$\alpha \approx 1 \qquad k_{ex} \approx \Delta\omega \qquad \text{intermediate exchange}$$
$$1 < \alpha \leq 2 \qquad k_{ex} > \Delta\omega \qquad \text{fast exchange}$$

with α being defined as $\alpha = 2(k_{ex}/\Delta\omega)^2/(1+(k_{ex}/\Delta\omega)^2)$ and $p_A \gg p_B$.

Chemical exchange changes the line widths, the peak positions and the transverse relaxation rates of the interconverting spins. In the absence of a magnetic field (free precession) the R_2 relaxation rate of state A becomes ($p_A \gg p_B$) (Woessner 1961, Palmer 2004):

$$R_{2A} = R_2^0 + \frac{k_{ex}}{2} - \frac{1}{\sqrt{8}}\left\{k_{ex}^2 - \Delta\omega^2 + \left[(k_{ex}^2 + \Delta\omega^2)^2 - 16p_A p_B \Delta\omega^2 k_{ex}^2\right]^{1/2}\right\}^{1/2} \tag{34}$$

with $R_{2A}^0 = R_{2B}^0 = R_2^0$ and $R_{ex} = R_{2A}^0 - R_2^0$. In the absence of a magnetic field (free precession) the chemical shift of state A is given by ($p_A \gg p_B$) (Woessner 1961, Palmer 2004):

$$\omega_A = \frac{\omega_A + \omega_B}{2} - \frac{1}{\sqrt{8}}\left\{\Delta\omega^2 - k_{ex}^2 + \left[(k_{ex}^2 + \Delta\omega^2)^2 - 16p_A p_B \Delta\omega^2 k_{ex}^2\right]^{1/2}\right\}^{1/2} \tag{35}$$

The kinetic and thermodynamic parameters of the chemical exchange equilibrium (Eq. 33) are usually determined by fitting the R_2 relaxation rate. The complex functional dependence of R_{ex} with k_{ex}, p_A, p_B and $\Delta\omega$ (Eq. 34) makes the determination of these parameters from a single measurement of a R_2 value per residue unfeasible. However, the conformational exchange contribution to R_2 can be quenched by the application of a radio frequency field in form of a spin echo sequence. In these so-called Carr-Purcell-Meiboom-Gill (CPMG) relaxation dispersion experiments the relaxation of transverse magnetization is observed during a $(\tau_{cp}/2\text{-}180°\text{-}\tau_{cp}\text{-}180°\text{-}\tau_{cp}/2)_n$ spin-echo sequence, where τ_{cp} is the delay between the

180° pulses and *n* is an integer (Loria and Palmer 1999). The effective field dependency of the transverse relaxation generates a relaxation dispersion curve (Figure 3.2). The shape of these curves is dependent on the chemical exchange time-scale and they can be fitted to a model (Eq. 33) that describes the conformational exchange process.
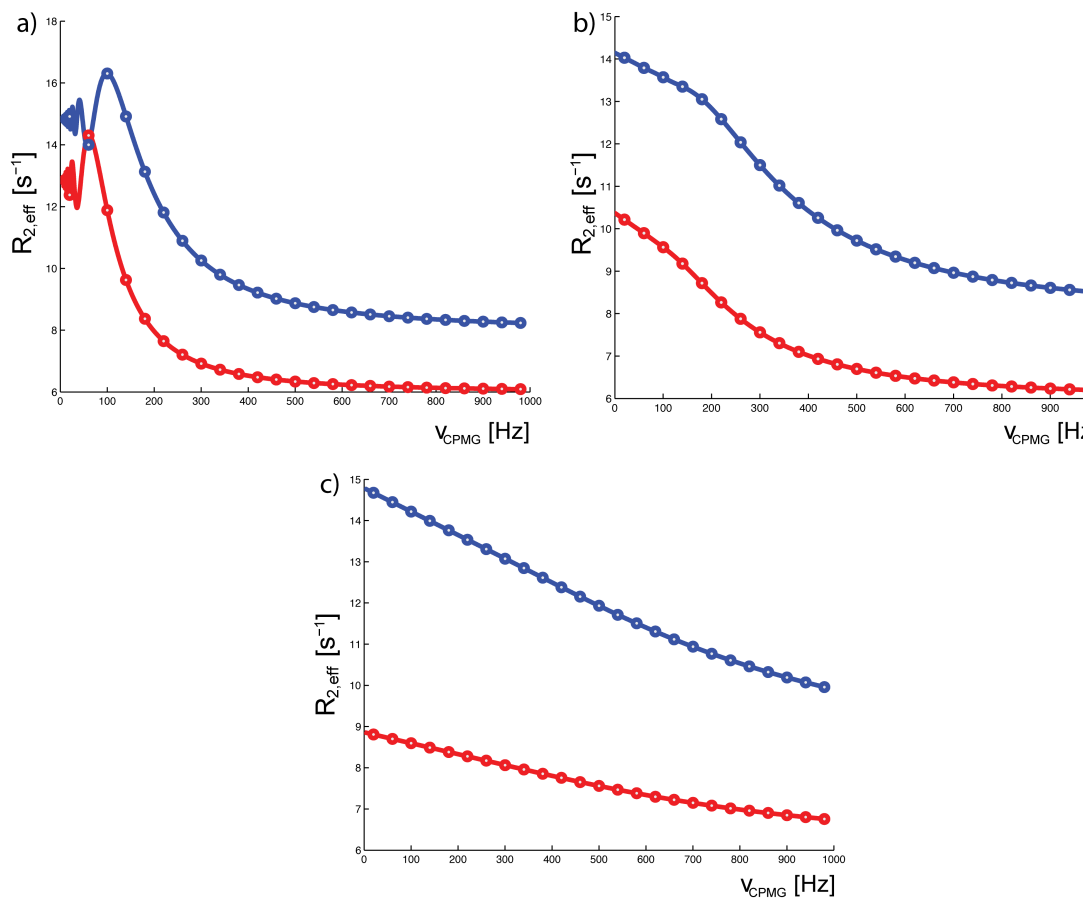
Figure 3.2. *CPMG relaxation dispersion curves at different time-scales.* a) slow exchange. b) intermediate exchange. c) fast exchange.

In the presence of a radio frequency field, the transverse relaxation rate R_2 of state A in the two-site chemical exchange process (Eq. 33) is given by (Carver and Richards 1972, Palmer 2001):

$$R_{2A}\left(1/\tau_{cp}\right) = R_2^0 + \frac{1}{2}\left(k_{ex} - \frac{1}{\tau_{cp}}\cosh^{-1}\left[D_+\cosh(\eta_+) - D_-\cos(\eta_-)\right]\right) \tag{36}$$

in which

$$D_\pm = \frac{1}{2}\left[\pm 1 + \frac{\psi + 2\Delta\omega^2}{\left(\psi^2 + \zeta^2\right)^{1/2}}\right]^{1/2}$$

$$\eta_\pm = \frac{\tau_{cp}}{2}\left[\pm\psi + \left(\psi^2 + \zeta^2\right)^{1/2}\right]^{1/2}$$

$\psi = k_{ex}^2 + \Delta\omega^2$ and $\zeta = -2\Delta\omega k_{ex}\left(p_A - p_B\right)$. Eq. 38 is valid for all chemical exchange time regimes if $p_A \gg p_B$.

CPMG experiments allow the determination of the kinetic and thermodynamic parameters if i) $\Delta\omega \neq 0$, ii) the exchange rate k_{ex} is between $10000s^{-1}$ and $1s^{-1}$ and iii) the population of excited-state is larger than 1%.

Chapter 4

Native Mass Spectrometry of Proteins

4.1 Analyzing Gas Phase Structures using ECD MS

For proteins that are ionized and transferred to the gas phase using electrospray ionization (ESI) the solution structure is retained as a metastable conformation at least on the milliseconds time-scale (Breuker and McLafferty 2008, Meyer et al. 2009). However, after milliseconds to seconds the "dry" protein will, in most cases, have undergone significant structural rearrangements to minimize its ionic interactions and the stable gas phase structure will most likely not resample the solution structure. There is evidence that this structural evolution is a stepwise process (Breuker and McLafferty 2008). The first step in the transition of solution to gas phase during ESI MS is the production of charged droplets. Evaporation of the water in these droplets leads to structural rearrangements of the proteins on the nanosecond time-scale. These findings are based on molecular dynamics simulations (Steinberg et al. 2007, Meyer et al. 2009). After full desolvation of charged residues (Lys, Arg, Glu, Asp) on the surface of the protein, they start (~ ps) forming very strong ionic interactions with each other which leads to the stabilization of secondary structure and compaction of the protein structures, however, the structures still resemble the solution state structures. These compact proteins are stable in the vacuum for milliseconds (Breuker and McLafferty 2008, Steinberg et al. 2008, Meyer et al. 2009). On the sub-second to second time-scale, hydrophobic bonds and electrostatic interactions are broken and the proteins fold into their stable gas phase structures. This was shown experimentally by electron capture dissociation experiments (ECD) (Horn et al. 2001, Breuker et al. 2002). In ECD MS experiments protein ions $(M + n\text{H})^{n+}$, which are ESI-produced interact with low energy electrons (≤ 0.2 eV) the capture of a low energy e^- leads to the fragmentation of the $(M + n\text{H})^{(n-1)+}\bullet$ protein ion radical. The fragmentation reaction yields **c** and **z**$\bullet$ product ions (Eq. 37), in addition some minor amounts of **a**$\bullet$ and **y** ions are produced (Eq. 38) (Zubarev et al. 1998, Zubarev et al. 1999).

$$\left[\begin{array}{c} \overset{O\cdots\,-H^{\underline{+}}\cdots NH_2}{\underset{R'C-NH-CHR}{\|}} \end{array}\right]^{n+} \xrightarrow{+e^-} \left[\begin{array}{c} \overset{OH\qquad NH_2}{\underset{R'\overset{\bullet}{C}-NH-CHR}{|}} \end{array}\right]^{n+} \longrightarrow \left[\begin{array}{c} \overset{OH}{\underset{R'C=NH}{|}} \end{array}\right]^{m+} + \left[\begin{array}{c} \overset{NH_2}{\bullet\,CHR} \end{array}\right]^{(n-m)+}$$
$$\qquad\qquad\qquad\qquad\qquad\qquad\qquad\qquad\qquad\qquad\qquad\qquad \boldsymbol{c}\qquad\quad \boldsymbol{z^{\cdot}} \qquad\qquad (37)$$

$$\left[\begin{array}{c} \overset{O\quad H^{\underline{+}}\cdots NH_2}{\underset{R'C-NH-CHR}{\|}} \end{array}\right]^{n+} \xrightarrow{+e^-} \left[\begin{array}{c} \overset{O\qquad\quad NH_2}{\underset{R'C-\overset{\bullet}{N}H_2-CHR}{\|}} \end{array}\right]^{n+} \longrightarrow R'^{\cdot m+} + \overset{O}{\underset{C}{\||\|}} + \left[\begin{array}{c} \overset{NH_2}{NH_2CHR} \end{array}\right]^{(n-m)+}$$
$$\qquad\qquad\qquad\qquad\qquad\qquad\qquad\qquad\qquad\qquad\qquad\qquad \boldsymbol{a^{\cdot}}\qquad\qquad\qquad \boldsymbol{y} \qquad\qquad (38)$$

In this sense ECD is unique from other fragmentation techniques such as collisional activation (CAD) as all of these techniques result in the same **b** and **y** type fragment ions (McLafferty et al. 2001). In addition ECD has the unique property, that it produces little cleavage of sites with small H• affinity. Most importantly, this includes noncovalent bonds such as hydrogen bonds and salt bridges, which are all broken by conventional backbone dissociation methods. This particular feature of ECD allows for the determination of the folding/unfolding equilibrium constant and of secondary structure stability in the gas phase (McLafferty et al. 2001, Horn et al. 2001, Breuker et al. 2002).

Bibliography

Abragam A (1961) Principles of nuclear magnetism. *Clarendon Press*, Oxford, UK.

Allen MP, Tildesley DJ (1987) Computer simulation of liquids. *Clarendon Press*, Oxford, UK.

Baldwin AJ, Kay LE (2009) NMR spectroscopy brings invisible protein states into focus. *Nat Chem Biol* **5:** 808-814

Battiste JL, Wagner G (2000) Utilization of site-directed spin labeling and high-resolution heteronuclear nuclear magnetic resonance for global fold determination of large proteins with limited nuclear Overhauser effect data. *Biochemistry* **39:** 5355-5365

Bax A, Kontaxis G, Tjandra N (2001) Dipolar couplings in macromolecular structure determination. *Methods Enzymol* **339:** 127-174

Bhabha G, Lee J, Ekiert DC, Gam J, Wilson IA, Dyson HJ, Benkovic SJ, Wright PE (2011) A dynamic knockout reveals that conformational fluctuations influence the chemical step of enzyme catalysis. *Science* **332:** 234-238

Bouvignies G, Meier S, Grzesiek S, Blackledge M (2006) Ultrahigh-resolution backbone structure of perdeuterated protein GB1 using residual dipolar couplings from two alignment media. *Angew Chem, Inter Ed* **45:** 8166-8169

Braun W, Bösch C, Brown LR, Go N, Wüthrich K (1981) Combined use of proton-proton Overhauser enhancements and a distance geometry algorithm for determination of polypeptide conformations - Application to micelle-bound glucagon. *Biochim Biophys Acta* **667:** 377-396

Breuker K, McLafferty FW (2008) Stepwise evolution of protein native structure with electrospray into the gas phase, 10(-12) to 10(2) S. *Proc Nat Acad Sci US A* **105:** 18145-18152

Breuker K, Oh HB, Horn DM, Cerda BA, McLafferty FW (2002) Detailed unfolding and folding of gaseous ubiquitin ions characterized by electron capture dissociation. *J Am Chem Soc* **124:** 6407-6420

Brindle P, Nakajima T, Montminy M (1995) Multiple protein-kinase A-regulated events are required for transcriptional induction by cAMP. *Proc Natl Acad Sci USA* **92:** 10521-10525

Brivanlou AH, Darnell JE (2002) Transcription - Signal transduction and the control of gene expression. *Science* **295:** 813-818

Brockwell DJ, Radford SE (2007) Intermediates: Ubiquitous species on folding energy landscapes? *Curr Opin Struct Biol* **17:** 30-37

Brünger AT, Nilges M (1993) Computational challenges for macromolecular structure determination by X-ray crystallography and solution NMR-spectroscopy. *Q Rev Biophys* **26:** 49-125

Brüschweiler R, Liao XB, Wright PE (1995) Long-range motional restrictions in a multidomain zinc-finger protein from anisotropic tumbling. *Science* **268:** 886-889

Carver JP, Richards RE (1972) General 2-site solution for chemical exchange produced dependence of t2 upon Carr-Purcell pulse separation. *J Mag Reson* **6:** 89-105

Cavanagh J, Fairbrother WJ, Palmer AG, Rance M, Skelton NJ (2007) Protein NMR spectroscopy. *Academic Press*, London, UK.

Chen L, Glover JNM, Hogan PG, Rao A, Harrison SC (1998) Structure of the DNA binding domains from NFAT, Fos and Jun bound specifically to DNA. *Nature* **392:** 42-48

Clore GM, Gronenborn AM, Brünger AT, Karplus M (1985) Solution conformation of a heptadecapeptide comprising the DNA-binding helix-f of the cyclic-AMP receptor

Protein of rscherichia-coli - Combined use of H-1 nuclear magnetic-resonance and restrained molecular-dynamics. *J Mol Biol* **186:** 435-455

Clore GM, Nilges M, Sukumaran DK, Brünger AT, Karplus M, Gronenborn AM (1986) The 3-dimensional structure of alpha-1-purothionin in solution - Combined use of nuclear-magnetic-resonance, distance geometry and restrained molecular-dynamics. *Embo J* **5:** 2729-2735

Clore GM, Szabo A, Bax A, Kay LE, Driscoll PC, Gronenborn AM (1990) Deviations from the simple 2-parameter model-free approach to the interpretation of N-15 nuclear magnetic-relaxation of proteins. *J Am Chem Soc* **112:** 4989-4991

Courey AJ (2008) Mechanisms in transcriptional regulation. *Blackwell Publishing*, Oxford, UK.

Cornilescu G, Delaglio F, Bax A (1999) Protein backbone angle restraints from searching a database for chemical shift and sequence homology. *J Biomol NMR* **13:** 289-302

De Alba E, Tjandra N (2004) Residual dipolar couplings in protein structure determination. *Methods Mol Biol* **278**: 89-106

De Guzman RN, Goto NK, Dyson HJ, Wright PE (2006) Structural basis for cooperative transcription factor binding to the CBP coactivator. *J Mol Biol* **355:** 1005-1013

De-Leon SBT, Davidson EH (2007) Gene regulation: Gene control network in development. *A Rev Biophys Biomol Struct* **36:** 191-212

del Sol A, Tsai C-J, Ma B, Nussinov R (2009) The Origin of allosteric functional modulation: Multiple pre-existing pathways. *Structure* **17:** 1042-1050

Ernst P, Wang J, Huang M, Goodman RH, Korsmeyer SJ (2001) MLL and CREB bind cooperatively to the nuclear coactivator CREB-binding protein. *Mol Cell Biol* **21:** 2249-2258

Escalante CR, Brass AL, Pongubala JMR, Shatova E, Shen LY, Singh H, Aggarwal AK (2002) Crystal structure of PU.1/IRF-4/DNA ternary complex. *Mol Cell* **10:** 1097-1105

Farrow NA, Muhandiram R, Singer AU, Pascal SM, Kay CM, Gish G, Shoelson SE, Pawson T, Formankay JD, Kay LE (1994) Backbone dynamics of a free and a phosphopeptide-complexed SRC homology-2 domain studied by N-15 NMR relaxation. *Biochemistry* **33:** 5984-6003

Frederick KK, Marlow MS, Valentine KG, Wand AJ (2007) Conformational entropy in molecular recognition by proteins. *Nature* **448:** 325-U323

Furnham N, Blundell TL, DePristo MA, Terwilliger TC (2006) Is one solution good enough? *Nat Struct Mol Biol* **13:** 184-185

Fushman D, Tjandra N, Cowburn D (1998) Direct measurement of N-15 chemical shift anisotropy in solution. *J Am Chem Soc* **120:** 10947-10952

Gautier A, Mott HR, Bostock MJ, Kirkpatrick JP, Nietlispach D (2010) Structure determination of the seven-helix transmembrane receptor sensory rhodopsin II by solution NMR spectroscopy. *Nat Struct Mol Biol* **17:** 768-U147

Goodman RH, Smolik S (2000) CBP/p300 in cell growth, transformation, and development. *Genes Dev* **14:** 1553-1577

Goto NK, Zor T, Martinez-Yamout M, Dyson HJ, Wright PE (2002) Cooperativity in transcription factor binding to the coactivator CREB-binding protein (CBP) - The mixed lineage leukemia protein (MLL) activation domain binds to an allosteric site on the KIX domain. *J Biol Chem* **277:** 43168-43174

Graf T (1992) Myb: A transcriptional activator linking proliferation and differentiation in hematopoietic cells. *Curr Opin Genet Dev* **2:** 249-255

Güntert P (1998) Structure calculation of biological macromolecules from NMR data. *Q Rev Biophys* **31:** 145-237

Hardy JA, Wells JA (2004) Searching for new allosteric sites in enzymes. *Curr Opin Struct Biol* **14:** 706-715

Henzler-Wildman K, Kern D (2007) Dynamic personalities of proteins. *Nature* **450:** 964-972

Henzler-Wildman KA, Lei M, Thai V, Kerns SJ, Karplus M, Kern D (2007) A hierarchy of timescales in protein dynamics is linked to enzyme catalysis. *Nature* **450:** 913-U927

Horn DM, Breuker K, Frank AJ, McLafferty FW (2001) Kinetic intermediates in the folding of gaseous protein ions characterized by electron capture dissociation mass spectrometry. *J Am Chem Soc* **123:** 9792-9799

Jackson SE (1998) How do small single-domain proteins fold? *Folding Des* **3:** R81-R91

Jeziorska DM, Jordan KW, Vance KW (2009) A systems biology approach to understanding cis-regulatory module function. *Semin Cell Dev Biol* **20:** 856-862

Kalkhoven E (2004) CBP and p300: HATs for different occasions. *Biochem Pharm* **68:** 1145-1155

Karamouzis MV, Konstantinopoulos PA, Papavassiliou AG (2007) Roles of CREB-binding protein (CBP)/p300 in respiratory epithelium tumorigenesis. *Cell Res* **17:** 324-332

Karplus M, Ichiye T, Pettitt BM (1987) Configurational entropy of native proteins. *Biophys J* **52:** 1083-1085

Karplus M, Kuriyan J (2005) Molecular dynamics and protein function. *Proc Natl Acad Sci USA* **102:** 6679-6685

Kirkpatrick S, Gelatt CD, Vecchi MP (1983) Optimization by simulated annealing. *Science* **220:** 671-680

Kleinjan DA, van Heyningen V (2005) Long-range control of gene expression: Emerging mechanisms and disruption in disease. *Am J Hum Genet* **76:** 8-32

Kornberg RD (2005) Mediator and the mechanism of transcriptional activation. *Trends Biochem Sci* **30:** 235-239

Kornberg RD (2007) The molecular basis of eukaryotic transcription. *Proc Natl Acad Sci USA* **104:** 12955-12961

Korzhnev DM, Religa TL, Banachewicz W, Fersht AR, Kay LE (2010) A transient and low-populated protein-folding intermediate at atomic resolution. *Science* **329:** 1312-1316

Leach AR (2001) Molecular modelling: Principles and application. *Prentice Hall*, Essex, UK.

Levitt MH (2001) Spin dynamics. *Wiley*, Chichester, UK.

Lipari G, Szabo A (1982a) Model-free approach to the interpretation of nuclear magnetic-resonance relaxation in macromolecules .1. Theory and range of validity. *J Am Chem Soc* **104:** 4546-4559

Lipari G, Szabo A (1982b) Model-free approach to the interpretation of nuclear magnetic-resonance relaxation in macromolecules .2. Analysis of experimental results. *J Am Chem Soc* **104:** 4559-4570

Loria JP, Rance M, Palmer AG (1999) A relaxation-compensated Carr-Purcell-Meiboom-Gill sequence for characterizing chemical exchange by NMR spectroscopy. *J Am Chem Soc* **121:** 2331-2332

Losonczi JA, Andrec M, Fischer MWF, Prestegard JH (1999) Order matrix analysis of residual dipolar couplings using singular value decomposition. *J Magn Reson* **138:** 334-342

Mandel AM, Akke M, Palmer AG (1995) Backbone dynamics of escherichia-coli ribonuclease HI - Correlations with structure and function in an active enzyme. *J Mol Biol* **246:** 144-163

Markwick PRL, Bouvignies G, Salmon L, McCammon JA, Nilges M, Blackledge M (2009) Toward a unified representation of protein structural dynamics in solution. *J Am Chem Soc* **131:** 16968-16975

McLafferty FW, Horn DM, Breuker K, Ge Y, Lewis MA, Cerda B, Zubarev RA, Carpenter BK (2001) Electron capture dissociation of gaseous multiply charged ions by Fourier-transform ion cyclotron resonance. *J Am Soc Mass Spectrom* **12:** 245-249

Meyer T, de la Cruz X, Orozco M (2009) An Atomistic View to the Gas Phase Proteome. *Structure* **17:** 88-95

Millet O, Loria JP, Kroenke CD, Pons M, Palmer AG (2000) The static magnetic field dependence of chemical exchange linebroadening defines the NMR chemical shift time scale. *J Am Chem Soc* **122:** 2867-2877

Mittermaier A, Kay LE (2006) Review - New tools provide new insights in NMR studies of protein dynamics. *Science* **312:** 224-228

Montminy M (1997) Transcriptional regulation by cyclic AMP. *Annu Rev Biochem* **66:** 807-822

Neri D, Szyperski T, Otting G, Senn H, Wuthrich K (1989) Stereospecific nuclear magnetic-resonance assignments of the methyl-groups of valine and leucine in the DNA-binding domain of the 434-repressor by biosynthetically directed fractional C-13 labeling. *Biochemistry* **28:** 7510-7516

Neuhaus D, Williamson MP (2000) The nuclear Overhauser effect in structural and conformational analysis. *Wiley-VCH*, New York, USA.

Nietlispach D, Clowes RT, Broadhurst RW, Ito Y, Keeler J, Kelly M, Ashurst J, Oschkinat H, Domaille PJ, Laue ED (1996) An approach to the structure determination of larger proteins using triple resonance NMR experiments in conjunction with random fractional deuteration. *J Am Chem Soc* **118:** 407-415

Nilges M, Clore GM, Gronenborn AM (1988) Determination of 3-dimensional structures of proteins from interproton distance data by hybrid distance geometry-dynamical simulated annealing calculations. *Febs L* **229:** 317-324

Overhauser AW (1953) Paramagnetic relaxation in metals. *Phys Rev* **89:** 689-700

Palmer AG (2004) NMR characterization of the dynamics of biomacromolecules. *Chem Rev* **104:** 3623-3640

Panne D, Maniatis T, Harrison SC (2007) An atomic model of the interferon-beta enhanceosome. *Cell* **129:** 1111-1123

Pervushin K, Riek R, Wider G, Wuthrich K (1997) Attenuated T-2 relaxation by mutual cancellation of dipole-dipole coupling and chemical shift anisotropy indicates an avenue to NMR structures of very large biological macromolecules in solution. *Proc Natl Acad Sci USA* **94:** 12366-12371

Prestegard JH, Bougault CM, Kishore AI (2004) Residual dipolar couplings in structure determination of biomolecules. *Chem Rev* **104:** 3519-3540

Reményi A, Scholer HR, Wilmanns M (2004) Combinatorial control of gene expression. *Nat Struct Mol Biol* **11:** 812-815

Rule GS and Hitchens TK (2006) Fundamentals of protein NMR spectroscopy. *Springer*, Dordrecht, The Netherlands.

Saupe A (1964) Kernresonanzen in kristallinen flüssigkeiten + in kristallinflussigen lösungen .I. *Z Naturforsch* **A 19:** 161-+

Schanda P, Brutscher B, Konrat R, Tollinger M (2008) Folding of the KIX domain: Characterization of the equilibrium analog of a folding intermediate using N-15/C-13 relaxation dispersion and fast H-1/H-2 amide exchange NMR spectroscopy. *J Mol Biol* **380:** 726-741

Schurr JM, Babcock HP, Fujimoto BS (1994) A test of the model-free formulas - Effects of anisotropic rotational diffusion and dimerization. *J Magn Reson B* **105:** 211-224

Solomon I (1955) Relaxation processes in a system of 2 spins. *Phys Rev* **99:** 559-565

Steinberg MZ, Breuker K, Elber R, Gerber RB (2007) The dynamics of water evaporation from partially solvated cytochrome c in the gas phase. *Phys Chem Chem Phys* **9:** 4690-4697

Steinberg MZ, Elber R, McLafferty FW, Gerber RB, Breuker K (2008) Early structural evolution of native cytochrome c after solvent removal. *Chembiochem* **9:** 2417-2423

Sterner DE, Berger SL (2000) Acetylation of histones and transcription-related factors. *Microbiol Mol Biol Rev* **64:** 435-459

Stone MJ (2001) NMR relaxation studies of the role of conformational entropy in protein stability and ligand binding. *Acc Chem Res* **34:** 379-388

Tjandra N, Bax A (1997) Direct measurement of distances and angles in biomolecules by NMR in a dilute liquid crystalline medium. *Science* **278:** 1111-1114

Tjandra N, Feller SE, Pastor RW, Bax A (1995) Rotational diffusion anisotropy of human ubiquitin from N-15 NMR relaxation. *J Am Chem Soc* **117:** 12562-12566

Tjandra N, Omichinski JG, Gronenborn AM, Clore GM, Bax A (1997) Use of dipolar H-1-N-15 and H-1-C-13 couplings in the structure determination of magnetically oriented macromolecules in solution. *Nat Struct Biol* **4:** 732-738

Tjian R, Maniatis T (1994) Transcriptional activation - A complex puzzle with few easy pieces. *Cell* **77:** 5-8

Tollinger M, Kloiber K, Agoston B, Dorigoni C, Lichtenecker R, Schmid W, Konrat R (2006) An isolated helix persists in a sparsely populated form of KIX under native conditions. *Biochemistry* **45:** 8885-8893

Tugarinov V, Choy WY, Orekhov VY, Kay LE (2005) Solution NMR-derived global fold of a monomeric 82-kDa enzyme. *Proc Natl Acad Sci USA* **102:** 622-627

Tugarinov V, Kay LE (2003) Ile, Leu, and Val methyl assignments of the 723-residue malate synthase G using a new labeling strategy and novel NMR methods. *J Am Chem Soc* **125:** 13868-13878

Tzeng SR, Kalodimos CG (2011) Protein dynamics and allostery: An NMR view. *Curr Opin Struct Biol* **21:** 62-67

Vo N, Goodman RH (2001) CREB-binding protein and p300 in transcriptional regulation. *J Biol Chem* **276:** 13505-13508

Wishart DS, Sykes BD, Richards FM (1992) The chemical-shift index - A fast and simple method for the assignment of protein secondary structure through NMR-spectroscopy. *Biochemistry* **31:** 1647-1651

Woessner DE (1961) Nuclear transfer effects in nuclear magnetic resonance pulse experiments. *J Chem Phys* **35:** 41-48

Zor T, De Guzman RN, Dyson HJ, Wright PE (2004) Solution structure of the KIX domain of CBP bound to the transactivation domain of c-Myb. *J Mol Biol* **337:** 521-534

Zubarev RA, Kelleher NL, McLafferty FW (1998) Electron capture dissociation of multiply charged protein cations. A nonergodic process. *J Am Chem Soc* **120:** 3265-3266

Zubarev RA, Kruger NA, Fridriksson EK, Lewis MA, Horn DM, Carpenter BK, McLafferty FW (1999) Electron capture dissociation of gaseous multiply-charged proteins is favored at disulfide bonds and other sites of high hydrogen atom affinity. *J Am Chem Soc* **121:** 2857-2862

Zweckstetter M (2008) NMR: prediction of molecular alignment from structure using the PALES software. *Nat Prot* **3:** 679-690

Article I

Direct Observation of the Dynamic Process Underlying Allosteric Signal Transmission

Sven Brüschweiler,[†] Paul Schanda,[‡,§] Karin Kloiber,[†] Bernhard Brutscher,[‡]
Georg Kontaxis,[†] Robert Konrat,[†] and Martin Tollinger*,[†]

Department of Computational & Structural Biology, Max F. Perutz Laboratories, Campus Vienna Biocenter 5, A-1030 Vienna, Austria and Institut de Biologie Structurale Jean-Pierre Ebel, CNRS, CEA, UJF, 41 rue Jules Horowitz, F-38027 Grenoble, France

Received December 20, 2008; E-mail: martin.tollinger@univie.ac.at

Abstract: Allosteric regulation is an effective mechanism of control in biological processes. In allosteric proteins a signal originating at one site in the molecule is communicated through the protein structure to trigger a specific response at a remote site. Using NMR relaxation dispersion techniques we directly observe the dynamic process through which the KIX domain of CREB binding protein communicates allosteric information between binding sites. KIX mediates cooperativity between pairs of transcription factors through binding to two distinct interaction surfaces in an allosteric manner. We show that binding the activation domain of the mixed lineage leukemia (MLL) transcription factor to KIX induces a redistribution of the relative populations of KIX conformations toward a high-energy state in which the allosterically activated second binding site is already preformed, consistent with the Monod−Wyman−Changeux (WMC) model of allostery. The structural rearrangement process that links the two conformers and by which allosteric information is communicated occurs with a time constant of 3 ms at 27 °C. Our dynamic NMR data reveal that an evolutionarily conserved network of hydrophobic amino acids constitutes the pathway through which information is transmitted.

Introduction

Allostery requires that information about the presence (or absence) of a biological target can be communicated between remote sites of protein molecules. While allosteric regulation plays a key role in many biological events on a molecular level,[1] the exact biophysical characterization of the mechanisms by which allosteric communication occurs remains a major challenge in structural biology.[2−4] Traditionally, allosteric mechanisms have been investigated by comparing static three-dimensional structures of proteins in their limiting states, i.e., the structures of unliganded beginning and ligand-bound end states.[5] Allosteric communication is, however, intimately linked to protein dynamics[6−11] and can be characterized at atomic resolution by NMR spin relaxation techniques.[12] With the

exception of purely dynamics-driven allostery,[13] allosteric information is typically transmitted by means of conformational changes along a defined pathway.[14] To characterize conformational transitions in proteins, NMR relaxation dispersion techniques can be employed. These experiments allow the quantitative study of transitions between states even in cases with highly skewed populations where low-populated (minor) states are not directly observable and allow extracting information about the time-scale of the transition as well as the structures of these low-populated states in terms of chemical shifts and residual anisotropic interactions.[15,16]

Here, we characterize the molecular mechanism through which the KIX domain of CREB-binding protein, CBP, propagates allosteric information between two remote binding sites. CBP is a transcriptional coactivator that is involved in a variety of biological processes such as cellular differentiation, development, and growth control.[17] CBP acts as a scaffold for the assembly of the transcriptional machinery through binding of transcription factors, which in turn bind to DNA promoter sequences. Interactions with transcription factors are mediated by independently folded protein modules; one such modular

[†] Max F. Perutz Laboratories.
[‡] Institut de Biologie Structurale Jean-Pierre Ebel.
[§] Current address: Physical Chemistry, ETH Zürich, Wolfgang-Pauli Strasse 10, CH-8093 Zürich, Switzerland.
(1) Hardy, J. A.; Wells, J. A. *Curr. Opin. Struct. Biol.* **2004**, *14*, 706–715.
(2) Goodey, N. M.; Benkovic, S. J. *Nat. Chem. Biol.* **2008**, *4*, 474–482.
(3) Cui, Q.; Karplus, M. *Protein Sci.* **2008**, *17*, 1295–1307.
(4) Kumar, S.; Ma, B.; Tsai, C. J.; Sinha, N.; Nussinov, R. *Protein Sci.* **2000**, *9*, 10–19.
(5) Daily, M. D.; Gray, J. J. *Proteins* **2007**, *67*, 385–399.
(6) Swain, J. F.; Gierasch, L. M. *Curr. Opin. Struct. Biol.* **2006**, *16*, 102–108.
(7) Kern, D.; Zuiderweg, E. R. *Curr. Opin. Struct. Biol.* **2003**, *13*, 748–757.
(8) Volkman, B. F.; Lipson, D.; Wemmer, D. E.; Kern, D. *Science* **2001**, *291*, 2429–2433.
(9) Velyvis, A.; Yang, Y. R.; Schachman, H. K.; Kay, L. E. *Proc. Natl. Acad. Sci. U.S.A.* **2007**, *104*, 8815–8820.
(10) Popovych, N.; Sun, S.; Ebright, R. H.; Kalodimos, C. G. *Nat. Struct. Mol. Biol.* **2006**, *13*, 831–838.
(11) Gunasekaran, K.; Ma, B.; Nussinov, R. *Proteins* **2004**, *57*, 433–443.
(12) Mittermaier, A.; Kay, L. E. *Science* **2006**, *312*, 224–228.
(13) Cooper, A.; Dryden, D. T. *Eur. Biophys. J.* **1984**, *11*, 103–109.
(14) Tsai, C. J.; del Sol, A.; Nussinov, R. *J. Mol. Biol.* **2008**, *378*, 1–11.
(15) Hansen, D. F.; Vallurupalli, P.; Kay, L. E. *J. Biomol. NMR* **2008**, *41*, 113–120.
(16) Korzhnev, D. M.; Kay, L. E. *Acc. Chem. Res.* **2008**, *41*, 442–451.
(17) Goodman, R. H.; Smolik, S. *Genes Dev.* **2000**, *14*, 1553–1577.

protein-binding domain in CBP is KIX, a small single-domain protein whose fold is composed of a bundle of three α helices and two short 3_{10} helices (see Figure S1 in the Supporting Information).[18] The KIX domain interlinks a great variety of different transcription factors by simultaneous binding through two interaction sites. One of these sites binds, for example, the activation domain of the mixed lineage leukemia (MLL) protein,[19] whereas the activation domain of the transcription factor c-Myb (among others) binds to the remote second site on KIX.[20] In vitro, binding of the MLL activation domain to KIX cooperatively enhances the interaction with c-Myb through an unknown allosteric mechanism:[19] KIX in complex with MLL displays a ~2-fold higher affinity for the c-Myb activation domain than the KIX domain alone.[21] Our dynamic NMR analysis of allosteric communication in KIX provides a quantitative description of the mechanism through which this domain mediates cooperativity between transcription factors.

Materials and Methods

Sample Preparation. Samples of uniformly ^{13}C- and/or ^{15}N-labeled KIX (residues 586−672) were prepared by bacterial growth using standard procedures and purified as described.[22] Selective ^{13}C labeling at backbone C^{α} and isoleucine side chain $C^{\delta 1}$ positions was obtained by supplementing growth media with 2-^{13}C-glucose[23] and 4-^{13}C-α-ketobutyrate,[24,25] respectively. Peptides that include the minimal activation domains of transcription factors, corresponding to residues 2840−2858 of MLL[19] (with Ala substituting for Cys2841),[21] residues 291−315 of c-Myb,[26] and residues 116−149 of CREB (with Ser-133 phosphorylated),[27] were purchased from PSL (Heidelberg, Germany).

NMR Spectroscopy and Data Analysis. NMR samples contained 0.4−1.0 mM KIX, 50 mM potassium phosphate buffer, pH 5.8, 25 mM NaCl, and 1 mM NaN_3 in 8% D_2O/92% H_2O. ^{15}N, $^{13}C^{\alpha}$, and $^{13}C^{\delta 1}$ Carr−Purcell−Meiboom−Gill (CPMG) relaxation dispersion experiments were performed at ^{1}H Larmor frequencies of 500, 600, and 800 MHz and 27 °C as described,[28−30] yielding data for 73 ^{15}N, 42 $^{13}C^{\alpha}$, and 3 Ile-$^{13}C^{\delta 1}$ sites. All dispersion profiles were numerically fitted to a common two-state process (assuming a more complicated kinetic scheme by inclusion of a third state into the model did not lead to a statistically significant improvement

of the fit, as judged by *F*-test criteria).[31] For Tyr648 (^{15}N) the data could not be fitted by a common process, and this residue was excluded from further analysis. In the first step of the fitting procedure, data from residues with exchange contributions exceeding 3 s^{-1} at 800 MHz (18 residues) were employed to determine the time-scale of the exchange process, τ_{ex}, and the populations of states, p_i (assuming identical values of τ_{ex} and p_i for all nuclei but residue-specific values for $\Delta\omega$). Data for residues with exchange contributions < 3 s^{-1} were subsequently fitted individually with τ_{ex} and p_i constrained to the values obtained by this procedure to determine their $\Delta\omega_{disp}$ values. Uncertainties were estimated via a Monte Carlo approach using 1000 synthetic data sets generated on the basis of repeat experiments, and standard deviations are reported in all cases. Backbone amide H/D exchange rates were measured using the SOFAST real-time approach and compared to the exchange rates of unprotected amide hydrogens as described.[32]

Results and Discussion

Figure 1a shows experimental relaxation dispersion data obtained for backbone amide ^{15}N and $^{13}C^{\alpha}$ nuclei in the binary complex formed by KIX and the activation domain of MLL. Nonflat relaxation dispersion profiles are detected for most residues in KIX·MLL, suggesting the presence of a conformational transition on the micro- to millisecond time-scale. Analysis of the data shows that this process occurs with a time constant of 3.0 ± 0.3 ms at 27 °C between two states that are populated to 93.0 ± 0.3% and 7.0 ± 0.3%, respectively. Dispersion profiles for all nuclei can be consistently fitted to the same dynamic parameters, indicative of a collective nature of the underlying conformational transition. All observed ^{15}N and $^{13}C^{\alpha}$ chemical shift differences between the two conformers, $\Delta\omega_{disp}$, are small (Figure 1b). Protein NMR chemical shifts are sensitive reporters of local structure;[33] the small magnitude of the $\Delta\omega_{disp}$ values suggests that the two states differ only marginally in their backbone conformation, ruling out (local) unfolding as an underlying process. Rather, the ^{15}N and $^{13}C^{\alpha}$ data imply that the minor (7%) state represents an alternative, folded conformer. Consistently, backbone amide hydrogen/deuterium exchange data on the KIX·MLL complex show that both states represent solvent exchange protected and fully folded conformers (Figure S2 in the Supporting Information), and temperature-dependent relaxation dispersion data show that the equilibrium between these conformers is almost invariant with temperature, indicating that the two states are of similar enthalpy (Figure S3 in the Supporting Information). Notably, the relaxation dispersion $\Delta\omega_{disp}$ values (^{15}N/$^{13}C^{\alpha}$) exceed 0.5 ppm only for residues close to the carboxy-terminal region of helix α_1 as well as residues in the center of helix α_3, encompassing parts of the MLL and c-Myb binding sites, respectively.

While the minor population is not directly observable in NMR spectra, the conformational transition between the two states gives rise to population-weighted resonance positions. Upon addition of the c-Myb activation domain to the binary KIX·MLL complex, KIX resonances gradually approach the chemical shifts of the ternary KIX·MLL·c-Myb complex (Figure 2a). The absolute values of the ^{15}N chemical shift differences that we measure between the ternary and the binary complex, $\Delta\omega_{ternary-binary}$, clearly correlate with the chemical shift differences between major and minor populations of the binary complex determined by relaxation

(18) De Guzman, R. N.; Goto, N. K.; Dyson, H. J.; Wright, P. E. *J. Mol. Biol.* **2006**, *355*, 1005–1013.

(19) Ernst, P.; Wang, J.; Huang, M.; Goodman, R. H.; Korsmeyer, S. J. *Mol. Cell. Biol.* **2001**, *21*, 2249–2258.

(20) Parker, D.; Rivera, M.; Zor, T.; Henrion-Caude, A.; Radhakrishnan, I.; Kumar, A.; Shapiro, L. H.; Wright, P. E.; Montminy, M.; Brindle, P. K. *Mol. Cell. Biol.* **1999**, *19*, 5601–5607.

(21) Goto, N. K.; Zor, T.; Martinez-Yamout, M.; Dyson, H. J.; Wright, P. E. *J. Biol. Chem.* **2002**, *277*, 43168–43174.

(22) Rutledge, S. E.; Volkman, H. M.; Schepartz, A. *J. Am. Chem. Soc.* **2003**, *125*, 14336–14347.

(23) Lundström, P.; Teilum, K.; Carstensen, T.; Bezsonova, I.; Wiesner, S.; Hansen, D. F.; Religa, T. L.; Akke, M.; Kay, L. E. *J. Biomol. NMR* **2007**, *38*, 199–212.

(24) Goto, N. K.; Gardner, K. H.; Mueller, G. A.; Willis, R. C.; Kay, L. E. *J. Biomol. NMR* **1999**, *13*, 369–374.

(25) Lichtenecker, R.; Ludwiczek, M. L.; Schmid, W.; Konrat, R. *J. Am. Chem. Soc.* **2004**, *126*, 5348–5349.

(26) Parker, D.; Jhala, U. S.; Radhakrishnan, I.; Yaffe, M. B.; Reyes, C.; Shulman, A. I.; Cantley, L. C.; Wright, P. E.; Montminy, M. *Mol. Cell* **1998**, *2*, 353–359.

(27) Parker, D.; Ferreri, K.; Nakajima, T.; LaMorte, V. J.; Evans, R.; Koerber, S. C.; Hoeger, C.; Montminy, M. R. *Mol. Cell. Biol.* **1996**, *16*, 694–703.

(28) Tollinger, M.; Skrynnikov, N. R.; Mulder, F. A.; Forman-Kay, J. D.; Kay, L. E. *J. Am. Chem. Soc.* **2001**, *123*, 11341–11352.

(29) Hansen, D. F.; Vallurupalli, P.; Lundstrom, P.; Neudecker, P.; Kay, L. E., J. *Am. Chem. Soc.* **2008**, *130*, 2667–2675.

(30) Skrynnikov, N. R.; Mulder, F. A.; Hon, B.; Dahlquist, F. W.; Kay, L. E. *J. Am. Chem. Soc.* **2001**, *123*, 4556–4566.

(31) McConnell, H. M. *J. Chem. Phys.* **1958**, *28*, 430–431.

(32) Schanda, P.; Brutscher, B.; Konrat, R.; Tollinger, M. *J. Mol. Biol.* **2008**, *380*, 726–741.

(33) Shen, Y.; et al. *Proc. Natl. Acad. Sci. U.S.A.* **2008**, *105*, 4685–4690.
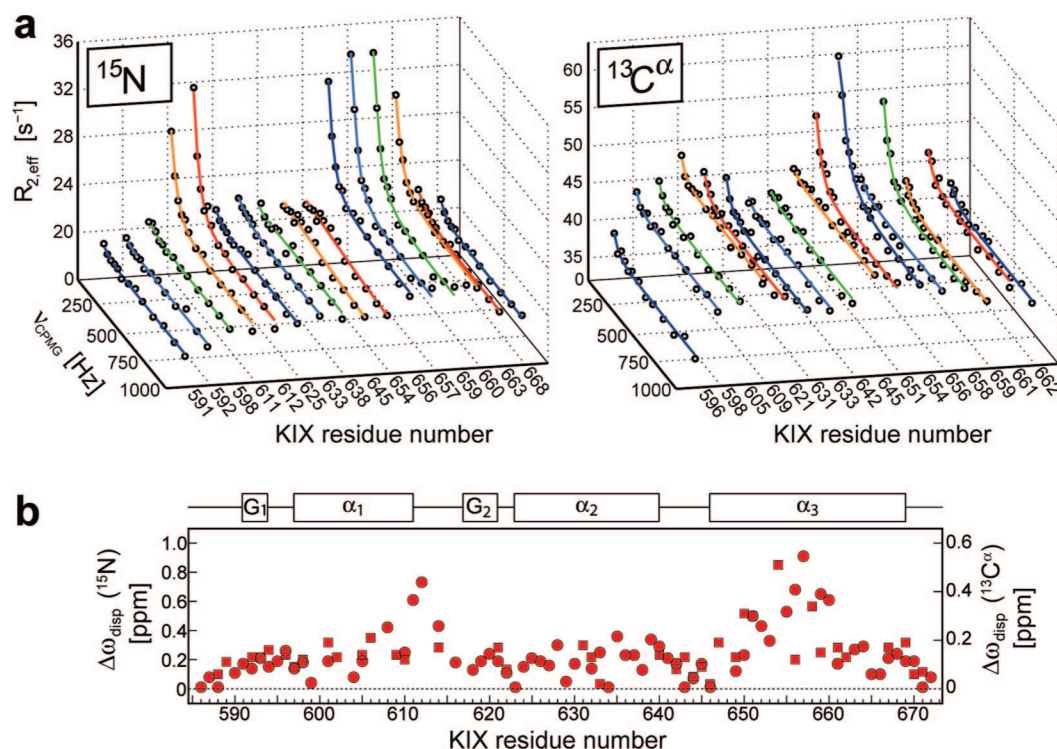
**Figure 1.** NMR relaxation dispersion data for the KIX·MLL complex. (a) ^{15}N (left) and ^{13}C$^{\alpha}$ (right) relaxation dispersion profiles for representative residues of KIX bound to MLL (concentration ratio KIX:MLL = 1:2.2), recorded at 800 MHz and 27 °C, along with best fits (lines). Under these conditions, >99.7% of KIX molecules are bound to MLL (K_d = 2.8 μM).[21] (b) Absolute values of backbone ^{15}N (circles) and ^{13}C$^{\alpha}$ (squares) chemical shift differences between the two KIX conformations, $\Delta\omega_{disp}$, as determined from the relaxation dispersion data for KIX·MLL. The location of the α helices and 3_{10} helices in KIX is indicated (PDB entry code 2AGH).[18]

dispersion measurements (Figure 2b). The linear correlation coefficient between the two data sets is 0.79 (Figure 2c), and a similar correlation is obtained for ^{13}C$^{\alpha}$ nuclei (Figure S4 in the Supporting Information), demonstrating that the conformation of KIX in the minor state of binary KIX·MLL is similar to KIX in the ternary KIX·MLL·c-Myb complex. Moreover, these data suggest that chemical shift changes upon binding of c-Myb to KIX·MLL are governed by conformational changes of KIX in response to ligand binding rather than local effects caused by direct contacts with the ligand peptide. This is corroborated by the chemical shift changes that we observe upon ternary complex formation using an alternative ligand: binding of the phosphorylated kinase-inducible domain (pKID) of CREB to KIX·MLL results in very similar backbone ^{15}N and ^{13}C$^{\alpha}$ chemical shift changes for the majority of KIX residues with the exception of residues that are involved in specific interactions with charged and/or aromatic pKID side chains that are absent in c-Myb (Figure S5).

It is of particlar interest to clarify whether the minor state of KIX that is populated to 7% in the binary KIX·MLL complex is populated prior to MLL binding. To address this question we performed backbone ^{15}N relaxation dispersion experiments at variable KIX:MLL concentration ratios, ranging between 1:0 and 1:2.2 (Figure 3). The data clearly show that the minor state of KIX is not populated to an appreciable degree (<~0.5%) in the absence of MLL but becomes progressively populated as the binary KIX·MLL complex is formed. This indicates that binding the activation domain of the MLL transcription factor to KIX induces a redistribution of the relative populations of KIX conformations toward a state in which the c-Myb (pKID) binding site is already preformed.

Because the conformation of KIX in the minor state of KIX·MLL already resembles the ternary complex, this state might be expected to display a higher affinity for c-Myb (or pKID).[34] This can be verified in a straightforward manner: As either c-Myb or pKID bind to KIX·MLL to form a ternary complex, the equilibrium between major and minor states will shift toward the state that binds ligand with higher affinity. The observation that ^{15}N and ^{13}C$^{\alpha}$ $\Delta\omega_{ternary-binary}$ values are of similar magnitude as the relaxation dispersion $\Delta\omega_{disp}$ values (Figure 2c) implies that it is the minor state toward which the equilibrium shifts and therefore represents the higher affinity conformation. The interaction between KIX and ligands thus involves selection from a pre-existing ensemble of conformations.[35,36] In the presence of saturating amounts of ligands binding to both KIX interaction sites relaxation dispersion profiles are flat (Figure 4).

Taken together, our data unequivocally establish that in the binary KIX·MLL complex KIX spontaneously interconverts between a major (lower energy) state and a minor (higher energy) state, which adopts a conformation similar to that of the ternary complex and binds c-Myb with higher affinity. Such a mechanism is consistent with the WMC model of allostery, which implies that the conformational transition that mediates information transfer between binding sites involves states that

(34) Tsai, C. J.; Kumar, S.; Ma, B.; Nussinov, R. *Protein Sci.* **1999**, *8*, 1181–1190.
(35) Ma, B.; Kumar, S.; Tsai, C. J.; Nussinov, R. *Protein Eng.* **1999**, *12*, 713–720.
(36) Lange, O. F.; Lakomek, N. A.; Fares, C.; Schröder, G. F.; Walter, K. F.; Becker, S.; Meiler, J.; Grubmüller, H.; Griesinger, C.; de Groot, B. L. *Science* **2008**, *320*, 1471–1475.

37
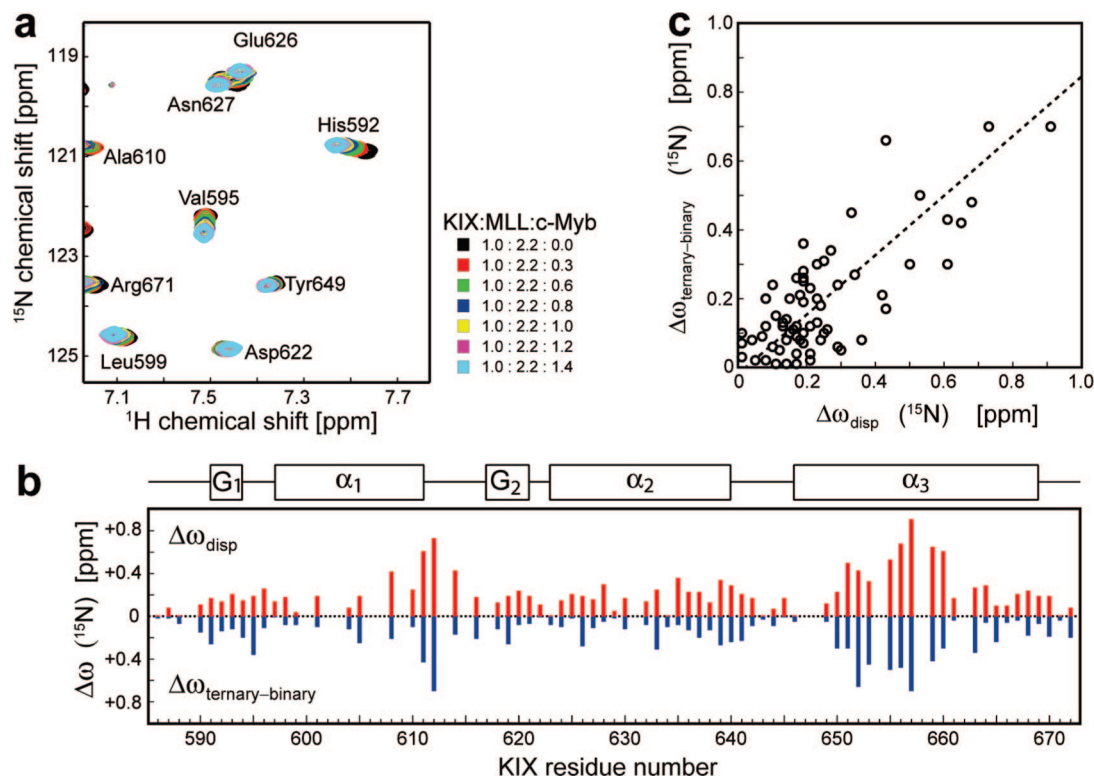
Figure 2. Chemical shift changes on c-Myb binding to the binary KIX·MLL complex. (a) [^{1}H–^{15}N]-HSQC spectra of ^{15}N-KIX bound to unlabeled MLL are shown with c-Myb concentrations ranging from 0 (black) to saturating (cyan), corresponding to KIX:MLL:c-Myb concentration ratios between 1:2.2:0 and 1:2.2:1.4. (b) Comparison of absolute values of backbone amide ^{15}N chemical shift differences obtained from relaxation dispersion data for the binary KIX·MLL complex, $\Delta\omega_{disp}$ (red bars), with absolute values of chemical shift differences between ternary KIX·MLL·c-Myb and binary KIX·MLL, $\Delta\omega_{ternary-binary}$ (blue bars). Values of $\Delta\omega_{ternary-binary}$ were determined from the titration of KIX·MLL with c-Myb and confirmed using triple-resonance NMR experiments. The location of KIX secondary structure elements in KIX·MLL·c-Myb is indicated. (c) Correlation of ^{15}N $\Delta\omega_{ternary-binary}$ and $\Delta\omega_{disp}$ values with a slope of 0.86. Because resonances are observed at population-averaged frequencies in HSQC spectra (fast exchange on the NMR chemical shift time-scale), $\Delta\omega_{ternary-binary}$ as observed upon transition from binary KIX·MLL (7% binding competent state) to fully saturated ternary KIX·MLL·c-Myb amounts to 93% of $\Delta\omega_{disp}$ values (corresponding to a slope of 0.93).

Figure 3. ^{15}N relaxation dispersion profiles for KIX at 800 MHz and 27 °C recorded at KIX:MLL concentration ratios between 1:0 and 1:2.2. Two residues distal to the MLL binding site with $\Delta\omega_{disp}$ exceeding the mean by $>2\sigma$ in the binary KIX·MLL complex are shown. For these residues $\Delta\omega_{KIX·MLL-KIX}$ (due to MLL binding) < 0.2 ppm, ensuring minimal exchange contributions arising from the reversible MLL binding process under conditions where MLL is not present in excess. In addition, partial unfolding for unliganded KIX does not contribute significantly to the relaxation dispersion profiles of these residues.[49] Due to the low number of residues that fulfill these criteria we abstained from quantitative analysis of the experimental relaxation dispersion data at variable KIX:MLL concentration ratios. It is clear, however, that the higher energy state of KIX becomes progressively populated as the binary KIX·MLL complex is formed.

Figure 4. ^{15}N NMR relaxation dispersion profiles for representative residues of KIX bound to MLL and pKID (concentration ratio KIX:MLL:pKID = 1:2.2:1.2) recorded at 800 MHz and 27 °C. pKID was chosen as a ligand because of the ~6-fold higher affinity of KIX·MLL for pKID than for c-Myb,[21] which minimizes contributions to relaxation dispersion profiles arising from the reversible ligand binding process. Under the conditions used, >99.7% of KIX is bound to pKID.

are populated in the absence of ligand.[37] The direct experimental observation of the dynamic transition between these two

(37) Monod, J.; Wyman, J.; Changeux, J. P. *J. Mol. Biol.* **1965**, *12*, 88–118.

38

Figure 5. Allosteric network of KIX. (a) Ribbon representation of the ternary KIX·MLL·c-Myb complex (PDB entry code 2AGH).[18] The backbone of KIX (residues 586−672) is shown in blue, and elements of secondary structure are labeled. The MLL backbone (only the structured part, residues 2843−2857) is shown as red ribbon, while the backbone of c-Myb (residues 291−309), which was absent in the relaxation dispersion experiments, is shown in green (partly transparent). Yellow spheres are drawn for nuclei with $\Delta\omega_{disp}$ values exceeding the average by more than two standard deviations σ ($\Delta\omega_{disp} > 0.60$ ppm for ^{15}N, $\Delta\omega_{disp} > 0.27$ ppm for $^{13}C^{\alpha}$), and the side chains of these residues are shown. The positions of these residues largely agree with those inferred from an exhaustive compilation of chemical shift data.[18] Isoleucine side chain-$\delta1$ carbons of Ile660, Ile611, and Ile657 are indicated by yellow spheres (see Figure 6). (b) Close-up view of the allosteric network of KIX·MLL showing the residues that bridge the MLL and c-Myb binding sites. For side chains of residues with $\Delta\omega_{disp}$ exceeding the mean by $>2\sigma$ van der Waals surfaces are drawn (yellow) and labeled, while the van der Waals surface of MLL is represented by a red wire frame. Notably, only a subset of the KIX residues that interact with MLL form part of the allosteric network.

conformers in KIX·MLL by NMR relaxation dispersion spectroscopy provides insight into the communication mechanism that links the two binding sites and mediates signal transduction: The subset of residues that display the largest chemical shift changes during this conformational transition form a tightly coupled network of interactions (Figure 5a). These residues include Tyr650, His651, Ala654, Ile657, and Tyr658. Their side chains participate in formation of a shallow hydrophobic groove on the surface of KIX, which is located between helices α_1 and α_3 and serves as docking interface for the hydrophobic face of the amphipathic helix of the c-Myb activation domain (as well as the activation domain of CREB, pKID).[18,38] Others, such as Phe612, are located distal to the c-Myb/pKID binding site, in particular at the carboxy-terminal region of helix α_1 and the short loop between helix α_1 and the 3_{10}-helix G_2. This specific region of KIX has been shown to be critical for the interaction with MLL: Upon MLL binding this loop and the 3_{10}-helix G_2 are repositioned to allow the side chain of Phe612 to make close hydrophobic contacts with the MLL amphipathic helix.[18]

Further residues that display significant chemical shift changes upon major/minor state transition and serve to bridge the two binding sites are shown in Figure 5b. Ile611, located at the carboxy terminus of helix α_1, is close to the MLL binding site and has contacts with Phe612. Its side chain does not interact with MLL but protrudes into the hydrophobic core of the KIX domain, where it interacts with Ile657 through extensive hydrophobic contacts, thereby interlinking the carboxy terminus of helix α_1 with the remote c-Myb/pKID binding surface. Likewise, Ile660 has contacts with residues in the N-terminal region of the structured part of the MLL peptide and with Ile611. To further explore the allosteric network we performed ^{13}C relaxation dispersion experiments on the side chains of isoleucine residues ($\delta1$ methyl groups), Figure 6a. The side chain data can be fitted to the same conformational transition process

as the backbone ^{15}N and $^{13}C^{\alpha}$ data with a time constant of 3 ms and a population ratio of 93:7, suggesting that the conformational rearrangements within the isoleucine cluster formed by Ile611, Ile657, and Ile660 and the protein backbone occur in a collective manner. Again, the $^{13}C^{\delta1}$ relaxation dispersion $\Delta\omega_{disp}$ values agree well with the chemical shift changes upon formation of the ternary complex with c-Myb (Figure 6b). We conclude that the side chains of these isoleucine residues participate in formation of the allosteric network and constitute the link through which allosteric information is transmitted. Sequence comparison shows that these three residues are highly conserved in KIX domains (Figure S6 in the Supporting Information) in line with the notion that functional coupling between residues in proteins represents an evolutionary constraint.[39,40]

Cooperativity has also been reported for binding of MLL to KIX in complex with c-Myb or pKID.[21] To study allosteric communication in this direction we performed relaxation dispersion experiments on a binary complex where the c-Myb/pKID binding site was occupied by ligand (Figure S7 in the Supporting Information). Flat dispersion profiles were obtained so that the communication process cannot be monitored by this technique either because the population of any higher energy state(s) that might be present is too low and/or the time scale of the process is outside the micro- to millisecond window. This finding is in line with predictions from computer simulations, which show that allosteric communication pathways are not necessarily bidirectional.[41,42]

Transcription factors stimulate gene transcription by binding to gene-specific DNA promoter sites and recruiting the basal

(38) Radhakrishnan, I.; Perez-Alvarado, G. C.; Parker, D.; Dyson, H. J.; Montminy, M. R.; Wright, P. E. *Cell* **1997**, *91*, 741–752.

(39) Süel, G. M.; Lockless, S. W.; Wall, M. A.; Ranganathan, R. *Nat. Struct. Biol.* **2003**, *10*, 59–69.

(40) Lockless, S. W.; Ranganathan, R. *Science* **1999**, *286*, 295–299.

(41) Hilser, V. J.; Dowdy, D.; Oas, T. G.; Freire, E. *Proc. Natl. Acad. Sci. U.S.A.* **1998**, *95*, 9903–9908.

(42) Chen, J.; Dima, R. I.; Thirumalai, D. *J. Mol. Biol.* **2007**, *374*, 250–266.
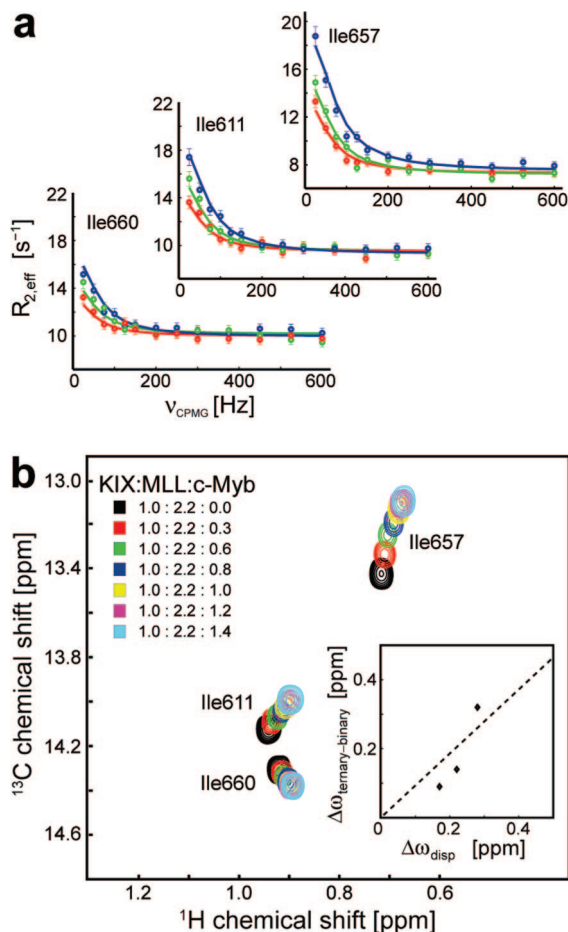
Figure 6. (a) Isoleucine $^{13}C^{\delta1}$ relaxation dispersion profiles recorded at 500 (red), 600 (green), and 800 MHz (blue) at 27 °C along with best fits. (b) Portions of [^{1}H$-^{13}$C]-HSQC spectra of KIX bound to MLL showing the positions of isoleucine side chain methyl (δ1) cross peaks at c-Myb concentrations ranging from 0 (black) to saturating (cyan) corresponding to KIX:MLL:c-Myb concentration ratios between 1:2.2:0 and 1:2.2:1.4. The insert shows the correlation of absolute values of $^{13}C^{\delta1}$ $\Delta\omega_{ternary-binary}$ and $\Delta\omega_{disp}$. A dashed line with a slope of 0.93 is drawn.

transcriptional complex through their activation domains.[43] CBP plays a central role in this process because it functions as a direct link between a variety of transcription factors and components of the transcriptional machinery.[17] Because it is present at limiting concentrations in vivo, competition of

different transcription factors for CBP is believed to be crucial for the regulation of gene transcription.[44] Moreover, since specificity of transcription is achieved by unique combinations of promoter-bound transcription factors, any (cooperative) effects that enhance or decrease their affinities to CBP can potentially promote specificity.[45] Our quantitative analysis of the allosteric transition in the KIX domain of CBP provides an atom-resolved description of the mechanism through which this domain mediates pairwise cooperativity between transcription factors. Binding of MLL induces a population shift of KIX conformations by ∼7% toward a higher affinity conformer, which results in a ∼2-fold increase of the affinities for c-Myb and pKID.[21] This population shift mechanism allows, in principle, the modulation of binding affinities in a versatile manner by the extent to which the higher affinity conformer is populated. Such pairwise fine tuning of affinities may be critical for regulation of the specificity of gene transcription, and several lines of evidence indicate that cooperative interactions between transcription factors (mediated by CBP) can promote synergism in transcriptional activation.[46,47] Moreover, the rate at which allosteric information is transmitted between binding sites might pose an essential constraint for the flow of information through the networks of proteins that regulate gene transcription in the cell.[48] Our results underline that knowledge of both structure and dynamics are required to understand the intricate molecular mechanisms by which proteins process information to fulfill their biological tasks.

Supporting Information Available: Seven supporting figures, showing backbone hydrogen/deuterium exchange and temperature dependent data, supplementary relaxation dispersion data, a chemical shift comparison, and a sequence alignment of KIX domains, and supporting references. This material is available free of charge via the Internet at http://pubs.acs.org.

JA809947W

(43) Brivanlou, A. H.; Darnell, J. E., Jr. *Science* **2002**, *295*, 813–818.

(44) Vo, N.; Goodman, R. H. *J. Biol. Chem.* **2001**, *276*, 13505–13508.
(45) Merika, M.; Thanos, D. *Curr. Opin. Genet. Dev.* **2001**, *11*, 205–208.
(46) Carey, M. *Cell* **1998**, *92*, 5–8.
(47) Ptashne, M.; Gann, A. *Nature* **1997**, *386*, 569–577.
(48) Rousseau, F.; Schymkowitz, J. *Curr. Opin. Struct. Biol.* **2005**, *15*, 23–30.
(49) Tollinger, M.; Kloiber, K.; Agoston, B.; Dorigoni, C.; Lichtenecker, R.; Schmid, W.; Konrat, R. *Biochemistry* **2006**, *45*, 8885–8893.

Supplementary Material:

Direct Observation of the Dynamic Process Underlying Allosteric Signal Transmission

Sven Brüschweiler[†], Paul Schanda[‡], Karin Kloiber[†], Bernhard Brutscher[‡], Georg Kontaxis[†], Robert Konrat[†], and Martin Tollinger[†]*

[†] Department of Biomolecular Structural Chemistry, Max F. Perutz Laboratories, Campus Vienna Biocenter 5, A-1030 Vienna, Austria

[‡] Institut de Biologie Structurale Jean-Pierre Ebel, CNRS; CEA; UJF; 41 rue Jules Horowitz, F-38027 Grenoble, France
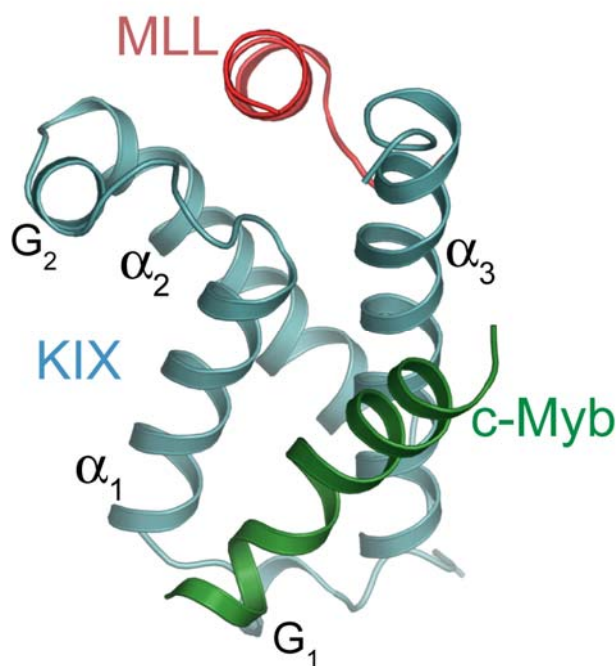
Supplementary Figure 1. Structure of the ternary KIX·MLL·c-Myb complex (PDB entry 2AGH).[1] KIX residues 586–672 are shown as light blue ribbon and elements of secondary structure are labeled. The backbone of the structured parts of the MLL (residues 2843–2857) and the c-Myb (residues 291–309) activation domains are shown as red and green ribbon, respectively.

S1
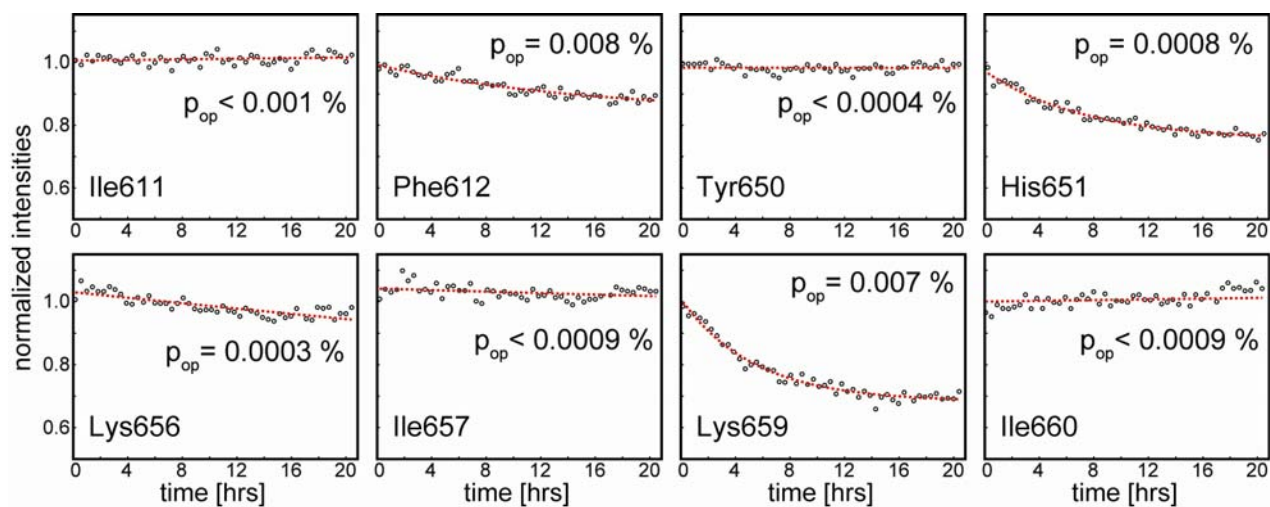
Supplementary Figure 2. Backbone amide H/D exchange data (populations of exchange-competent states, p_{op}) recorded on the binary KIX·MLL complex (concentration ratio 1:2.2) at 27°C for selected residues with $\Delta\omega_{disp}$ exceeding the mean by $>2\sigma$ in the binary KIX·MLL complex. For all residues in KIX·MLL values of p_{op} are $< 0.04\%$.
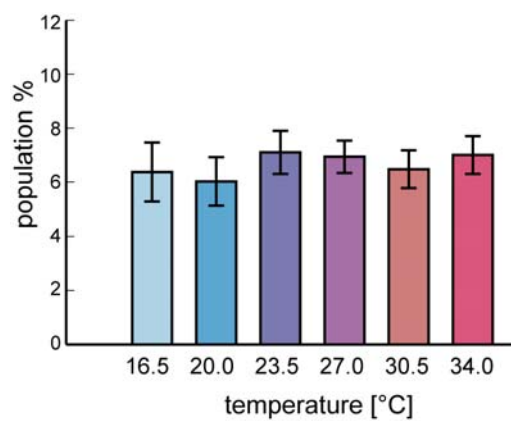
Supplementary Figure 3. Temperature dependence of the population of the higher energy state that is present in KIX·MLL, obtained from ^{15}N NMR relaxation dispersion experiments recorded at 16.5, 20.0, 23.5, 27.0, 30.5 and 34.0°C.
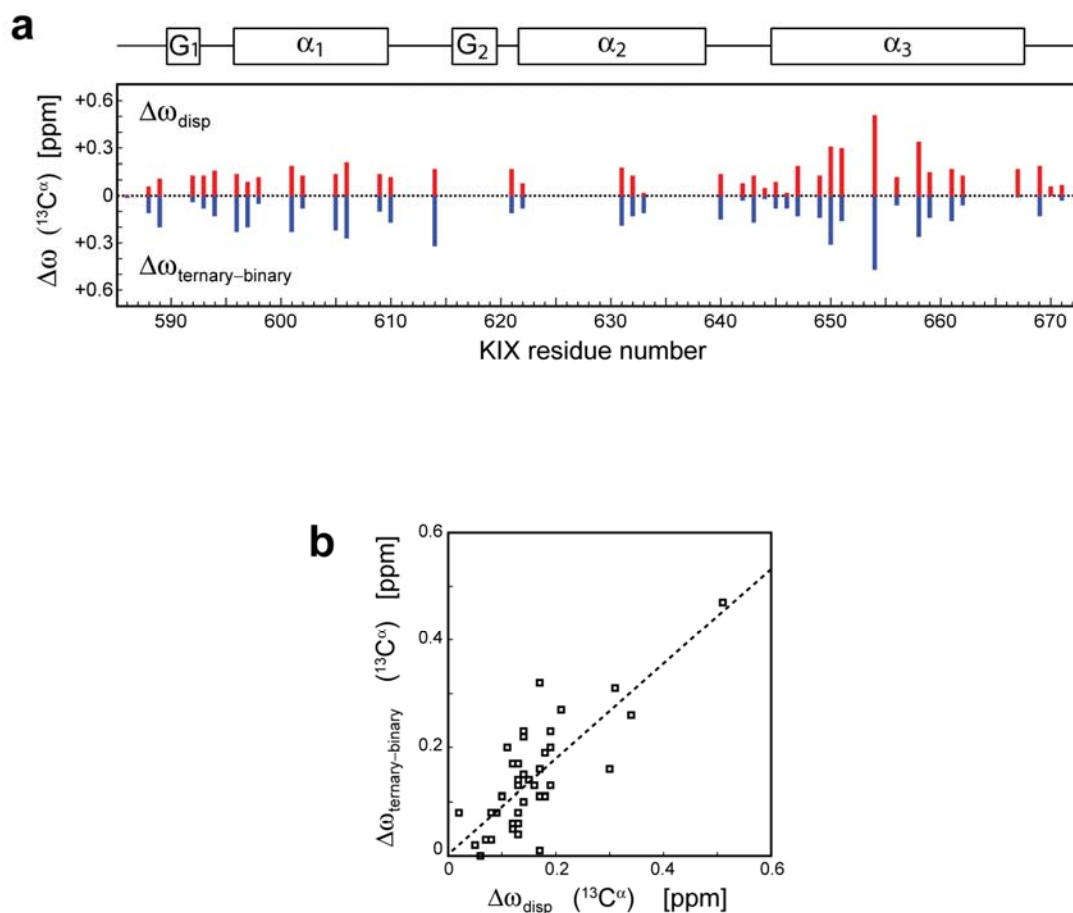
Supplementary Figure 4. KIX $^{13}C^\alpha$ chemical shift changes upon binding c-Myb to the KIX·MLL complex. (**a**) Comparison of absolute values of $^{13}C^\alpha$ chemical shift differences obtained from relaxation dispersion data for the binary KIX·MLL complex, $\Delta\omega_{disp}$, (red bars) with absolute values of $^{13}C^\alpha$ chemical shift differences between the ternary KIX·MLL·c-Myb complex and the binary KIX·MLL complex, $\Delta\omega_{ternary-binary}$, (blue bars). Values of $\Delta\omega_{ternary-binary}$ were determined using triple-resonance NMR experiments (HNCA and HN(CO)CA). The location of KIX secondary structure elements in the ternary KIX·MLL·c-Myb complex is indicated. (**b**) Correlation of $^{13}C^\alpha$ $\Delta\omega_{ternary-binary}$ and $\Delta\omega_{disp}$ values. The linear correlation coefficient is 0.78, the slope is 0.89.
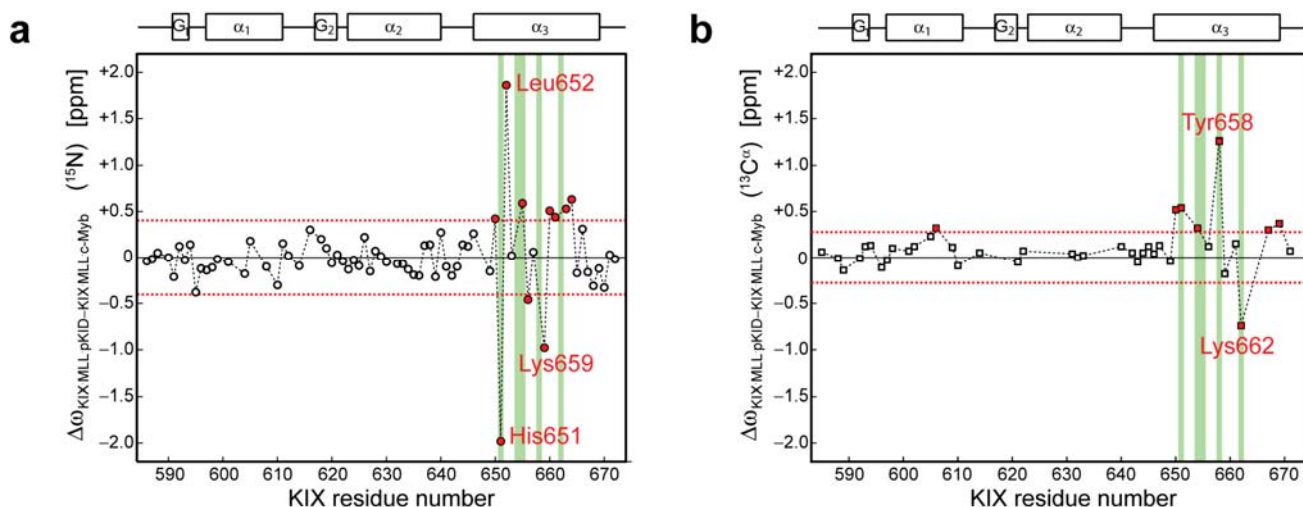
Supplementary Figure 5. Comparison of chemical shifts in the two ternary complexes KIX·MLL·c-Myb and KIX·MLL·pKID. Differences of backbone amide ^{15}N (**a**) and ^{13}C$^{\alpha}$ (**b**) chemical shift values between the ternary complexes, $\Delta\omega_{\text{KIX·MLL·pKID–KIX·MLL·c-Myb}}$, are plotted as a function of KIX residue number. Red dashed lines are drawn at $\pm\sigma$, where σ is the standard deviation of all $\Delta\omega_{\text{KIX·MLL·pKID–KIX·MLL·c-Myb}}$ values (σ (^{15}N)=0.40, σ (^{13}C$^{\alpha}$)=0.28). Residues with values of $\Delta\omega_{\text{KIX·MLL·pKID–KIX·MLL·c-Myb}}$ exceeding σ are indicated in red. KIX residues Tyr658 and Lys662, which specifically interact with the charged phosphate group of the phosphoserine 133 of pKID (the equivalent residue is Arg294 in c-Myb), as well as KIX residues Tyr651, Ala654, Glu655 and Tyr658, which interact with the aromatic side chain of Tyr134 of pKID (the equivalent residue in c-Myb is Ile297, and c-Myb does not contain any aromatic amino acids) are highlighted in light green. $\Delta\omega_{\text{KIX·MLL·pKID–KIX·MLL·c-Myb}}$ values are only shown for residues for which relaxation dispersion data were obtained.

S5

45
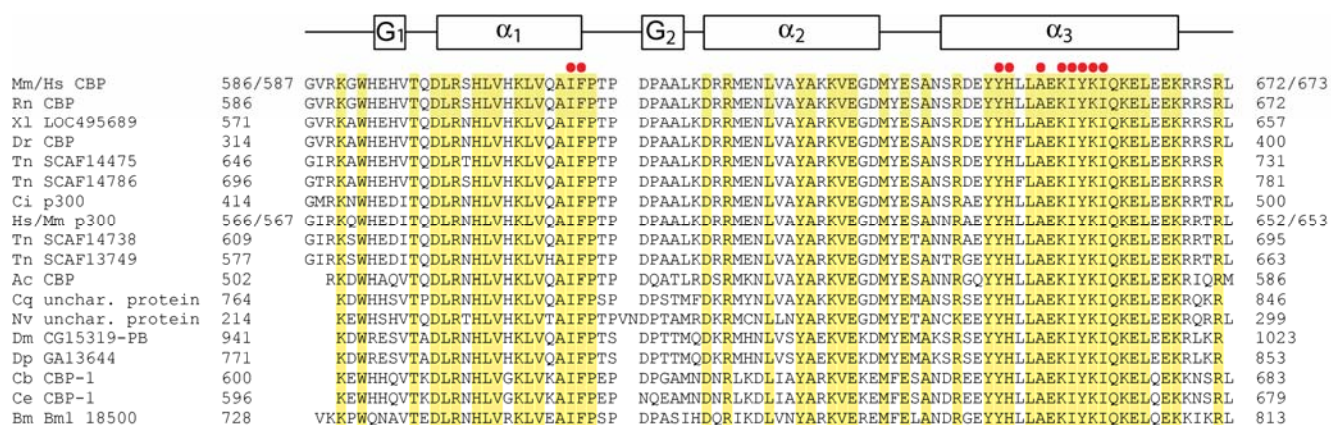
Supplementary Figure 6. Alignment of KIX domain sequences from various species (prefix abbreviations; Mm, *Mus musculus*; Hs, *Homo sapiens*; Rn, *Rattus norvegicus*; Xl, *Xaenopus laevis*; Dr, *Danio rerio*; Tn, *Tetraodon nigroviridis*; Ci, *Ctenopharyn-godon idella*; Ac, *Aplysia californica*; Cq, *Culex quinquefasciatus*; Nv, *Nemato-stella vectensis*; Dm, *Drosophila melanogaster*; Dp, *Drosophila pseudoobscura*; Cb, *Caenorhabditis briggsae*; Ce, *Caenorhabditis elegans*; Bm, *Brugia malayi*). Residues that are invariant in these proteins are highlighted in yellow, and residues that participate in the allosteric network of the binary KIX·MLL complex ($\Delta\omega_{disp}$ values exceed the average by $>2\sigma$ for ^{15}N and/or ^{13}C$^{\alpha}$) are indicated by red dots. The location of KIX secondary structure elements is shown.
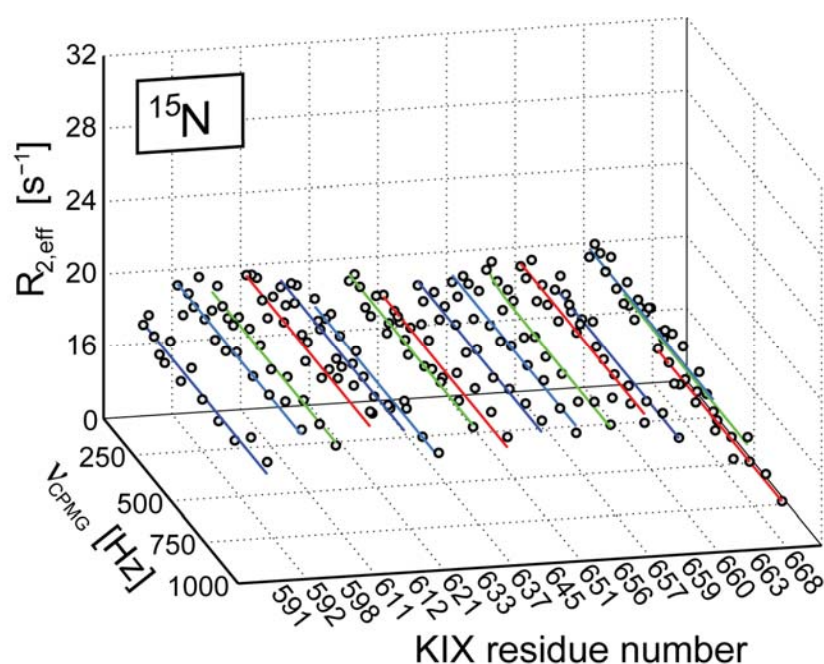
Supplementary Figure 7. NMR ^{15}N relaxation dispersion profiles of representative residues in the binary KIX·pKID complex (concentration ratio KIX: pKID=1:1.2, higher concentrations of pKID were avoided to prevent binding of pKID to the MLL binding site,[2] recorded at 600 MHz and 27°C. pKID was chosen as a ligand for the c-Myb/pKID binding site because of the ~8-fold higher affinity of KIX for pKID than for c-Myb.[3] Under the conditions used, >99.6% of KIX is bound to pKID.

References.

1. De Guzman, R.N., Goto, N.K., Dyson, H.J. & Wright, P.E. Structural basis for cooperative transcription factor binding to the CBP coactivator. *J Mol Biol* **355**, 1005−1013 (2006).

2. Sugase, K., Dyson, H.J. & Wright, P.E. Mechanism of coupled folding and binding of an intrinsically disordered protein. *Nature* **447**, 1021−1025 (2007).

3. Goto, N.K., Zor, T., Martinez-Yamout, M., Dyson, H.J. & Wright, P.E. Cooperativity in transcription factor binding to the coactivator CREB-binding protein (CBP). *J Biol Chem* **277**, 43168−43174 (2002).

Article II

VIP **Gaseous Proteins**

Electrostatic Stabilization of a Native Protein Structure in the Gas Phase**

Kathrin Breuker,* Sven Brüschweiler, and Martin Tollinger

Recently, a general picture has been proposed of how long, and to what extent, native protein structure can be retained in the gas phase.[1a] In particular, molecular dynamics simulations suggest that salt bridges and ionic hydrogen bonds on the protein surface can transiently stabilize the global fold shortly after desolvation.[1b] However, the use of native mass spectrometry[2] for studying protein solution structure is still controversial, mostly because site-specific experimental gas-phase data[3] is scarce. Here we report electron capture dissociation (ECD)[4] data on the gas-phase structures of the three-helix bundle protein KIX[5] (Figure 1) that indicate
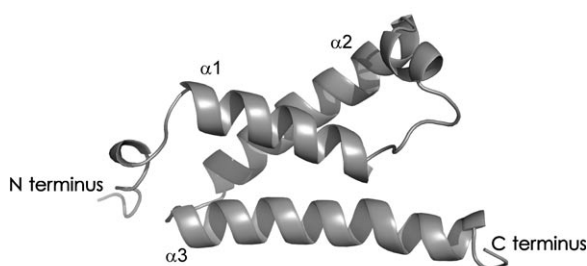
Figure 1. Structure of KIX in aqueous solution at pH 5.5 and 27°C, as determined by NMR spectroscopic experiments (PDB entry: 2AGH, model 1).[5]

substantial preservation of the native solution structure on a timescale of at least 4 s. We demonstrate that in the gas phase, the most stable regions are those stabilized by salt bridges and ionic hydrogen bonds.

[*] Dr. K. Breuker
Institut für Organische Chemie and
Center for Molecular Biosciences Innsbruck (CMBI)
Universität Innsbruck, Innrain 52a, 6020 Innsbruck (Austria)
Fax: (+43) 512-507-2892
E-mail: kathrin.breuker@uibk.ac.at
Homepage: http://www.bioms-breuker.at/
S. Brüschweiler, Priv.-Doz. Dr. M. Tollinger
Max F. Perutz Laboratories
Dr. Bohr-Gasse 9, 1030 Vienna (Austria)
Priv.-Doz. Dr. M. Tollinger
Institut für Organische Chemie, Universität Innsbruck (Austria)

Supporting information for this article is available on the WWW under http://dx.doi.org/10.1002/anie.201005112.

Figure 2 shows site-specific yields of c and $z^{\cdot}$ fragment ions[6] from ECD of $(M + nH)^{n+}$ ions of KIX (see Figure S1 in the Supporting Information) formed by electrospray ionization (ESI).[7] For the 7+ ions, separated c and $z^{\cdot}$ products were observed only from backbone cleavage near the termini (residues 1–13 and 89–91), but not from the three-helix bundle region, which forms a globular fold around a hydrophobic core (residues 16–88).[5] This observation is consistent with intramolecular interactions in the three-helix bundle region preventing separation of c and $z^{\cdot}$ backbone-cleavage products[3a–c] in the gaseous 7+ ions. Collisional activation of the 7+ ions (laboratory-frame energy: 28 eV) prior to ECD effected only marginal unfolding near the N terminus (see Figure S2 in the Supporting Information), revealing a notable stability of the three-helix bundle in the absence of solvent.

For the 8+ ions (Figure 2), the appearance of cleavage products from the N-terminal ends of helices α1 (residues 16–30) and α2 (residues 42–61) indicates partial unfolding, with helix α1 separating from the bundle, and helices α1 and α2 starting to unravel from their N-terminal ends. Unraveling of α1 and α2 continues in the 9+ ions, while helices α2 and α3 appear to largely retain their native antiparallel bundle structure. Separation of α2 and unraveling of α3 (residues 65–88), also from its N-terminal end, is evident from the fragmentation pattern observed for the 10+ ions. However, c- and $z^{\cdot}$-ion yields in the 65–88 region remained relatively small for the 10+ and 11+ ions, suggesting that partially intact α3 helix structure limits fragment ion separation. Further increasing the precursor ion charge gave increased c- and $z^{\cdot}$-ion yields and unfolding, similar to ECD data for Ubiquitin[3c] (see Figure S3 in the Supporting Information), with the fragmentation pattern of the 16+ KIX ions being largely unselective with respect to backbone cleavage site.

The data in Figure 2 provide substantial evidence for a correlation between the solution- and gas-phase structures of KIX. This supposition is corroborated by ECD of 12+ ions generated by nano-ESI from a solution (in H_2O at pH 4.5) that better resembles the native protein environment,[8] which gave decreased c- and $z^{\cdot}$-ion yields in the α2 and α3 regions (see Figure S4 in the Supporting Information), along with a smaller total fragment ion yield (37%) relative to that resulting from ECD of 12+ ions from ESI of solutions in H_2O/CH_3OH (80:20) at pH 4 (total fragment-ion yield: 49%; see Figure S3 in the Supporting Information).

The temporal stability of nativelike KIX 7+ ions was studied by introducing a delay between ion trapping and structural probing by ECD. However, the ECD fragmentation patterns showed no significant differences for delay times of 1 μs and 2 s (see Figure S5 in the Supporting Information). To

Figure 2. Yields of *c* (black bars) and *z*⁺ (open bars) fragment ions from ECD of (M + nH)ⁿ⁺ ions of KIX versus backbone cleavage site; helix regions are shaded gray. Ions with n = 7–12 and n = 13–16 were electrosprayed from quasinative (80:20 H₂O/CH₃OH, pH 4) and denaturing (50:50 H₂O/CH₃OH, pH 2.5) protein solutions (1–2 μM), respectively.

strikingly similar.[9] Apparently, the three-helix bundle structure of KIX is sufficiently stabilized by specific noncovalent interactions that outweigh the loss of hydrophobic bonding in the gas phase.

Figure 4a shows integrated *c*- and *z*⁺-ion yields for helix regions α1, α2, and α3 versus precursor ion charge. The data exhibit sigmoidal behavior, with transition charge values (at 50% of the plateau value) of 9.2, 10.7, and 12.4 for α1, α2, and α3, respectively. This order of helix stability (α3 > α2 > α1) in the gas phase agrees with that in solution as determined by NMR spectroscopic experiments.[10] However, in solution, each helix unfolds cooperatively,[10] whereas the gas-phase data (Figure 1) show incremental unraveling from their N-terminal ends. This behavior is also reflected in the site-specific transition charge values from analysis of site-specific *c*- and *z*⁺-ion yields (see Figure S6 in the Supporting Information), which generally increase from the N to the C terminus (Figure 4b). Transition charge values for cleavage sites between helix regions (31–41, 62–64) are similar to values for adjacent helix ends, indicating that helix separation does not precede helix unraveling.

Although the ECD data in Figures 2 and 3 demonstrate extensive preservation of the native solution structure in the 7 + ions, its stabilization in the gas phase must be based on interactions other than hydrophobic bonding.[3d,e] These include neutral[11] and ionic[1b,12] hydrogen bonds, charge–dipole interactions,[13] and salt bridges.[1b,14] Figure 5 shows helices α1, α2, and α3 with all basic (H, K, R) and acidic (D, E) residues highlighted in color. The density of charged residues is smallest for α1 (5 out of 15 residues, 0.33) and largest for α3 (14 out of 24 residues, 0.58); α2 exhibits an intermediate density of 0.4 (8 out of 20 residues). Importantly, the charge density values

expedite possible structural transitions, we next activated the gaseous 7 + ions by 28 eV collisions (see Figure S2 in the Supporting Information) prior to ion trapping. Despite the increase in ion internal energy, the fragmentation patterns from ECD with delays of 1 μs, 2 s, and 4 s (Figure 3) are

50
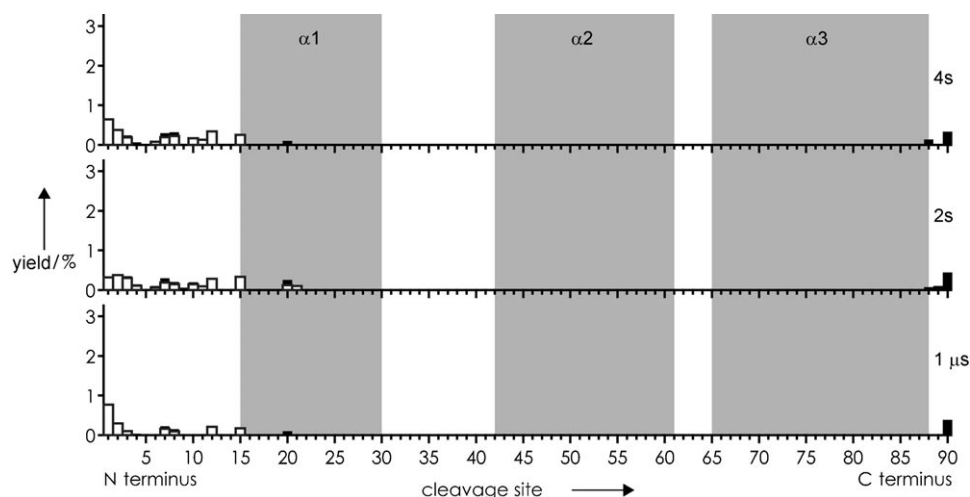
Figure 3. Yields of *c* and *z* fragment ions from ECD of $(M + 7H)^{7+}$ ions of KIX electrosprayed from a solution in H_2O/CH_3OH (80:20) at pH 4.0 versus backbone cleavage site. The experiments were carried out with collisional ion activation (laboratory-frame energy: 28 eV) and delays between ion trapping and structural probing by ECD of 1 µs (bottom), 2 s (center), and 4 s (top).
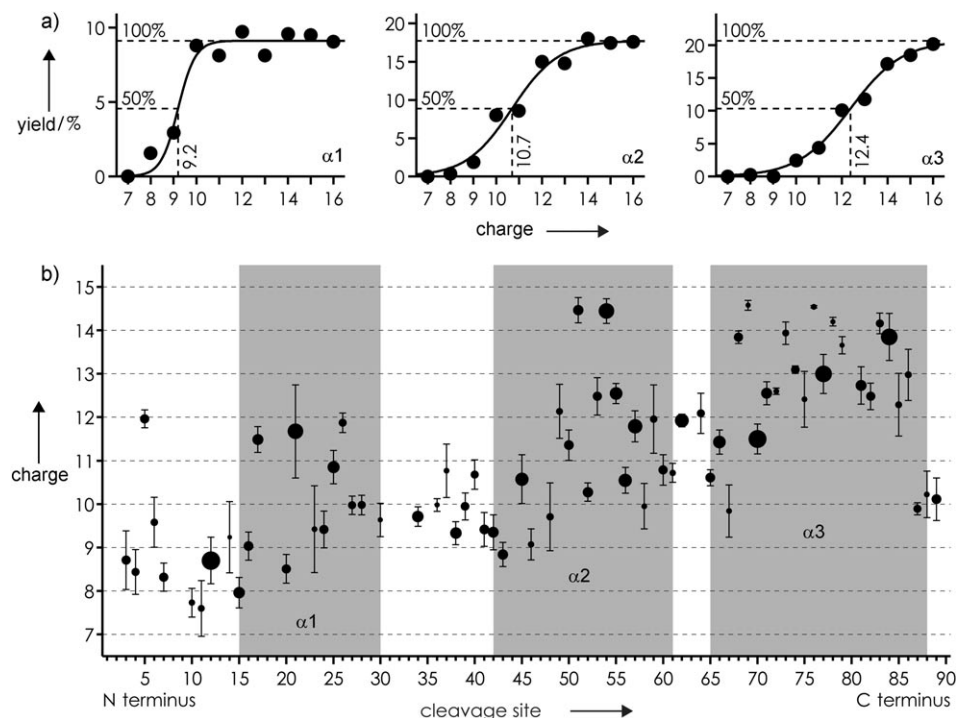
Figure 4. Analysis of the data in Figure 2: a) integrated *c*- and *z*-ion yields for helix regions α1, α2, and α3 versus precursor ion charge; b) site-specific transition charge values (at 50% of plateau value) versus backbone cleavage site; symbol size and error bars represent plateau values and standard deviations for transition charge values from sigmoidal fit functions, respectively.

Close inspection of the native KIX structure revealed that one (D17/H21), three (R42/E45, K52/E55, K53/D57), and six (R65/D66, E67/H70, E74/K75, K78/E82, K81/E84, E85/R88) intrahelix salt bridges can stabilize helices α1, α2, and α3, respectively (Figure 5). The density of salt bridges correlates ($r = 0.9999$) with transition charge values (Figure 6b) even better than the density of charged residues, suggesting that salt bridges are major determinants for protein structural stabilization in the gas phase. However, this conclusion does not exclude additional stabilization by ionic hydrogen bonds as well as charge–dipole interactions. In particular, interaction of the positive net charge at the C-terminal end of helix α3 (Figure 5) with its electric dipole moment can further stabilize the α3 helix structure,[13] and is consistent with helix unraveling from the N-terminal end.

Stabilization of the global fold by interactions between the three helices probably involves helix dipole/dipole interactions;[15] the antiparallel helices α2 and α3 with larger dipole moments than that of the shorter helix α1 separate and unfold last. Additional stabilization of tertiary structure by ionic hydrogen bonding between charged residues and backbone amides[1b] is indicated by the scatter of site-specific transition charge values (Figure 4b).

We show here that electrostatic interactions can compensate for the loss of hydrophobic bonding and stabilize the native three-helix bundle structure of KIX in the gas phase on a timescale of at least 4 s. Among these interactions, salt bridges were found to play a dominant role. However, a high number of surface-exposed charged residues alone does not guarantee protein stability in the gas phase: equine Cytochrome *c* has 24 basic and 12 acidic residues,[3a] with the number of salt bridges on the protein surface increasing from 6 in solution to an average value of 17.3 in the gas phase

correlate ($r = 0.9775$) with transition charge values (as a measure of helix stability in the gas phase) for α1, α2, and α3 (Figure 6a). This observation strongly suggests that interactions involving charged residues, that is, ionic hydrogen bonds and salt bridges, largely determine helix stability in the gas phase.
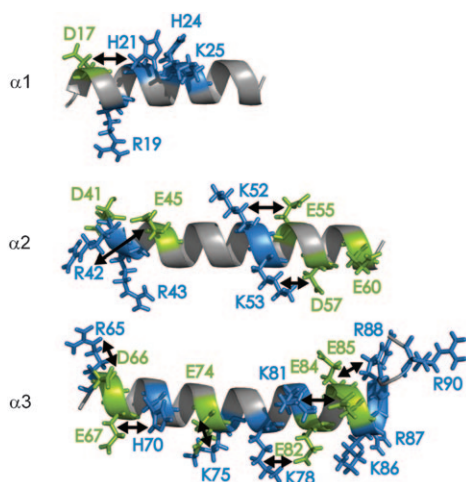
Figure 5. KIX α helices with possible salt bridges between basic (blue) and acidic (green) residues indicated by arrows.
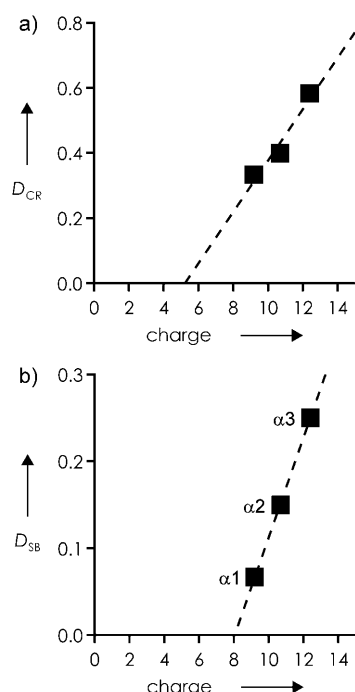
Figure 6. a) Density of charged residues (D_{CR}, number of charged residues/number of residues) and b) density of salt bridges (D_{SB}, number of salt bridges/number of residues) versus transition charge value for helices α1, α2, and α3 (linear-fit functions with Pearson correlation coefficients of $r = 0.9775$ (a) and $r = 0.9999$ (b) shown as dashed lines).

within 10 ps after desolvation,[1b] yet its native fold disintegrates on a timescale of milliseconds.[3e, 16] The outstanding stability of gaseous KIX ions observed in this study must be attributed to the combination of favorable electrostatic interactions, including salt bridges, neutral and ionic hydrogen bonds, as well as charge–dipole interactions. Whether or not native mass spectrometry can reveal information about the

solution structure of a protein critically depends on the timescale of the experiment[1a] and the extent of intramolecular stabilization by electrostatic interactions. KIX is the first protein for which site-specific ECD data indicate preservation of the solution structure in the gas phase. We propose KIX as a model protein for the evaluation of new and emerging methodology for the structural probing of gaseous proteins.

Experimental Section

KIX protein (91 residues, GSHMGVRKGW HEHVTQDLRS HLVHKLVQAI FPTPDPAALK DRRMENLVAY AKKVEGD-MYE SANSRDEYYH LLAEKIYKIQ KELEEKRRSR L) was expressed in *Escherichia coli* cells by using a plasmid that included the CBP KIX coding region[5] (residues 586–672; residue 586 corresponds to residue 5 in this study) and purified by Ni-affinity and size-exclusion chromatography.[10] The purified protein was desalted as described previously.[17] Solution pH was adjusted by addition of acetic acid. Experiments were performed on a 7 T Fourier transform ion cyclotron resonance (FT-ICR) mass spectrometer (Bruker) equipped with an ESI source (flow rate: 1.5 µL min^{-1}) and a hollow dispenser cathode operated at 1.6 A for ECD. The desolvation gas temperature was 200 and 150 °C for 80:20 and 50:50 H_2O/CH_3OH solutions, respectively. Before ion trapping, precursor isolation (using radiofrequency waveforms), and irradiation with low-energy (< 1 eV) electrons for 17–50 ms in the FT-ICR cell, ions were accumulated in the hexapole ion cells for 0.3–2.0 s. Ion activation prior to ECD was realized in the second hexapole by energetic collisions with Ar gas. Between 250 and 500 scans were added for each ECD spectrum. ECD fragment ion yields were calculated as percentage values relative to all ECD products excluding $a^{•}/y$ ions,[6] considering that backbone dissociation of a parent ion gives a pair of complementary c and $z^{•}$ ions ($100\% = 0.5[c] + 0.5[z^{•}] +$ [other products], in which other products are reduced molecular ions and products from loss of small neutral species from the latter).[3c]

[1] a) K. Breuker, F. W. McLafferty, *Proc. Natl. Acad. Sci. USA* **2008**, *105*, 18145–18152; b) M. Z. Steinberg, R. Elber, F. W. McLafferty, R. B. Gerber, K. Breuker, *ChemBioChem* **2008**, *9*, 2417–2423.
[2] J. A. Loo, *Mass Spectrom. Rev.* **1997**, *16*, 1–23; A. J. R. Heck, R. H. H. van den Heuvel, *Mass Spectrom. Rev.* **2004**, *23*, 368–389; B. T. Ruotolo, C. V. Robinson, *Curr. Opin. Chem. Biol.* **2006**, *10*, 402–408.
[3] a) K. Breuker in *Principles of Mass Spectrometry Applied to Biomolecules* (Eds.: J. Laskin, C. Lifshitz), Wiley, Hoboken, **2006**, pp. 177–212; b) D. M. Horn, K. Breuker, A. J. Frank, F. W. McLafferty, *J. Am. Chem. Soc.* **2001**, *123*, 9792–9799; c) K. Breuker, H. B. Oh, D. M. Horn, B. A. Cerda, F. W. McLafferty, *J. Am. Chem. Soc.* **2002**, *124*, 6407–6420; d) K. Breuker, F. W. McLafferty, *Angew. Chem.* **2003**, *115*, 5048–5052; *Angew. Chem. Int. Ed.* **2003**, *42*, 4900–4904; e) K. Breuker, F. W. McLafferty, *Angew. Chem.* **2005**, *117*, 4989–4992; *Angew. Chem. Int. Ed.* **2005**, *44*, 4911–4914.
[4] R. A. Zubarev, N. L. Kelleher, F. W. McLafferty, *J. Am. Chem. Soc.* **1998**, *120*, 3265–3266; R. A. Zubarev, D. M. Horn, E. K.

Fridriksson, N. L. Kelleher, N. A. Kruger, M. A. Lewis, B. K. Carpenter, F. W. McLafferty, *Anal. Chem.* **2000**, *72*, 563–573.

[5] R. N. De Guzman, N. K. Goto, H. J. Dyson, P. E. Wright, *J. Mol. Biol.* **2006**, *355*, 1005–1013.

[6] *a*ˑ and *y* ions were of much lower abundance (total yield < 4 %) with correspondingly small signal-to-noise ratios, and were not included in the analysis.

[7] J. B. Fenn, M. Mann, C. K. Meng, S. F. Wong, C. M. Whitehouse, *Science* **1989**, *246*, 64–71.

[8] Initial experiments using nano-ESI (flow rate: 100 nL min⁻¹) and unbuffered, aqueous solutions at pH 4.5–5.5 showed a tendency of KIX to aggregate and clog the emitter, so in further experiments we used solutions containing at least 20 % CH_3OH at pH < 5 and regular ESI.

[9] Delays > 4 s led to significantly decreased electron capture efficiency, presumably as a result of increased ion magnetron radii; see, for example: C. L. Hendrickson, S. A. Hofstadler, S. C. Beu, D. A. Laude, *Int. J. Mass Spectrom. Ion Processes* **1993**, *123*, 49–58.

[10] P. Schanda, B. Brutscher, R. Konrat, M. Tollinger, *J. Mol. Biol.* **2008**, *380*, 726–741.

[11] H. B. Oh, K. Breuker, S. K. Sze, Y. Ge, B. K. Carpenter, F. W. McLafferty, *Proc. Natl. Acad. Sci. USA* **2002**, *99*, 15863–15868; C. S. Hoaglund-Hyzer, A. E. Counterman, D. E. Clemmer, *Chem. Rev.* **1999**, *99*, 3037–3079; H. B. Hamidane, H. He, O. Y. Tsybin, M. R. Emmett, C. L. Hendrickson, A. G. Marshall, Y. O. Tsybin, *J. Am. Soc. Mass Spectrom.* **2009**, *20*, 1182–1192.

[12] M. Meot-Ner, *Chem. Rev.* **2005**, *105*, 213–284.

[13] M. F. Jarrold, *Phys. Chem. Chem. Phys.* **2007**, *9*, 1659–1671.

[14] P. D. Schnier, W. D. Price, R. A. Jockusch, E. R. Williams, *J. Am. Chem. Soc.* **1996**, *118*, 7178–7189; E. F. Strittmatter, E. R. Williams, *J. Phys. Chem. A* **2000**, *104*, 6069–6076.

[15] D. T. Kaleta, M. F. Jarrold, *J. Am. Chem. Soc.* **2003**, *125*, 7186–7187; L. W. Zilch, D. T. Kaleta, M. Kohtani, R. Krishnan, M. F. Jarrold, *J. Am. Soc. Mass Spectrom.* **2007**, *18*, 1239–1248.

[16] E. R. Badman, C. S. Hoaglund-Hyzer, D. E. Clemmer, *Anal. Chem.* **2001**, *73*, 6000–6007.

[17] M. Hartl, A. M. Mitterstiller, T. Valovka, K. Breuker, B. Hobmayer, K. Bister, *Proc. Natl. Acad. Sci. USA* **2010**, *107*, 4051–4056.

53

Supporting Information

Electrostatic Stabilization of a Native Protein Structure in the Gas Phase**

Kathrin Breuker,* Sven Brüschweiler, and Martin Tollinger

ange_201005112_sm_miscellaneous_information.pdf
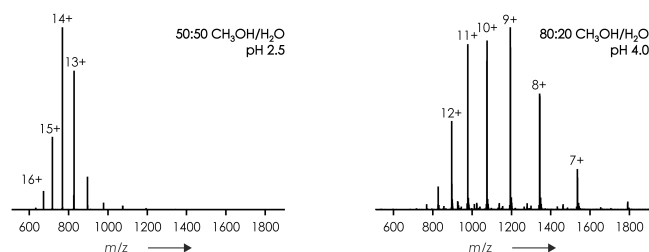
Figure S1: ESI mass spectra of KIX (1-2 μM) electrosprayed from 50:50 H_2O/CH_3OH solution at pH 2.5 (left) and 80:20 H_2O/CH_3OH solution at pH 4.0 (right).
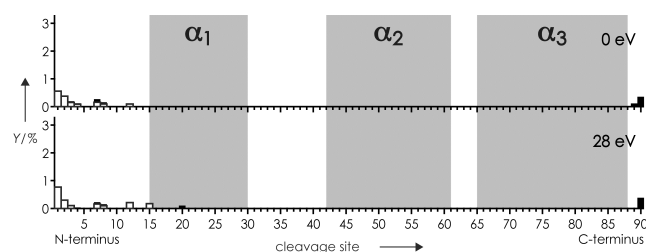
Figure S2: c (black bars) and $z^\bullet$ (open bars) ion yields from ECD of $(M + 7H)^{7+}$ ions of KIX (2 μM) electrosprayed from 80:20 H_2O/CH_3OH solution at pH 4.0 versus backbone cleavage site, without collisional activation (top, which is the same data as in Figure 2) and with 28 eV (laboratory frame energy) collisional activation (bottom) prior to ECD.
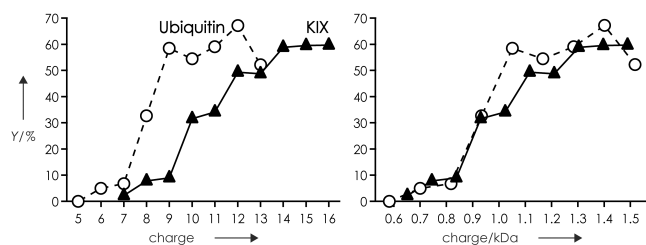
Figure S3: For the data in Figure 1, total c, $z^\bullet$ ion yields from ECD of $(M + nH)^{n+}$ ions of KIX (triangles) versus precursor charge (left) and precursor charge divided by protein mass (right); data for Ubiquitin (circles, from reference 3c) are shown for comparison.
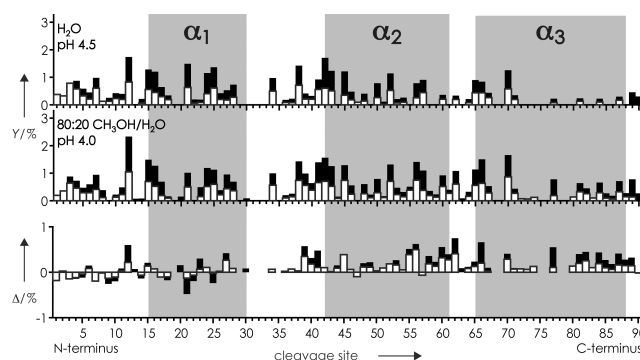
Figure S4: c (black bars) and $z^{\bullet}$ (open bars) ion yields from ECD of $(M + 12H)^{12+}$ ions of KIX generated by nano-electrospray ionization from H_2O solution at pH 4.5 (top) and electrospray ionization from 80:20 H_2O/CH_3OH solution at pH 4.0 (center, which is the same data as in Figure 2) versus backbone cleavage site, the bottom trace shows the yield difference.
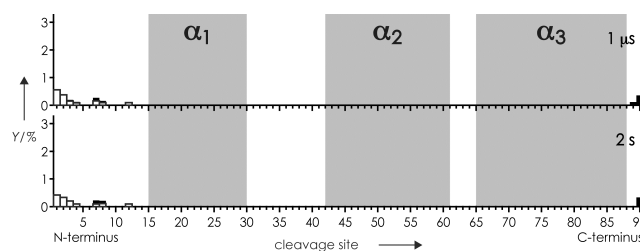
Figure S5: c (black bars) and $z^{\bullet}$ (open bars) ion yields from ECD of $(M + 7H)^{7+}$ ions of KIX (2 μM) electrosprayed from 80:20 H_2O/CH_3OH solution at pH 4.0 versus backbone cleavage site, with delay times between ion trapping and ECD of 1 μs (top, which is the same data as in Figure 2) and 2 s (bottom).
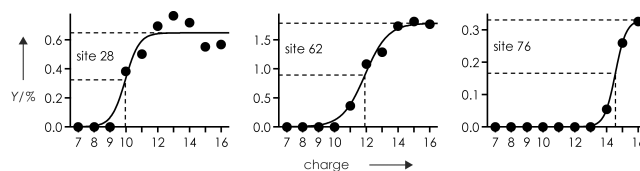
Figure S6: Representative examples for site-specific c, $z^{\bullet}$ ion yields versus precursor ion charge, solid lines show sigmoidal fit functions from which transition charge values (50% of plateau value) were calculated: 10.0, 11.9, and 14.6 for cleavage sites 28, 62, and 76, respectively.

Article III

Allosteric communication in the KIX domain proceeds through re-packing of the hydrophobic core

Sven Brüschweiler 1,2, Reiner Ribarics 1, Robert Konrat 1 and Martin Tollinger 2,#

1 Structural and Computational Biology, Max F. Perutz Laboratories, Campus Vienna Biocenter 5, A-1030 Vienna, Austria
2 Institute of Organic Chemistry, University of Innsbruck, Innrain 52A, A-6020 Innsbruck, Austria

To whom correspondence should be addressed.
Phone: +43 512 507 5230. Fax: +43 512 507 2892. E-mail:
martin.tollinger@uibk.ac.at

Abstract

The KIX domain of the transcriptional co-activator CREB binding protein (CBP) mediates cooperativity between transcription factors in an allosteric manner. Ligand binding to one surface of the KIX domain enhances interactions with transcription factores to the second, remote binding site of the protein. Nuclear magentic resonance (NMR) spin relaxation studies showed that binding of a single transcription factor molecule, the activation domain of mixed lineage leukemia protein (MLL) induces the formation of a low-populated conformer of KIX that resembles the conformation of the protein in the presence of the second ligand. The data revealed the mechanistic significance of the hydrophobic core of the KIX domain for the observed binding cooperativity, suggesting that a subset of the hydrophobic core residues constitutes an allosteric network that bridges the two binding sites. Here we describe the three-dimensional NMR solution structures of the binary complex of KIX with MLL and the ternary complex of KIX formed with MLL and the phosphorylated kinase inducible domain of CREB (pKID), as well as unliganded KIX. The data show that binding of pKID to the binary complex of KIX with MLL induces a defined conformational transition of the hydrophobic core residues that form part of the allosteric network, enabling a structural rationalization of allosteric communication in the KIX domain. In addition, NMR spin relaxation experiments to further characterize dynamic processes in KIX reveal the involvement of pico-to-nanosecond time-scale dynamic processes in allosteric coupling of the two binding surfaces.

Introduction

Cooperativity plays a central role for the regulation of gene transcription.[1; 2; 3] Transcription factors along with transcriptional co-activators assemble cooperatively on DNA promoter sequences, and transcription is stimulated by recruitment of RNA polymerase II.[4] These interactions are mediated by transcriptional co-activators, such as CBP, its paralog p300 or Mediator co-activator,[5; 6] which act as a scaffold for the recruitment of the transcriptional machinery. It has been observed in various studies that combination of a number of DNA-bound transcription factors results in synergistic transcriptional response[1] and, more specifically, several lines of evidence indicate that cooperative interactions between transcription factors and CBP are pivotal to promote synergism in transcriptional activation.[3; 7] CBP participates in the regulation of gene transcription by linking transcription factors with components of the basal transcriptional machinery.[5] CBP is present at only low (and possibly limiting) concentrations in vivo, suggesting that competition of different transcription factors for CBP may be crucial for the regulation of gene transcription.[8] The characterization of the biophysical mechanism by which cooperiativity modulates the affinities of transcription factors for binding to CBP is a prerequisite for understanding how gene transcription is regulated.

CBP is a modular protein that contains a number of structured domains, as well as long stretches that are intrinsically disordered and represent linker regions and/or interactions motifs that fold only upon binding their biological targets.[9] From a regulatory perspective, the KIX domain is of particular interest, since it is capable of binding two transcription factors simultaneously through two different binding sites, thereby directly mediating interactions between bound transcription factors. The three-dimensional structure of the KIX domain is composed of a bundle of three α-helices and two short 3_{10}-helices, with the two binding sites for transcription factors, which are isolated from each other, being located at remote surfaces of the protein.[10] Homologous KIX domains have also been identified and characterized in p300 as well as in human and yeast Mediator co-activator subunits and their structures were determined recently, revealing a high degree of functional and structural similarity.[11; 12]

The KIX domain of CBP thus physically interlinks transcription factors by simultaneous binding through two interaction sites, and it does so in a co-operative manner.[13] In vitro, binding of the mixed-lineage leukemia (MLL) activation domain to KIX co-operatively enhances the interaction with the activation domain of the transcription factor c-Myb: KIX in complex with MLL displays a ~2-fold higher affinity for c-Myb than the KIX domain alone.[14] Likewise, positive cooperativity has been demonstrated for the interaction of the activation domain of pKID (the phosphorylated kinase inducible domain of CREB, which binds to KIX through the c-Myb interaction site) with KIX in complex with MLL.[14] These cooperative effects provide a potential mechanism through which transcriptional activity might be modulated in the cell. Several observations relating to communication between transcription factors mediated by CBP have indeed been described in the literature, suggesting transcriptional synergy between various transcription factors.[7; 15]

We recently monitored directly the conformational re-arrangement process by which the KIX domain communicates information about the presence of a biological target at the MLL binding site to the allosterically regulated c-Myb/pKID binding site using backbone and side chain NMR relaxation dispersion techniques.[16] The data revealed that binding the activation domain of MLL to KIX causes a re-distribution of the relative populations of KIX conformers towards a state that adopts a conformation that is similar to that of the ternary complex. Titration experiments showed that this higher energy (excited) conformational sub-state of KIX·MLL, which is populated to 7% in the KIX·MLL binary complex, displays a higher affinity for c-Myb/pKID ligands than the 93% populated lower-energy (ground) state of the protein complex. These results suggest that binding of c-Myb/pKID involves the selection of the higher-energy conformer, whose structure is complementary to the ligand, from a pre-existing ensemble of conformations, reminiscent of the conformational selection mechanism of molecular recognition.[17; 18; 19] In solution, KIX in complex with MLL is in an equilibrium between these two conformational sub-states within ~3 ms. As the higher-affinity conformational sub-state is depleted from the equilibrium upon ligand binding, the equilibrium is recovered through the allosteric transition.

The exact structural basis of the allosteric transition is, however, unknown. The relaxation dispersion data indicate that a network of hydrophobic amino acids, which bridge the two binding sites of the KIX domain, constitutes the pathway through which allosteric information is communicated. The data suggest subtle conformational differences between lower and higher energy conformers, with chemical shift differences δω between 0.4 and 1.0 ppm found for the small subset of ^{15}N and ^{13}C nuclei that form part of the allosteric network. This is contrasted by the remainder of the protein backbone, for which with δω values < 0.4 ppm were detected, indicating that the structure of the three-helix scaffold is not affected by the transition between lower and higher energy conformers. Intriguingly, side chain methyl relaxation dispersion experiments performed on isoleucine δ1 methyl ^{13}C nuclei suggested a small but significant conformational adaption of the part of the hydrophobic core that bridges the two binding sites. In addition, backbone amide ^{1}H/^{2}H exchange data showed that both (lower and higher energy) sub-states represent fully folded and solvent exchange protected conformers.[16]

Here we report the NMR derived three-dimensional solution structures of the binary complex of KIX formed with the activation domain of MLL, the ternary complex of KIX bound to MLL and pKID and the structure of KIX not bound to ligand peptides. Together with the structure of the binary complex of KIX and pKID,[20] our results facilitate a comprehensive description of the structural adaption of the KIX domain in response to binding ligand molecules. In combination with pico-to-nanosecond dynamic NMR and ITC experimental data, the results enable us to draw a structural and dynamic picture of the molecular mechanism through which the KIX domain of CBP mediates cooperativity between transcription factors.

Results

Solution structures of binary and ternary complexes of KIX

NMR solution structures of the KIX domain of CBP (residues 586-672) were determined in the presence of the activation domain of the transcription factor MLL as well as in the presence of the activation domains of both MLL and pKID using triple-resonance resolved NMR techniques (Figure 1). Structural statistics are shown in Table 1. The overall structures of these complexes are very similar to the structures that were determined for KIX in complex with pKID,[20] KIX in complex with c-Myb[21] and the ternary complex of KIX with the MLL and c-Myb activation domains.[10] The central scaffold of the KIX domain is formed by a bundle of three α-helices (residues 597-611: α1, residues 623-642: α2, residues 646-669: α3) together with two short 3_{10}-helices (residues 591-593: G1 and residues 617-620: G2). The three helices α1- α3 pack together in an antiparallel fashion to form an extended hydrophobic core which is capped by the first 3_{10}-helix G1 on one side, while the loop L12, which encompasses the 3_{10}-helix G2 and connects helices α1 and α2, partly caps the other side of the hydrophobic core.[10]

In the binary complex KIX·MLL as well as in ternary KIX·MLL·pKID, residues 2847 to 2855 of MLL form an amphipathic helix that binds to the hydrophobic groove on the surface of the KIX domain at the C-terminus of helix α1, similar to the ternary complex formed by KIX with the activation domains of MLL and c-Myb.[10] Through the insertion of MLL into the hydrophobic groove, several hydrophobic residues (I2849, M2850, F2852, V2853, and L2853) of MLL are in the position to form hydrophobic contacts with a number of KIX residues (I611, F612, A619, R624 (aliphatic region), L628, Y631, I660 and L664), which are part of the hydrophobic groove. In addition, the NMR structures indicate electrostatic interactions between the side chain of N2856 of MLL and two KIX side chains, T614 and D616. The structures of KIX·MLL and KIX·MLL·pKID complexes show no significant difference with respect to the binding mode of the MLL ligand peptide.

In the ternary complex KIX·MLL·pKID, the activation domain of CREB binds into a shallow hydrophobic pocket on the surface of the KIX domain that is formed by

side chains of amino acid residues in helices α1 (N-terminal part) and α3 (central part). Bound pKID forms two almost perpendicular helices αA and αB, as observed previously for the binary complex of KIX formed with pKID [20]. The side chains of helix αB residues I137, L138 and L141 make close hydrophobic contacts with the pKID binding pocket formed by KIX helix α3 residues Y650, A654, I657 and Y658. In addition, the side chain of A145 packs against the side chains of L599 and L603. For the αA helix of pKID intermolecular NOEs were only found for I127 and L128. Both of these residues make van der Waals contacts with Y658. In addition, the hydroxyl group of Y658 forms a hydrogen bond with the phosphate group of pS133 of pKID [20]. There are no direct contacts between the bound activation domains of MLL and pKID.

The pair-wise rms between backbone atoms of the well structured parts of the KIX domain (residues 589-672) in KIX·MLL and KIX·MLL·pKID is 1.206 Å, which is comparable to the rms of the structural bundles of the two complexes. This is consistent with the observation of only small chemical shift differences of backbone (^{15}N, ^{1}HN, ^{13}Cα) resonances between the binary and ternary complexes.[16] It is therefore evident from the NMR structural analysis of the two complexes that the KIX protein backbone is not significantly affected by binding pKID.

To identify and characterize any conformational differences involving the hydrophobic core of the KIX domain in binary KIX·MLL and ternary KIX·MLL·pKID complexes, we put particular effort into site-specific and stereospecific assignments of KIX side chain methyl groups. For KIX·MLL and KIX·MLL·pKID isoleucine side chain γ2 and δ1 methyls are resolved in two-dimensional [^{1}H,^{13}C] correlation experiments and can be assigned individually. In addition, we obtained stereospecific assignments of Val and Leu side chain methyl resonances for all 15 Val and Leu residues. For the binary complex relatively strong NOEs are observed between the δ1 methyl group of I611 and both (δ1 and δ2) methyl groups of L628. These NOEs are absent in the ternary complex, indicating that the binding of pKID to the binary KIX·MLL complex is accompanied by a defined re-packing of the hydrophobic core of the domain. This is further corroborated by the observation that symmetry equivalent NOEs involving the δ1 and δ2

methyl groups of L628. In addition, the NOE patterns for the δ1 methyl group of I657 indicate a change in orientation of the I657 side chain upon binding pKID.

In Figure 2 the hydrophobic cores of KIX·MLL and KIX·MLL·pKID complexes are compared. In the hydrophobic core of the binary complex KIX·MLL, the δ1 methyl group of I660 is tightly packed to the γ1 methylene group of I611 and the methyl group of A610. Binding of pKID, however, is accompanied by an increase of the distance between the δ1 methyl group of I660 and residues I611, A610 and L607. Moreover, the side chain chi1 torsion angle of Ile I657 is rotated by about −110° upon transition from binary KIX·MLL to ternary KIX·MLL·pKID, thereby propagating the conformational adaption of the hydrophobic core to the c-Myb/pKID binding surface of the KIX domain. In KIX·MLL·pKID the δ1 methyl group of I657 forms close hydrophobic contacts with the side chains of I137 and L141 of the ligand peptide pKID (see below).

A comprehensive description of the conformational response of the KIX domain to the presence of ligand peptides requires structural information of all relevant states. In order to complement the set of available structures we also determined the solution structure of KIX in the absence of ligand peptides (Figure 3). As anticipated,[22; 23] unliganded KIX displays a measurably higher conformational flexibility of the three helix bundle, with a pair-wise rms between backbone atoms of the well structured parts of the protein (residues 589-672) of 1.231 Å. In particular, while the C-terminal part of helix α3 (residues 661-672) populates helical regions of the backbone dihedral angle ϕ/ψ space, its conformation is distorted from an ideal helical conformation in many of the structures, leading to a significant dynamic fraying of the structural bundle. The most significant difference between the backbones of unliganded KIX and the complexes KIX·MLL and KIX·MLL·pKID is found for the loop L12. This segment of the KIX domain forms part of the MLL binding site in the complexes, with F612 making direct hydrophobic interactions with the ligand peptide. While this part of the protein backbone is conformationally heterogeneous in unliganded KIX, it is significantly rigidifies upon binding the MLL peptide in both KIX·MLL and KIX·MLL·pKID complexes and shifts its position towards the MLL binding site, as observed for the ternary KIX·MLL·c-Myb complex.[10] We obtained stereospecific assignments for all

Val and 16 out of 18 Leu side chain methyl resonances in unliganded KIX. Although isoleucine side chain γ2 and δ1 methyls are only partly resolved in two-dimensional [^{1}H,^{13}C] correlation experiments. However, the overall NOE pattern suggests that the hydrophobic core of the protein in the absence of ligand peptides is similar to the one in KIX·MLL.

Pico-to-nanosecond time scale dynamics of KIX and KIX complexes

To characterize the dependence of the conformational flexibility of the KIX domain on the presence of bound ligands, we determined backbone amide order parameters, which are sensitive reporters of pico-to-nanosecond time scale dynamics,[24] for four different (complexed) states of the KIX domain: unliganded KIX, binary KIX·MLL, binary KIX·pKID and ternary KIX·MLL·pKID (Figure 4). In binary and ternary complexes of KIX, the three-helix scaffold of the protein is well ordered in solution, with backbone order parameters of ca. 0.9 for helices α1- α3. In agreement with the NMR solution structures, order parameters of the unliganded KIX domain are measurably lower (the average of all order parameters in helices α1- α3, S^2_{avg}, is 0.85), suggesting a higher level of flexibility on the pico-to-nanosecond time scale. Significantly lower than average order parameters are also found for the N-termini (including the 3_{10} helix G1) and the C-termini of the protein in all four states, consistent with the dynamic fraying of these segments of the protein that is observed in the structural bundles. In addition, the order parameters of the backbone amides in helix α3 suggest that the C-terminal half of this helix is more rigid in complexes containing MLL compared to unliganded KIX and KIX·pKID. This observation agrees with lower degree of dynamic fraying that is observed for the C-terminal half of helix α3 in the structural bundles of KIX·MLL and KIX·MLL·pKID compared to unliganded KIX (Figures 1 and 3).

The NMR relaxation data also indicate significant pico-to-nanosecond time scale dynamics in loop region L12, along with a clear difference between different complexes of KIX. For this part of the KIX backbone, average order parameters vary in a step-wise manner upon binding ligands, with S^2_{avg} values of 0.64 in the free form of the protein and 0.85 in the ternary complex KIX·MLL·pKID and intermediate levels of dynamics for binary complexes KIX·MLL and KIX·pKID (S^2_{avg} of 0.80 and 0.71, respectively). Contrary to the step-wise changes of the order

parameters in the L12 loop, the three-helix scaffold of the binary KIX complexes rigidifies upon binding a single ligand (either MLL or pKID) and shows no further rigidification upon binding an additional ligand molecule to form the ternary complex KIX·MLL·pKID. This behavior is most prominent for helices α1 and α2 of the KIX domain (helix α1: KIX S^2_{avg}=0.84, KIX·MLL: S^2_{avg}=0.90, KIX·pKID: S^2_{avg}=0.90, KIX·MLL·pKID: S^2_{avg}=0.91) and α2 (KIX S^2_{avg}=0.82, KIX·MLL: S^2_{avg}=0.90, KIX·pKID: S^2_{avg}=0.91, KIX·MLL·pKID: S^2_{avg}=0.91). For helix α3 resonance overlap in unliganded KIX prevents the measurement order parameters for four C-terminal residues of helix α 3 (666-669). Comparison of the order parameters of backbone amides in the N-terminal part of helix α3 (646-665), however, suggests that this part of the three-helix scaffold is less dynamic on a pico-to-nanosecond time scale in the unliganded protein and only slightly changes its dynamic properties when ligand(s) are bound to the protein (helix α3: KIX S^2_{avg}=0.90, KIX·MLL: S^2_{avg}=0.92, KIX·pKID: S^2_{avg}=0.91, KIX·MLL·pKID: S^2_{avg}=0.93).

An interesting phenomenon is found for unliganded KIX. The backbone amide order parameter data display a relatively large variation for α2 helix. An oscillatory behavior of the order parameters is observed for the segment of helix α2 between residues 625-637 with lowest order parameters found for residues M625, L628, V629, K632, K633 and E636, and higher order parameters for residues in between. Of note, the more dynamic backbone amides in helix α2 of unliganded KIX are located on the side of the helix that contacts helix α1. Upon binding ligand (MLL or pKID, or both), this oscillation is lost and helix α2 displays relatively uniform order parameters in ligand bound states, suggesting a tighter packing of helices α1 and α2 compared to the unliganded KIX domain. We have previously shown that helices α1 and α2, which are conformationally less stable than helix α3, have a tendency to unfold and refold (in milliseconds) in the unliganded form of the protein.[22] This local unfolding-refolding process is suppressed if MLL or pKID are bound to the KIX domain.[16]

Taken together, the average order parameters of residues in helical segments of the KIX domain (α1- α3) increase from 0.85 in free KIX to 0.91 and 0.90 in the binary complexes KIX·MLL and KIX·pKID, respectively, suggesting significant

rigidification of the KIX backbone upon peptide binding. Unlike for the loop L12, formation of the ternary complex KIX·MLL·pKID (average order parameter in α1-α3: S^2_{avg}=0.91) is not accompanied by further rigidification of the three-helix bundle scaffold.

Isothermal calorimetric data

We conducted a mutational analysis of the KIX domain by introducing isoleucine to valine substitutions for all the three isoleucine residues I611, I657 and I660 that form part of the allosteric signal transmission pathway and characterized their affinities for MLL and pKID ligand peptides using isothermic titration calorimetry (Table 2). The three mutants displayed similar binding affinities for MLL, along with very similar circular dichroism spectra (data not shown), indicative for the structural integrity of the mutants. However, only I611V and I657V mutant proteins showed a ~2-fold higher affinity for pKID when bound to MLL, while the I660V mutant protein displayed no cooperative binding of pKID.

Discussion

NMR relaxation dispersion experiments suggest that in the binary complex formed by KIX with MLL allosteric communication between the MLL and pKID/c-Myb binding sites involves conformational selection of a ca. 7% low-populated (excited state) conformer whose structure resembles the ternary complex.[16] A comparison of binary KIX·MLL and ternary KIX·MLL·pKID complexes of KIX are shown in Figure 1. It is evident that conformational changes of the KIX backbone upon binding of pKID to the binary KIX·MLL complex are minor, which is in agreement with the small magnitude of backbone amide carbon $^{13}C\alpha$ chemical shift changes that are observed upon ligand binding.[16] However, binding of the pKID activation domain to binary KIX·MLL is accompanied by considerable re-packing of the hydrophobic core of the KIX domain (Figure 2). As a result of this conformational transition, the side chain of residue I657 flips around its chi1 dihedral angle, positioning its $\delta 1$ methyl group at the surface of the KIX domain. In the ternary complex of KIX with MLL and pKID, the I657 side chain is part of the hydrophobic groove on the surface of KIX that represents the docking interface for pKID, where Ile657 hydrophobically packs to the residues I137 and L141 of the pKID amphipathic helix αB.

It is intriguing that the hydrophobic core residues for which we observe this re-packing upon ligand binding are identical to the ones that we have previously identified to be part of the hydrophobic cluster that constitutes the allosteric network in KIX.[16] Using side chain methyl relaxation dispersion studies we found a clear correspondence between the hydrophobic core chemical shifts of ternary KIX complex and the shifts of the excited state in the binary complex of KIX with MLL. These data suggest that the re-packing of the hydrophobic core that we observe in the NMR structures of binary (KIX·MLL) and ternary (KIX·MLL·pKID) complexes, shown in Figure 2, already occurs in binary KIX·MLL (i.e. before pKID binds) during the transition between the 93% populated ground and the 7% populated excited states. The three-dimensional solution structure of KIX·MLL·pKID, and in particular the change in conformation that we observe between this structure and the structure of the complex formed with MLL alone

(KIX·MLL), thus provide a structural picture of allosteric communication between the two remote ligand binding sites in the KIX domain.

Figure 5 shows a close-up view of the KIX/pKID binding surface in the ternary complex KIX·MLL·pKID. The δ1 methyl group of KIX residue I657 is exposed to the surface of the domain and forms part of the hydrophobic pocket that accommodates the amphipathic helix αB of the ligand peptide pKID.[20] The hydrophobic side chains of two residues of pKID, I137 and L141, pack to the I657 of the KIX domain. I137 and L141 of pKID are known to be critical for the molecular recognition of ligands binding to the KIX domain: both I137 and L141 are part of the conserved ΦXXΦΦ sequence motif, where Φ is a hydrophobic residue and X is an arbitrary residue, which is characteristic for ligands that bind to KIX.[25] Any conformational change at the pKID/c-Myb hydrophobic binding groove will thus very likely modulate the efficiency with which hydrophobic contacts with ligand peptides are formed, and affect their affinities. With respect to allosteric coupling, the presence of a higher affinity (excited state) conformer, even if populated only to a low extent, can act as a driving force for the ligand binding process. Recognition and binding of peptides will predominantly occur through the higher affinity conformer, whose structure is complementary to the ligand.

Results from Peter Wright's laboratory indeed show that the complementarity of the hydrophobic interactions between the pKID binding pocket and peptide ligands plays a critical role for the affinity with which these ligands are bound to the KIX domain.[21] NMR solution structures of KIX bound to the activation domain of the transcription factor c-Myb show that the positions that are equivalent to I137 and L141 in pKID are taken by two leucine residues in c-Myb (L298 and L302, both part of the c-Myb ΦXXΦΦ motif). It is evident from the KIX·c-Myb structures that the side chain of L302 of c-Myb penetrates more deeply into the hydrophobic pocket that is formed by the KIX domain than the equivalent L141 of pKID,[20] enabling the formation of hydrophobic contacts of its methyl groups with the side chain of KIX residue L607 at the bottom of the pocket. Based on these observations it was suggested that the hydrophobic interactions between pKID and KIX are less optimal than those between pKID and c-Myb, which explains the relatively low affinity of unphosphorylated KID to KIX.[21]

Allosteric communication in the opposite direction

While our relaxation dispersion experiments in combination with the high-resolution structures presented here provide insights into the mechanism by which KIX propagates information about the presence of MLL to the c-Myb/pKID binding site, the molecular mechanism of communication in the opposite direction (from the c-Myb/pKID binding site to the MLL binding site) is not obvious.[16] The lack of significant contributions of micro-to-millisecond time scale dynamic processes to NMR spin relaxation rates indicates that either the population of any higher energy state(s) that might be present in KIX·pKID or KIX·c-Myb binary complexes is too low and/or the time scale of the process is outside the micro-to-millisecond window that can be studied by relaxation dispersion NMR.

Indeed, the NMR spin relaxation data reported here argue for a contribution of pico-to-nanosecond time scale dynamic processes to the mechanism of allosteric coupling from the c-Myb/pKID binding site to the MLL binding site. Upon binding of pKID to the KIX domain, we observe a change in pico-to-nanosecond dynamics for the KIX backbone for segments of the protein that are remote from the binding site of the peptide (Figure 6). In particular, two of the three helices (α1 and α2) of the KIX domain that form the three-helix scaffold of the protein rigidify, along with the connecting loop L12 and the N-terminus of the domain. This is contrasted by the pKID binding surface itself, which is mostly formed by residues in helix α3 and which does not display a significant change in pico-to-nanosecond time scale dynamics upon binding. The rigidification of the linker L12, which has no direct contacts with pKID, is particularly interesting, because it is believed to play a critical role for binding MLL.[10] Based on the observation of chemical shift averaging and narrow backbone amide resonances it has been suggested that the linker L12 is conformationally flexible in order to enable the interaction of this binding surface of the KIX domain with a variety of disparate ligand sequences, while in complex with MLL the conformational flexibility is reduced.[10; 20] In addition, this part of the protein is considerably displaced upon MLL binding, allowing the side chain of KIX residue F612 to form hydrophobic contacts with the MLL ligand. In light of the significance of this loop domain for binding MLL, this long range dynamic coupling between the two binding sites is likely of functional significance.

A markedly different behavior is found for MLL binding to KIX. While the presence of bound MLL significantly increases the order parameters of amino acid residues that are part of the hydrophobic MLL binding pocket (loop L12) and the helices $\alpha 1$ and $\alpha 2$ of the three-helix scaffold of the protein as well as the C-terminal end of helix $\alpha 3$, we find no significant changes of order parameters at the pKID binding site. Thus, binding of the activation domain of MLL appears to cause local rigidification, but has no long-range effect on dynamic processes on the pico-to-nanosecond time scale. Interestingly, however, the loss of flexibility on the pico-to-nanosecond time scale upon MLL binding of the L12 loop is accompanied by a significant increase of dynamics on a millisecond time scale (the allosteric conformational transition) that involves a contiguous network of residues connecting the L12 loop to the remote pKID binding site of the KIX domain.[16]

Dynamics and allostery

Dynamic allosteric coupling has been reported for a variety of proteins.[26; 27] For example, binding of cAMP to the S62F variant of the transcriptional activator CAP causes a conformational redistribution of this protein towards the active conformations.[28] Likewise, phosphorylation of the bacterial nitrogen regulatory protein C shifts the balance of populations of the different forms of this protein from the inactive to the active form,[29] and the PBX1 homeodomain transiently folds into a conformation in which the binding sites for DNA and the transcription factor Hox are pre-organized even in the absence of ligands.[30] Together with our results for the KIX domain of CBP, these data underscore the mechanistic significance of dynamic equilibria for allosteric regulation and ligand recognition. Of note, such population shift mechanisms enable the modulation of binding affinities in a versatile manner by the extent to which the higher affinity conformer is populated, as well as by the difference in binding affinites of the different conformers.

It is tempting to speculate about the structural pre-requisites for dynamic allosteric coupling. Intriguingly, the hydrophobic core of the KIX domain displays a non-uniform distribution of aromatic and aliphatic residues: The part of the hydrophobic core that constitutes the allosteric network of the domain is formed by predominantly non-aromatic residues and contains mostly ioleucines, leucines, valines and alanines, while the adjacent part of the hydrophobic core that is located between the N-terminal half of helices $\alpha 1$ and $\alpha 3$ and the C-terminus of helix $\alpha 2$ comprises a cluster of aromatic residues. It thus seems aliphatic side chains may be more amenable to hydrophobic re-packing processes than aromatic side-chains. In addition, sequence comparison of KIX domains show that residues that form to aliphatic hydrophobic core are conserved to a higher level than the ones that are located in the aromatic hydrophobic, arguing for an evolutionary conservation of functional dynamics.[31; 32]

Materials and methods

Sample Preparation

Unlabeled, 10% ^{13}C-labeled, uniformly ^{13}C- and/or ^{15}N-labeled samples of the KIX domain (residues 586-672) of human CBP were prepared by bacterial growth in standard LB and M9 minimal media and purified as described [33]. KIX I611V, I657V and I660V mutants were generated using the Stratagene QuickChange II Site-Directed Mutagenesis Kit. The unlabeled mutant proteins were overexpressed and purified according to the same protocol established for wild-type KIX. Structural integrity of the mutant proteins was verified by circular dichroism (CD) and NMR spectroscopy.

Uniformly ^{13}C, ^{15}N-labeled MLL samples (residues 2840-2858; Cys2841 substituted through an Ala) were overexpressed in *Escherichia coli* as a N-terminal fusion to a hexa-histidine tagged MBP. The cells were grown at 37 °C in M9 minimal media containing ^{15}NH$_4$Cl and ^{13}C-glucose as sole nitrogen and carbon sources, in presence of kanamycin until OD$_{600}$≈0.6 then the temperature was lowered to 28 °C and after 30 minutes protein synthesis was induced by adding isopropyl-β-d-thiogalactopyranoside (IPTG) to a final concentration of 0.8 mM. The cells were harvested 5 hours after induction and resuspended in lysis buffer containing 20 mM Tris-HCl (pH 7.5), 250 mM NaCl, 10 mM imidazole and 5 mM β-mercaptoethanol. The cells were lysed using a French pressure cell and clarified by centrifugation. Subsequently, the supernatant was loaded onto a HisTrap FF crude (GE Healthcare) column. In the next step the MBP-MLL fusion protein was applied to a Superdex 75 (GE Healthcare) equilibrated with cleavage buffer that contained 50 mM Tris-HCl (pH 7.5), 0.5 mM EDTH and 2 mM DTT. The His-tagged MBP was cleaved by incubation with TEV, and it was removed using nickel affinity chromatography. In the final step, MLL was purified to homogeneity by size exclusion chromatography using a Superdex 30 (GE Healthcare). Mass spectrometry was used to conform the identity of MLL. For ITC measurements unlabeled MLL peptide (residue 116-149) was purchased from PSL (Heidelberg, Germany).

The human KID domain of CREB (residues 116-149) was prepared as a N-terminal fusion to a hexa-histidine tagged thioredoxin. Uniformly ^{13}C, ^{15}N-labeled samples for NMR studies were prepared by growing E. coli cells in M9 minimal media containing $^{15}NH_4Cl$ and ^{13}C-glucose as sole nitrogen and carbon sources at 37 °C. Protein overexpression was induced at $OD_{600} \approx 0.8$ by adding IPTC to a final concentration of 0.7 mM. Cells were harvested after 5 h and trx-KID purification followed the same 3-step procedure as established for MBP-MLL. Ser133 of KID was phosphorylated *in vitro* by incubation of 60μM purified KID with 0.05 μM PKA catalytic subunit, 1 mM ATP in a 25 mM Tris-HCl (pH 7) buffer containing 10 mM $MgCl_2$ and 2 mM DTT for 24 h at 30°C. pKID was purified by size exclusion chromatography using a Superdex 30 (GE Healthcare). Mass spectrometry was used to confirm that pKID was fully phosphorylated. For ITC measurements the unlabeled pKID peptide (residue 2840-2858) was purchased from PSL (Heidelberg, Germany).

Isothermal titration calorimetry

All ITC measurements were preformed at 27 °C in 50mM potassium phosphate (pH 5.8), 25 mM NaCl and 1 mM NaN_3 using an iTC_{200} (MicroCal). After an initial injection of 0.5 μl, 24 injections of 1.5 μl pKID or MLL were dispensed into the sample cell. Wild-type and mutant KIX domains I611V, I657V and I660V (80 μM) were titrated with pKID (~600 μM) and MLL (~1000 μM) stock solutions. pKID (~600 μM) was titrated to the binary wild-type and mutant KIX·MLL complexes (80 μM, MLL saturation >95%) using the same stock solutions as for unliganded KIX measurements. All experiments were recorded three times. The experimental binding isotherms were fitted to a one-site binding model using the MicroCal Origin software.

CD measurements

CD spectra of wild-type and mutant KIX domains (30 μM) were recorded at 27 °C in a buffer containing 50mM potassium phosphate (pH5.8), 25 mM NaCl and 1 mM NaN_3. The melting curve was determined, from 10 °C to 90 °C in 5 °C steps, by monitoring the circular dichroism signal at 222 nm. The melting temperature T_m was determined by fitting the sigmoidal melting curve to a Boltzmann equation [34] using Origin software.

NMR spectroscopy

NMR spectra were recorded at 27 °C on Varian Inova 500, 800 MHz and Varian Direct Drive 600 MHz spectrometers. Data were processed using NMRPipe [35] and analyzed using CcpNmr.[36] NMR samples contained 1 mM of labeled protein or peptide, unlabeled ligands in at least 2-fold excess, 50 mM potassium phosphate buffer, pH 5.8, 25 mM NaCl and 1 mM NaN_3 in 10% D_2O/90% H_2O. Backbone and side chain ^1H, ^{13}C, ^{15}N chemical shift assignments of KIX (unliganded KIX, KIX·MLL and KIX·MLL·pKID), pKID and MLL were obtained using standard triple-resonance experiments: HNCA/HN(CO)CA, HNCO/HN(CA)CO, CBCA(CO)NH/HNCACB, ^{15}N-edited TOCSY-HSQC, (H)CCONH-TOCSY and HCCH-TOCSY. For KIX (unliganded KIX, KIX·MLL and KIX·MLL·pKID), stereospecific assignment of the prochiral methyl groups of Val and Leu were obtained using the 10% fractional labeling method of Neri et al.[37] Intramolecular distance restraints for KIX (KIX, KIX·MLL and KIX·MLL·pKID), MLL and pKID were obtained from 3D ^1H-^1H-NOESY ^{15}N/^{13}C-HSQC experiments. For KIX (KIX, KIX·MLL and KIX·MLL·pKID), additional intramolecular distance restraints were obtained from 3D ^{13}C, ^{13}C methyl NOESY experiments.[38] Intermolecular distance restraints were obtained from a ω_1-^{13}C-filtered simultaneous inter-intramolecular three-dimensional ^1H-^1H NOESY-^{13}C-HSQC experiment.[39]

RDCs of KIX (KIX, KIX·MLL and KIX·MLL·pKID) and pKID were measured on samples partially aligned using strain-induced alignment in a 4% polyacrylamide gel.[40] HN-N RDCs ($^1D_{1H, 15N}$) were measured using an in-phase/anti-phase (IPAP) ^1H, ^{15}N HSQC experiment [41] or a 3D best-type HNCO experiment.[42]

Relaxation measurements and analysis

Heteronuclear ^1H, ^{15}N NOE, rotating-frame longitudinal relaxation time $T_{1\rho}$ and the longitudinal relaxation time T_1 were measured for KIX in the following states KIX, KIX·MLL, KIX·PKID and KIX·MLL·pKID, at 27°C at 800 MHz. The heteronuclear ^1H, ^{15}N NOE was obtained by recording, in an interleaved manner, one spectrum with a delay of 2 s followed by proton saturation for 3 s and another spectrum with a delay of 5 s without proton saturation. Relaxation delays of 10.9 ms, 54.4 ms, 108.9 ms, 217.6 ms, 326.4 ms, 435.2 ms, 598.4 ms and 707.2 ms were used for T1 experiments and delays of 10.0 ms, 20.0 ms, 30.0 ms, 40.0 ms, 60.0 ms, 80.0 ms, and 100.0 ms for the $T_{1\rho}$ measurements. The spherical diffusion tensor was

determined by the method of Brüschweiler *et al.*[43] using the program quadric_diffusion.[44] The internal dynamics and overall tumbling were fit with the program FAST-ModelFree.[45]

Structure calculations and refinement

Backbone dihedral angle restraints were set to ϕ = −60(±10)° and ψ = −45(±10)° for residues that were predicted to be α-helical, based on $^{13}C\alpha$, $^{13}C\beta$, $^{13}C'$, $^{1}H\alpha$, ^{15}N and ^{1}HN, using the software Talos plus.[46] Distance restraints derived from the 3D ^{13}C, ^{13}C methyl NOESY experiments were all set to an upper bond of 5.5 Å. All other intra- and intermolecular distance restraints were calibrated using the Aria2.3 program.[47] An initial structural ensemble was used to determine the alignment tensor of KIX and pKID using the PALES software.[48] The experimentally determined distance, dihedral angle and dipolar coupling restraints were used in a torsion angle simulated annealing protocol using CNS1.2/Aria2.3 [47; 49] to solve the solution structure of KIX, the binary KIX·MLL complex and the ternary KIX·MLL·pKID complex. The final NMR ensembles were refined in an explicit water shell.[50] The 20 lowest-energy solution structures (out of 100 calculated) were selected as a final representative ensemble of KIX, KIX·MLL and KIX·MLL·pKID.

Acknowledgements

References

1. Carey, M. (1998). The enhanceosome and transcriptional synergy. *Cell* **92**, 5-8.

2. Panne, D. (2008). The enhanceosome. *Curr. Opin. Struct. Biol.* **18**, 236-242.

3. Ptashne, M. & Gann, A. (1997). Transcriptional activation by recruitment. *Nature* **386**, 569-577.

4. Lemon, B. & Tjian, R. (2000). Orchestrated response: a symphony of transcription factors for gene control. *Genes Dev* **14**, 2551-69.

5. Goodman, R. H. & Smolik, S. (2000). CBP/p300 in cell growth, transformation, and development. *Genes Dev* **14**, 1553-1577.

6. Kornberg, R. D. (2005). Mediator and the mechanism of transcriptional activation. *Trends. Biochem. Sci.* **30**, 235-239.

7. Merika, M. & Thanos, D. (2001). Enhanceosomes. *Curr Opin Genet Dev* **11**, 205-208.

8. Vo, N. & Goodman, R. H. (2001). CREB-binding protein and p300 in transcriptional regulation. *J Biol Chem* **276**, 13505-13508.

9. Dyson, H. J. & Wright, P. E. (2005). Intrinsically unstructured proteins and their functions. *Nat Rev Mol Cell Biol* **6**, 197-208.

10. De Guzman, R. N., Goto, N. K., Dyson, H. J. & Wright, P. E. (2006). Structural basis for cooperative transcription factor binding to the CBP coactivator. *J Mol Biol* **355**, 1005-1013.

11. Yang, F., Vought, B. W., Satterlee, J. S., Walker, A. K., Jim Sun, Z. Y., Watts, J. L., DeBeaumont, R., Saito, R. M., Hyberts, S. G., Yang, S., Macol, C., Iyer, L., Tjian, R., van den Heuvel, S., Hart, A. C., Wagner, G. & Naar, A. M. (2006). An ARC/Mediator subunit required for SREBP control of cholesterol and lipid homeostasis. *Nature* **442**, 700-704.

12. Thakur, J. K., Arthanari, H., Yang, F., Pan, S. J., Fan, X., Breger, J., Frueh, D. P., Gulshan, K., Li, D. K., Mylonakis, E., Struhl, K., Moye-Rowley, W. S., Cormack, B. P., Wagner, G. & Naar, A. M. (2008). A nuclear receptor-like pathway regulating multidrug resistance in fungi. *Nature* **452**, 604-609.

13. Ernst, P., Wang, J., Huang, M., Goodman, R. H. & Korsmeyer, S. J. (2001). MLL and CREB bind cooperatively to the nuclear coactivator CREB-binding protein. *Mol Cell Biol* **21**, 2249-2258.

14. Goto, N. K., Zor, T., Martinez-Yamout, M., Dyson, H. J. & Wright, P. E. (2002). Cooperativity in transcription factor binding to the coactivator CREB-binding protein (CBP). *J Biol Chem* **277**, 43168-43174.

15. Cheng, X., Reginato, M. J., Andrews, N. C. & Lazar, M. A. (1997). The transcriptional integrator CREB-binding protein mediates positive cross talk between nuclear hormone receptors and the hematopoietic bZip protein p45/NF-E2. *Mol. Cell Biol.* **17**, 1407-1416.

16. Bruschweiler, S., Schanda, P., Kloiber, K., Brutscher, B., Kontaxis, G., Konrat, R. & Tollinger, M. (2009). Direct observation of the dynamic

process underlying allosteric signal transmission. *J Am Chem Soc* **131**, 3063-8.

17. Tsai, C. J., Kumar, S., Ma, B. & Nussinov, R. (1999). Folding funnels, binding funnels, and protein function. *Protein Sci* **8**, 1181-1190.

18. Weber, G. (1972). Ligand binding and internal equilibria in proteins. *Biochemistry* **11**, 864-878.

19. Tobi, D. & Bahar, I. (2005). Structural changes involved in protein binding correlate with intrinsic motions of proteins in the unbound state. *Proc. Natl. Acad. Sci. USA* **102**, 18908-18913.

20. Radhakrishnan, I., Perez-Alvarado, G. C., Parker, D., Dyson, H. J., Montminy, M. R. & Wright, P. E. (1997). Solution structure of the KIX domain of CBP bound to the transactivation domain of CREB: a model for activator:coactivator interactions. *Cell* **91**, 741-752.

21. Zor, T., De Guzman, R. N., Dyson, H. J. & Wright, P. E. (2004). Solution structure of the KIX domain of CBP bound to the transactivation domain of c-Myb. *J Mol Biol* **337**, 521-534.

22. Schanda, P., Brutscher, B., Konrat, R. & Tollinger, M. (2008). Folding of the KIX domain: characterization of the equilibrium analog of a folding intermediate using ^{15}N/^{13}C relaxation dispersion and fast ^{1}H/^{2}H amide exchange NMR spectroscopy. *J Mol Biol* **380**, 726-741.

23. Radhakrishnan, I., Perez-Alvarado, G. C., Parker, D., Dyson, H. J., Montminy, M. R. & Wright, P. E. (1999). Structural analyses of CREB-CBP transcriptional activator-coactivator complexes by NMR spectroscopy: implications for mapping the boundaries of structural domains. *J Mol Biol* **287**, 859-65.

24. Mittermaier, A. & Kay, L. E. (2006). New tools provide new insights in NMR studies of protein dynamics. *Science* **312**, 224-228.

25. Plevin, M. J., Mills, M. M. & Ikura, M. (2005). The LxxLL motif: a multifunctional binding sequence in transcriptional regulation. *Trends Biochem Sci* **30**, 66-9.

26. Swain, J. F. & Gierasch, L. M. (2006). The changing landscape of protein allostery. *Curr Opin Struct Biol* **16**, 102-108.

27. Kern, D. & Zuiderweg, E. R. (2003). The role of dynamics in allosteric regulation. *Curr Opin Struct Biol* **13**, 748-757.

28. Tzeng, S. R. & Kalodimos, C. G. (2009). Dynamic activation of an allosteric regulatory protein. *Nature* **462**, 368-72.

29. Volkman, B. F., Lipson, D., Wemmer, D. E. & Kern, D. (2001). Two-state allosteric behavior in a single-domain signaling protein. *Science* **291**, 2429-2433.

30. Farber, P. J. & Mittermaier, A. (2011). Concerted dynamics link allosteric sites in the PBX homeodomain. *J Mol Biol* **405**, 819-30.

31. Lockless, S. W. & Ranganathan, R. (1999). Evolutionarily conserved pathways of energetic connectivity in protein families. *Science* **286**, 295-299.

32. Süel, G. M., Lockless, S. W., Wall, M. A. & Ranganathan, R. (2003). Evolutionarily conserved networks of residues mediate allosteric communication in proteins. *Nat Struct Biol* **10**, 59-69.

33. Tollinger, M., Kloiber, K., Agoston, B., Dorigoni, C., Lichtenecker, R., Schmid, W. & Konrat, R. (2006). An isolated helix persists in a sparsely populated form of KIX under native conditions. *Biochemistry* **45**, 8885-8893.

34. Niesen, F. H., Berglund, H. & Vedadi, M. (2007). The use of differential scanning fluorimetry to detect ligand interactions that promote protein stability. *Nat Protoc* **2**, 2212-21.

35. Delaglio, F., Grzesiek, S., Vuister, G. W., Zhu, G., Pfeifer, J. & Bax, A. (1995). NMRPipe: a multidimensional spectral processing system based on UNIX pipes. *J Biomol NMR* **6**, 277-93.

36. Vranken, W. F., Boucher, W., Stevens, T. J., Fogh, R. H., Pajon, A., Llinas, M., Ulrich, E. L., Markley, J. L., Ionides, J. & Laue, E. D. (2005). The CCPN data model for NMR spectroscopy: development of a software pipeline. *Proteins* **59**, 687-96.

37. Neri, D., Szyperski, T., Otting, G., Senn, H. & Wuthrich, K. (1989). Stereospecific nuclear magnetic resonance assignments of the methyl groups of valine and leucine in the DNA-binding domain of the 434 repressor by biosynthetically directed fractional 13C labeling. *Biochemistry* **28**, 7510-6.

38. Zwahlen, C., Gardner, K. H., Sarma, S. P., Horita, D. A., Byrd, R. A. & Kay, L. E. (1998). An NMR experiment for measuring methyl-methyl NOEs in C-13-labeled proteins with high resolution. *J Am Chem Soc* **120**, 7617-7625.

39. Eichmuller, C., Schuler, W., Konrat, R. & Krautler, B. (2001). Simultaneous measurement of intra- and intermolecular NOEs in differentially labeled protein-ligand complexes. *J Biomol NMR* **21**, 107-16.

40. Chou, J. J., Gaemers, S., Howder, B., Louis, J. M. & Bax, A. (2001). A simple apparatus for generating stretched polyacrylamide gels, yielding uniform alignment of proteins and detergent micelles. *J Biomol NMR* **21**, 377-82.

41. Ottiger, M., Delaglio, F. & Bax, A. (1998). Measurement of J and dipolar couplings from simplified two-dimensional NMR spectra. *J Magn Reson* **131**, 373-8.

42. Ortega-Roldan, J. L., Jensen, M. R., Brutscher, B., Azuaga, A. I., Blackledge, M. & van Nuland, N. A. (2009). Accurate characterization of weak macromolecular interactions by titration of NMR residual dipolar couplings: application to the CD2AP SH3-C:ubiquitin complex. *Nucleic Acids Res* **37**, e70.

43. Bruschweiler, R., Liao, X. & Wright, P. E. (1995). Long-range motional restrictions in a multidomain zinc-finger protein from anisotropic tumbling. *Science* **268**, 886-9.

44. Lee, L. K., Rance, M., Chazin, W. J. & Palmer, A. G., 3rd. (1997). Rotational diffusion anisotropy of proteins from simultaneous analysis of 15N and 13C alpha nuclear spin relaxation. *J Biomol NMR* **9**, 287-98.

45. Cole, R. & Loria, J. P. (2003). FAST-Modelfree: a program for rapid automated analysis of solution NMR spin-relaxation data. *J Biomol NMR* **26**, 203-13.

46. Shen, Y., Delaglio, F., Cornilescu, G. & Bax, A. (2009). TALOS+: a hybrid method for predicting protein backbone torsion angles from NMR chemical shifts. *J Biomol NMR* **44**, 213-23.

47. Rieping, W., Habeck, M., Bardiaux, B., Bernard, A., Malliavin, T. E. & Nilges, M. (2007). ARIA2: automated NOE assignment and data integration in NMR structure calculation. *Bioinformatics* **23**, 381-2.

48. Zweckstetter, M., Hummer, G. & Bax, A. (2004). Prediction of charge-induced molecular alignment of biomolecules dissolved in dilute liquid-crystalline phases. *Biophys J* **86**, 3444-60.

49. Brunger, A. T. (2007). Version 1.2 of the Crystallography and NMR system. *Nat Protoc* **2**, 2728-33.

50. Linge, J. P., Williams, M. A., Spronk, C. A., Bonvin, A. M. & Nilges, M. (2003). Refinement of protein structures in explicit solvent. *Proteins* **50**, 496-506.
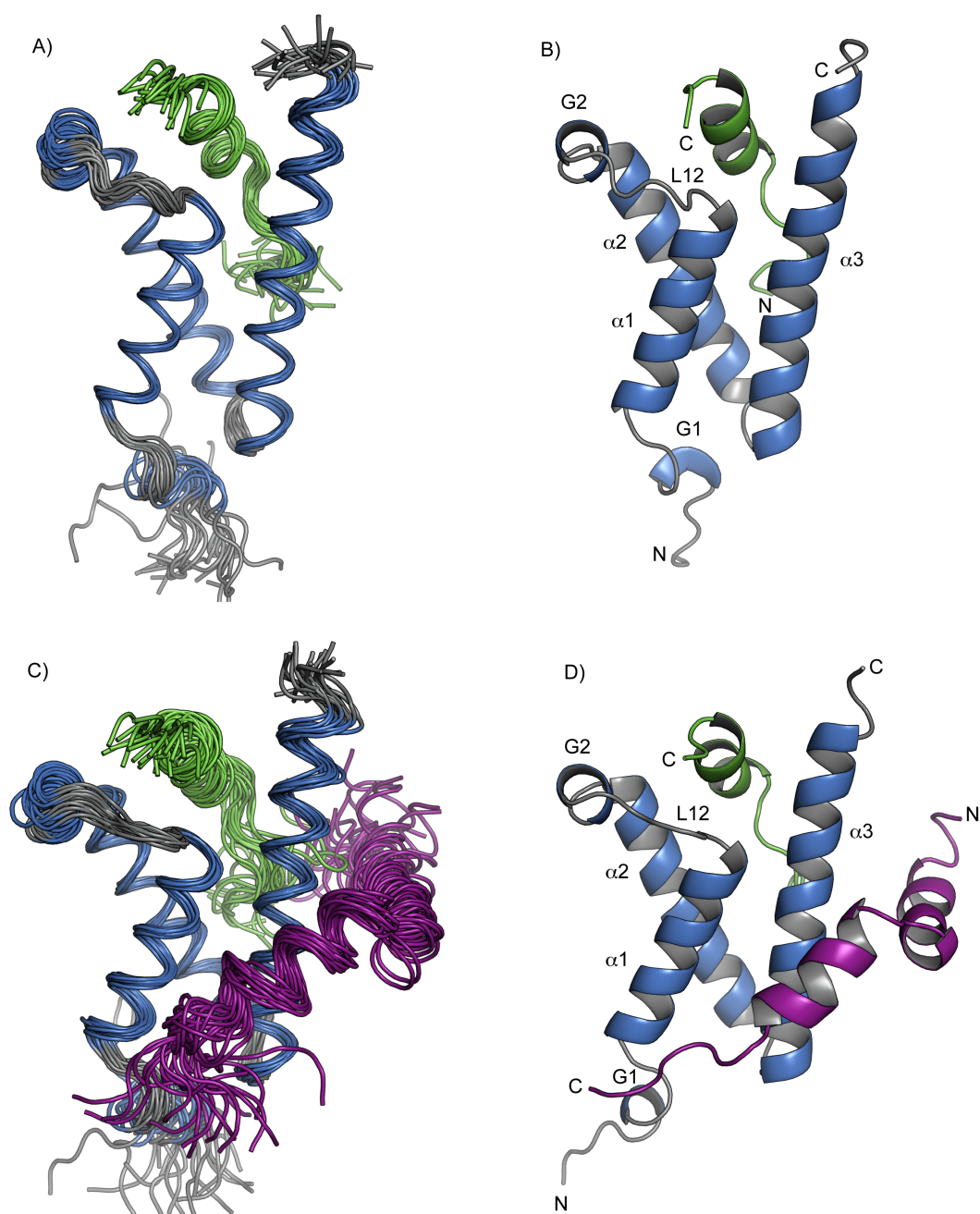
Figure 1

Solution structures of binary and ternary complexes of KIX. (a) NMR ensemble of 20 representative structures of KIX in complex with MLL. Secondary structure elements are labeled as suggested by Radhakrishnan et al.[20] and color coded (KIX: helices: blue, loops: grey, MLL: green). (b) Lowest energy structure of KIX·MLL, helices are displayed as ribbons. (c) NMR ensemble of 20 representative structures of KIX in complex with MLL (residues 2840-2858) and pKID (residues 116-149).

Secondary structure elements are color coded as in panel A (with pKID shown in magenta). (d) Lowest energy structure of KIX·MLL·pKID. All panels were generated using pymol.
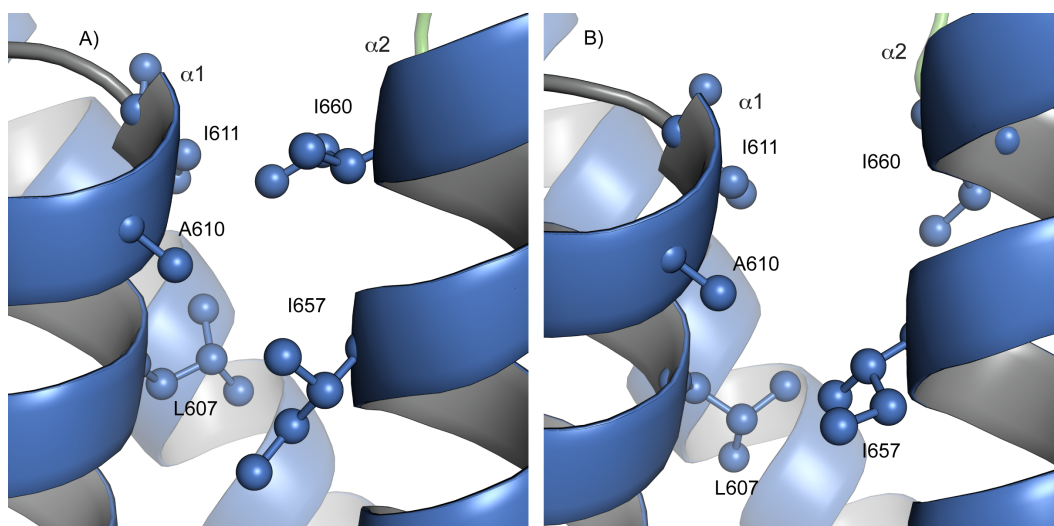
Figure 2

Close-up view of the hydrophobic core formed by residues L607, A610, I611, I657 and I660 in KIX·MLL (left) and KIX·MLL·pKID (right).
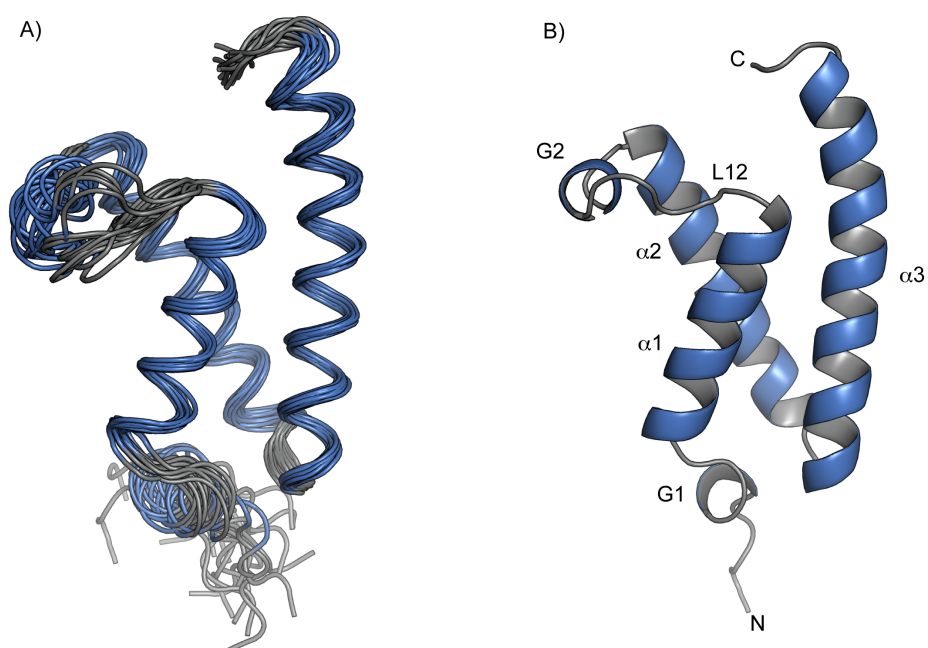
Figure 3

NMR ensemble of 20 representative structures of KIX. Color coding as in Figure 1.
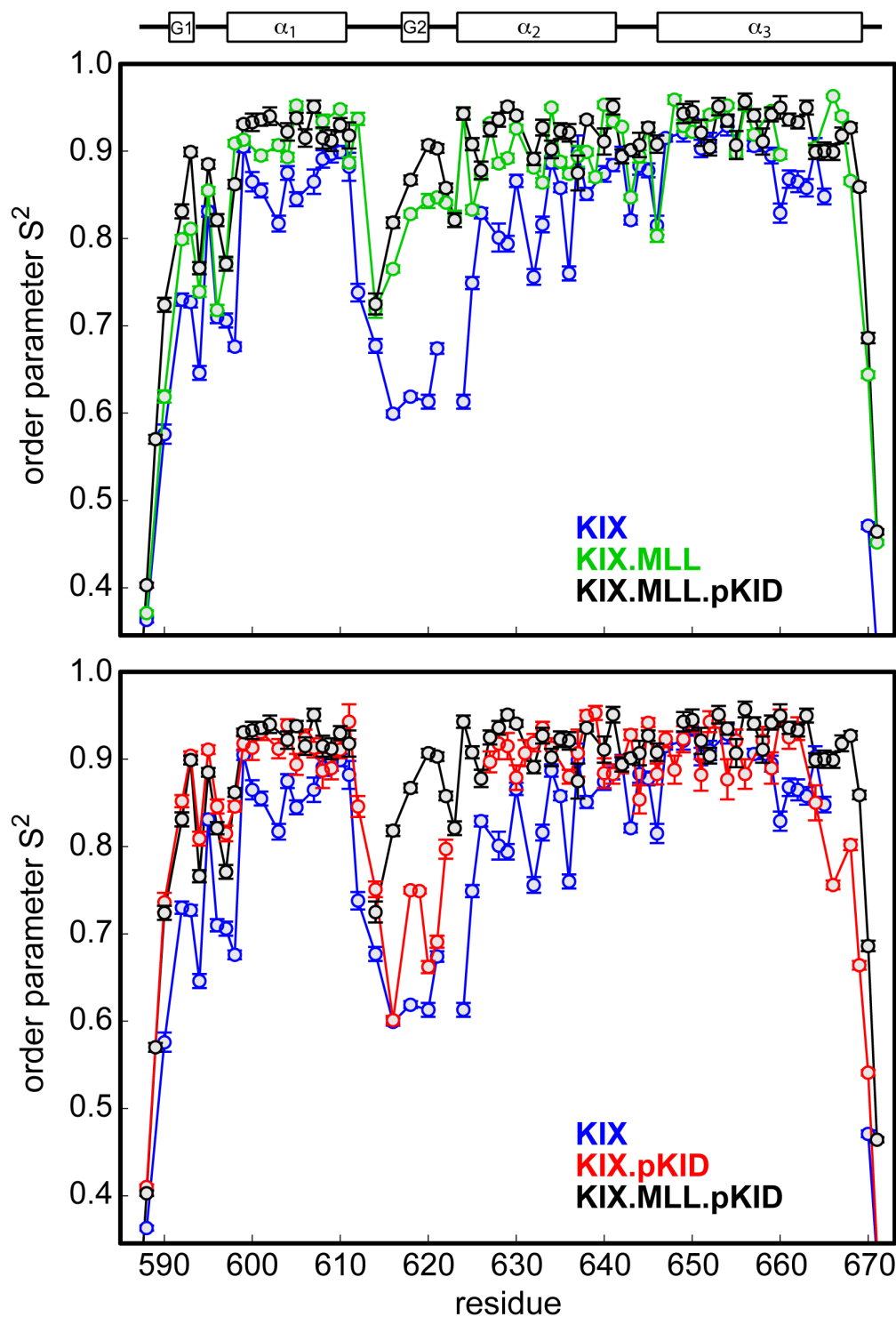
Figure 4

Comparison of backbone amide order parameters S^2 in (a) KIX (blue), binary KIX·MLL (green) and ternary KIX·MLL·pKID (black) and (b) KIX (blue), binary KIX·pKID (red) and ternary KIX·MLL·pKID (black). Error bars are shown and lines between data points are drawn unless in cases where S^2 could not be determined due to resonance overlap for 2 or more consecutive backbone amides.
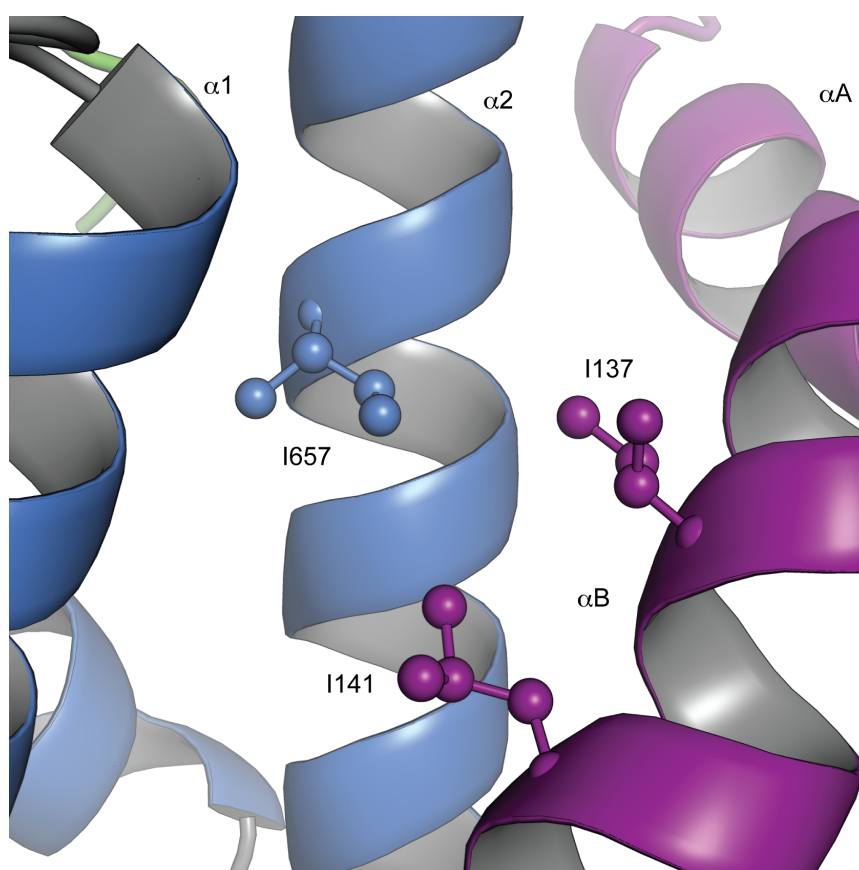
Figure 5

Close-up view of the solution structure of the ternary complex KIX·MLL·pKID showing the interaction surface of the KIX domain with the pKID peptide. The backbone of the KIX domain is displayed as blue ribbon, along with the side chain heavy atoms of I657 (blue spheres). The pKID backbone (magenta ribbon) and the side chains of pKID residues I137 and L141 (magenta spheres) which interact with the hydrophobic side chain of I657 are displayed.
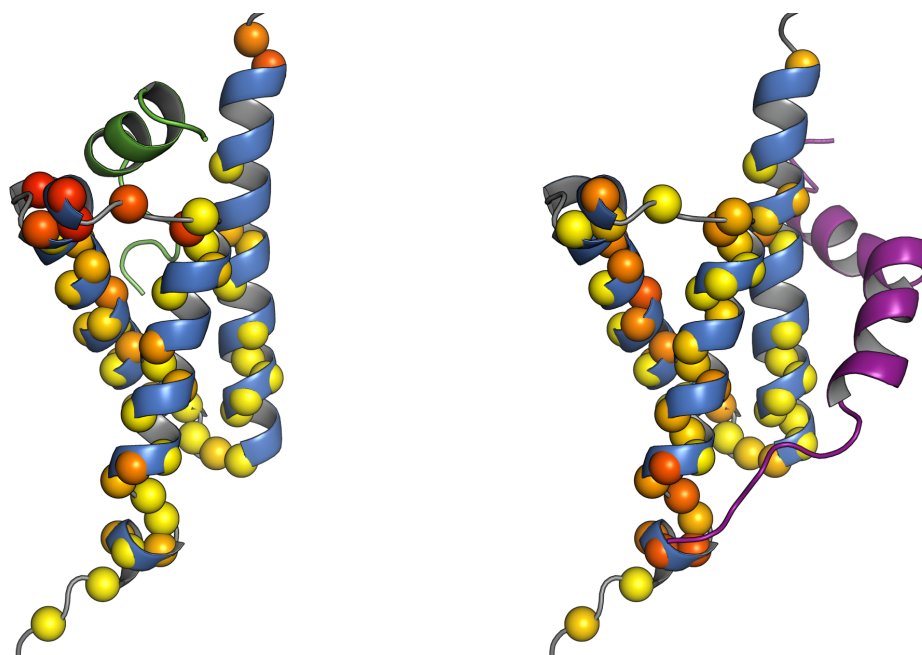
Figure 6

Effect of ligand binding on pico-to-nanosecond dynamics of the KIX domain. (A) Ribbon representation showing the increase in order parameters that is observed upon binding of the MLL peptide to KIX. Backbone amide nitrogens of KIX (residues 586-672) are displayed as spheres and color coded according to the difference in order parameters, ΔS^2, between KIX·MLL and KIX (red: $\Delta S^2 = 0.3$, linearly interpolated to yellow: $\Delta S^2 = 0$). Only nitrogens for which data in both KIX and KIX·MLL are available are shown. The structured part of MLL (residues 2840-2858) is shown in green. (B) Ribbon representation showing the increase in order parameters upon binding of the pKID peptide to KIX (color coding as in (A)).

	KIX	KIX.MLL	KIX.MLL.pKID
NMR restraints			
Distance restraints			
Total NOE	602	1052	983
Intra-residue	323	461/84	322/84/93
Inter-residue	279		
Sequential ($|i-j| = 1$)	160	250/34	190/34/59
Medium-range ($|i-j| \leq 4$)	70	125/3	78/3/13
Long-range ($|i-j| \geq 5$)	49	71	54/0/0
Intermolecular restraints		24	24/29
Total dihedral restraints	156	184	225
ϕ	78	78/13	78/13/20
ψ	78	78/13	78/13/21
Total $^1D_{1H-15N}$ RDCs	48	80/0	79/0/21
Structure statistics			
Violations (RMSD and S.D.)			
Distance restraints	0.026±0.002	0.018±0.001	0.021±0.002
Dihedral restraints	3.15± 1.59	3.3±1.52	2.7±1.14
$^1D_{1H-15N}$ RDCs	0.77±0.057	0.77±0.042	1.05±0.17
Deviation from idealized geometry			
Bond lengths (Å)	0.0038±0.0002	0.0040±0.0001	0.0041±0.0001
Bond angles (°)	0.55±0.02	0.55±0.02	0.61±0.02
Ramachandran statistics[a]			
Residues in most favored regions	91.0%	93.4%	91.7%
Residues in additional allowed regions	8.8%	6.6%	6.9%
Residues in generously allowed regions	0.1%	0.0%	1.4%
Residues in disallowed regions	0.1%	0.0%	0.0%
Average pairwise r.m.s. deviation (Å)			
Heavy atoms (2° struct)	1.18±0.11	0.77±0.08	1.23±0.12
Backbone atoms (2° struct)	0.44±0.11	0.39±0.07	0.63±0.10
Heavy atoms (all residues)	2.20±0.48	1.87±0.64	2.40±0.74
Backbone (all residues)	1.80±0.92	1.66±1.10	2.10±1.13

[a] Ramachadran statistics were obtained using the PROCHECK NMR software.

Table 1

NMR restraints and structural statistics for KIX·MLL, KIX·MLL·pKID and KIX.

Ligand	Binding to	K_d [µM]
pKID	KIX	4.1±0.5
pKID	KIX·MLL	2.28±0.05
pKID	KIXI611V	6.8±0.3
pKID	KIXI611V·MLL	3.0±0.2
pKID	KIXI657V	4.5±0.3
pKID	KIXI657V·MLL	2.0±0.2
pKID	KIXI660V	2.80±0.06
pKID	KIXI657V·MLL	3.6±0.3
MLL	KIX	2.74±0.04
MLL	KIXI611V	8.5±0.5
MLL	KIXI657V	2.9±0.2
MLL	KIXI660V	5.8±0.8

Table 2

Isothermal calorimetric data.

Summary – Zusammenfassung

Article I & III:

English: Allosteric regulation of protein function is a common and effective control mechanism in biological processes. Cooperativity plays a central role for the regulation of gene transcription. The KIX domain of the transcriptional co-activator CREB binding protein (CBP) cooperatively binds transcription factors. Binding of MLL to one surface of the KIX domain enhances binding of c-Myb or pKID to the second, remote binding site of the protein and vice versa. Our NMR spin relaxation studies revealed that binding the activation domain of MLL induces the formation of a low-populated (excited) conformer of KIX that resembles the conformation of the protein in the presence of the second ligand. Titration experiments showed that this excited conformational sub-state of KIX·MLL, which is populated to 7% in the KIX·MLL binary complex, displays a higher affinity for c-Myb/pKID than the 93% populated ground state of the protein complex. These results suggest that binding of c-Myb/pKID involves the selection of the higher-energy conformer, whose structure is complementary to the ligand, from a pre-existing ensemble of conformations, in agreement with the conformational selection mechanism of ligand recognition.

By solving the solution structures of the binary complex formed by KIX bound to the activation domain of MLL and the ternary complex of KIX bound to MLL and pKID we could show that binding of the pKID activation domain to binary KIX·MLL is accompanied by considerable re-packing of the hydrophobic core of the KIX domain. The $\delta 1$ methyl group of I657 is positioned at the surface of the KIX domain in the ternary complex, hydrophobically packing to the residues I137 and L141 of the pKID amphipathic helix αB. For the binary KIX·c-Myb/pKID complex we obtained flat relaxation dispersion curves either because the population of any higher energy state(s) that might be present is too low and/or the time scale of the process is outside the micro-to-millisecond window. However, we could show that rather pico-to-nanosecond time scale dynamic processes contribute to the mechanism of allosteric coupling from the c-Myb/pKID binding site to the MLL binding site. Upon binding of pKID to the KIX domain, we observed a change in pico-to-nanosecond dynamics for the KIX backbone in particular, helices α1 and α2 of the KIX domain rigidified, along with the connecting loop L12 and the N-terminus of the domain. The rigidification of the linker L12, which has no direct contacts with pKID, is particularly interesting, because it is directly involved in MLL binding.

Deutsch: Allostrische Regulation von Proteinfunktionen ist einer von der Natur häufig und effektiv eingesetzter Kontrollmechanismus für biologische Prozesse. Kooperativität kommt bei der Regulation von Gentranskription eine entscheidende Rolle zu. Die KIX Domäne des Transkriptionscoaktivators CREB Binding Protein (CBP) bindet Transkriptionsfaktoren kooperativ. Das Binden eines Transkriptionsfaktors MLL an einer der beiden Bindungsstellen der KIX Domäne führt zur erhöhten Affinität des zweiten Liganden pKID oder c-Myb an einer zweiten, räumlich entfernten Bindungsstelle. Unsere Relaxations-Dispersions Messungen mittels Kernresonanzspektroskopie zeigen, dass das Binden der Aktivierungsdomäne von MLL die Ausbildung einer zweiten, niedrig populierten Proteinkonformation, einem sogenannten angeregten Zustand induziert. Mittels Titrationsexperimenten zeigten wir, dass der angeregte Zustand des binären KIX·MLL, welcher zu 7% populiert ist, eine höhere Affinität für die Liganden pKID/c-Myb aufweist als der zu 93% populierte Grundzustand des binären Komplexes. Diese Resultate weisen darauf hin, dass c-Myb und pKID den angeregten Zustand aus dem Ensemble selektieren, da seine Konformation bereits dem ternären Komplex entspricht. Dies ist in Übereinstimmung mit dem Konformations-Selektions Modell, welches die Ligandenerkennung eines Proteins beschreibt. Durch die Bestimmung der Proteinstrukturen des binären KIX Komplexes mit MLL und des ternären KIX Komplexes mit MLL und pKID in wässriger Lösung konnten wir zeigen, dass das Binden von pKID an den binären KIX·MLL Komplex zu einer definierten konformationellen Umlagerung des hydrophoben Kern führt. Die δ1 Methylgruppe von I657 wird im ternären Komplex an der Oberfläche der KIX Domäne positioniert und kann dadurch hydrophobe Wechselwirkungen mit I137 und L141 der amphipathischen αB Helix von pKID eingehen.

Für den binären KIX·c-Myb/pKID Komplex ergaben unsere Relaxations-Dispersions Messungen ausschließlich flache Dispersionskurven. Dies kann zwei mögliche Ursachen haben: Entweder ist der angeregte Zustand nicht ausreichend populiert und/oder der Austausch geschieht nicht auf der Mikro- zu Millisekunden Zeitskala. Allerdings konnten wir zeigen, dass stattdessen Prozesse auf der Piko- zu Nanosekunden Zeitskala zum Mechanismus der allosterischen Kopplung zwischen der c-Myb/pKID Bindungsstelle und MLL Bindungsstelle beitragen. Nach dem Binden von pKID konnten wir eine Reduktion in der Pico- zu Nanosekunden Dynamik der Helix α1, α2, einschließlich des L12 Loops und des N-Terminus der KIX Domäne messen. Die Abnahme der Flexibilität des L12 Loop ist von besonderem Interesse da er direkt an der MLL Bindung involviert ist.

Article II:

English: It is known that proteins that are ionized and transferred to the gas phase using ESI the solution structure is retained as a metastable conformation at least on the milliseconds timescale. Using Fourier-transform ion cyclotron resonance mass spectrometry (FT-ICR MS) we were able to show that the solution structure of the KIX domain of the transcriptional co-activator CBP is substantially preserved in the gas phase for at least 4 s. ESI ionization produces protein ions of the form $[M+n\,\mathrm{H}]^{n+}$, these KIX ions were fragmentized using ECD. Different ion states (n=7-16) showed different amounts of fragmentation. For the 7+ ions only fragments of the unstructured N-terminus of KIX were observed. Little fragmentation was observed for the n=8-9 states, although the N-termini of helix α1 and α2 start to unravel. Unraveling of helix α3 and separation of all three helices becomes evident from our ECD data for the 10+ ions. Further increased ion charge leads to a fragmentation pattern largely unselective to the backbone cleavage site indicative for an unfolded protein. This order of helix stability (α3 > α2 > α1) in the gas phase is similar to the helix stability in solution.

Deutsch: Es ist bekannt dass Proteine welche mittels ESI ionisiert und verdampft werden ihre Lösungsstruktur als metastabile Konformation auf zumindest der Millisekunden Zeitskala beibehalten. Unter Verwendung von FT-ICR MS konnten wir zeigen dass die Lösungsstruktur der KIX Domäne des Transkriptionscoaktivators CBP für mindestens 4s substantiell erhalten bleibt. Ionisation mittels ESI erzeugt $[M+n\,\mathrm{H}]^{n+}$ Protein-Ionen, die entsprechenden KIX Ionen wurden mittels ECD fragmentiert. Unterschiedliche Ionisationsgrade (n=7-16) zeigten ein unterschiedliches Ausmaß an Fragmentierung. Für 7+ Ionen konnten nur Fragmente des unstrukturierten N-Terminus der KIX Domäne detektiert werden. Für die n=8-9 Zustände wurde nur sehr geringe Fragmentierung beobachtet, obwohl die N-Termini der Helix α1 und α2 sich zu entfalten beginnen. Bei den 10+ Ionen wird von den ECD Daten deutlich, dass sich die Helix α3 zu entfalten beginnt und dass sich die drei Helices räumlich von einander entfernt haben. Bei höheren Ladungszuständen kommt es zur unselektiven Fragmentierung der KIX Domäne, was indikativ für ein ungefaltetes Protein ist. Die Helixstabilität in der Gasphase (α3 > α2 > α1) ist ident mit der Helixstabilität in der flüssigen Phase.

Appendix A1

Chemical Shifts of KIX

Residue	Atom	Nuclei	Shift [ppm]
G586	C	13C	174.13
G586	CA	13C	45.453
G586	HN	1H	8.425
G586	HA1	1H	3.883
G586	HA2	1H	3.906
G586	N	15N	110.574
V587	C	13C	176.445
V587	CA	13C	62.403
V587	CB	13C	32.991
V587	CG1	13C	21.364
V587	CG2	13C	20.792
V587	HN	1H	7.976
V587	HA	1H	4.05
V587	HB	1H	1.981
V587	N	15N	119.627
V587	QG1	1H	0.846
V587	QG2	1H	0.848
R588	C	13C	176.286
R588	CA	13C	56.442
R588	CB	13C	30.859
R588	CD	13C	43.596
R588	CG	13C	27.644
R588	HN	1H	8.479
R588	HA	1H	4.276
R588	HB2	1H	1.738
R588	HB3	1H	1.738
R588	HD3	1H	3.123
R588	N	15N	125.63
R588	QG	1H	1.547
K589	C	13C	177.736
K589	CA	13C	55.153
K589	CB	13C	32.857
K589	CG	13C	32.874
K589	HN	1H	8.039
K589	HA	1H	4.129
K589	HB2	1H	0.575
K589	HB3	1H	1.099
K589	N	15N	121.413
G590	CA	13C	47.428
G590	HN	1H	8.644
G590	HA1	1H	3.697
G590	HA2	1H	3.904
G590	N	15N	112.357
W591	C	13C	178.199
W591	CA	13C	58.292
W591	CB	13C	28.071
W591	HN	1H	7.878
W591	HA	1H	4.467
W591	HB2	1H	3.132
W591	HB3	1H	3.555
W591	N	15N	118.944
H592	C	13C	176.851
H592	CA	13C	56.591
H592	CB	13C	29.067
H592	HN	1H	7.044
H592	HA	1H	3.48
H592	HB2	1H	2.867
H592	HB3	1H	2.848
H592	N	15N	119.615
E593	C	13C	176.863
E593	CA	13C	58.442
E593	CB	13C	29.568
E593	CG	13C	36.053
E593	HN	1H	7.619
E593	HA	1H	3.934
E593	HB2	1H	1.764
E593	HB3	1H	1.725
E593	HG2	1H	2.031
E593	HG3	1H	2.024
E593	N	15N	116.504
H594	C	13C	174.464
H594	CA	13C	54.92
H594	CB	13C	29.96
H594	HN	1H	7.527
H594	HA	1H	4.872
H594	HB2	1H	3.625
H594	HB3	1H	3.218
H594	N	15N	113.375
V595	C	13C	174.656
V595	CA	13C	62.321
V595	CB	13C	33.49
V595	CG1	13C	22.41
V595	CG2	13C	21.754
V595	HN	1H	7.484
V595	HA	1H	4.467
V595	HB	1H	2.203
V595	N	15N	120.753
V595	QG1	1H	1.116
V595	QG2	1H	1.218
T596	C	13C	175.644
T596	CA	13C	60.346
T596	CB	13C	71.209
T596	CG2	13C	22.208
T596	HN	1H	7.446
T596	HA	1H	4.524
T596	N	15N	115.192
T596	QG2	1H	1.274
Q597	C	13C	178.214

Q597	CA	13C	59.027		L603	CB	13C	40.591
Q597	CB	13C	28.205		L603	CD1	13C	25.681
Q597	CG	13C	33.807		L603	CD2	13C	22.843
Q597	HN	1H	8.895		L603	HN	1H	8.111
Q597	HB2	1H	2		L603	HA	1H	3.971
Q597	HB3	1H	2.058		L603	HB2	1H	1.348
Q597	HG2	1H	2.326		L603	HB3	1H	2.091
Q597	HG3	1H	2.329		L603	HG	1H	1.894
Q597	N	15N	120.295		L603	N	15N	121.593
D598	C	13C	178.619		L603	QD1	1H	0.903
D598	CA	13C	57.258		L603	QD2	1H	0.757
D598	CB	13C	40.588		V604	C	13C	178.047
D598	HN	1H	8.377		V604	CA	13C	67.817
D598	HA	1H	4.287		V604	CB	13C	31.813
D598	HB2	1H	2.539		V604	CG1	13C	21.623
D598	HB3	1H	2.539		V604	CG2	13C	24.029
D598	N	15N	117.764		V604	HN	1H	8.27
L599	C	13C	179.402		V604	HA	1H	3.382
L599	CA	13C	58.586		V604	HB	1H	2.144
L599	CB	13C	41.828		V604	N	15N	119.812
L599	CD1	13C	24.436		V604	QG1	1H	0.791
L599	CD2	13C	25.436		V604	QG2	1H	0.967
L599	HN	1H	7.576		H605	C	13C	177.232
L599	HA	1H	4.225		H605	CA	13C	59.584
L599	HB2	1H	1.986		H605	HN	1H	7.923
L599	HB3	1H	1.849		H605	HA	1H	4.185
L599	HG	1H	1.847		H605	HB2	1H	3.276
L599	N	15N	122.875		H605	HB3	1H	3.276
L599	QD1	1H	1.179		H605	N	15N	116.749
L599	QD2	1H	1.223		K606	C	13C	179.598
R600	C	13C	179.232		K606	CA	13C	59.338
R600	CA	13C	60.511		K606	HN	1H	8.01
R600	HN	1H	7.742		K606	N	15N	119.492
R600	HA	1H	4.022		L607	C	13C	178.278
R600	HB3	1H	1.789		L607	CA	13C	58.718
R600	HG3	1H	1.549		L607	CB	13C	42.605
R600	N	15N	118.334		L607	CD1	13C	26.088
S601	C	13C	177.555		L607	CD2	13C	24.822
S601	CA	13C	61.773		L607	HN	1H	7.915
S601	HN	1H	8.401		L607	HA	1H	3.924
S601	HA	1H	4.016		L607	HB2	1H	2.002
S601	N	15N	112.685		L607	HB3	1H	1.459
S601	QB	1H	3.895		L607	HG	1H	1.608
H602	C	13C	177.643		L607	N	15N	121.192
H602	CA	13C	59.389		L607	QD1	1H	0.806
H602	CB	13C	28.903		L607	QD2	1H	0.751
H602	HN	1H	7.997		V608	C	13C	177.835
H602	HA	1H	4.448		V608	CA	13C	67.607
H602	HB2	1H	3.388		V608	CB	13C	31.803
H602	HB3	1H	3.485		V608	CG1	13C	21.824
H602	N	15N	121.553		V608	CG2	13C	24.212
L603	C	13C	179.398		V608	HN	1H	8.059
L603	CA	13C	58.478		V608	HA	1H	3.394

V608	HB	1H	2.144		P613	HB2	1H	2.223
V608	N	15N	118.297		P613	HB3	1H	1.841
V608	QG1	1H	0.899		P613	HD2	1H	3.414
V608	QG2	1H	0.967		P613	HD3	1H	3.415
Q609	C	13C	177.361		P613	HG3	1H	1.872
Q609	CA	13C	58.097		T614	C	13C	172.909
Q609	CB	13C	29.08		T614	CA	13C	58.98
Q609	CG	13C	34.463		T614	CB	13C	70.061
Q609	HN	1H	7.983		T614	CG2	13C	21.463
Q609	HA	1H	3.901		T614	HN	1H	7.804
Q609	HB2	1H	1.942		T614	HA	1H	4.506
Q609	HB3	1H	1.942		T614	HB	1H	4.03
Q609	HE21	1H	6.801		T614	N	15N	114.208
Q609	HE22	1H	7.283		T614	QG2	1H	1.071
Q609	HG2	1H	2.253		P615	C	13C	176.303
Q609	HG3	1H	2.209		P615	CA	13C	63.522
Q609	N	15N	116.132		P615	CB	13C	32.059
Q609	NE2	15N	111.433		P615	CD	13C	51.194
A610	C	13C	178.319		P615	CG	13C	27.411
A610	CA	13C	54.1		P615	HA	1H	4.325
A610	CB	13C	19.195		P615	HB3	1H	2.225
A610	HN	1H	7.456		P615	HD2	1H	3.8
A610	HA	1H	4.098		P615	HD3	1H	3.605
A610	N	15N	119.245		P615	HG3	1H	1.883
A610	QB	1H	1.472		D616	C	13C	175.274
I611	C	13C	175.825		D616	CA	13C	51.752
I611	CA	13C	63.071		D616	CB	13C	41.917
I611	CB	13C	39.378		D616	HN	1H	7.92
I611	CD1	13C	14.411		D616	HA	1H	4.83
I611	CG1	13C	28.906		D616	HB2	1H	2.718
I611	CG2	13C	18.356		D616	HB3	1H	2.572
I611	HN	1H	7.49		D616	N	15N	120.672
I611	HA	1H	3.803		P617	C	13C	178.223
I611	HB	1H	1.766		P617	CA	13C	64.828
I611	N	15N	114.314		P617	CB	13C	32.144
I611	QD1	1H	0.809		P617	CD	13C	51.088
I611	QG1	1H	1.126		P617	CG	13C	27.518
I611	QG2	1H	0.757		P617	HA	1H	4.206
F612	C	13C	179.229		P617	HB3	1H	2.267
F612	CB	13C	40.117		P617	HD2	1H	3.817
F612	HN	1H	8.087		P617	HD3	1H	3.82
F612	HA	1H	4.831		P617	HG2	1H	1.915
F612	HB2	1H	2.7		P617	HG3	1H	1.976
F612	HB3	1H	3.102		A618	C	13C	178.985
F612	N	15N	120.266		A618	CA	13C	53.708
F612	QD	1H	7.183		A618	CB	13C	18.759
F612	QE	1H	7.182		A618	HN	1H	8.194
P613	C	13C	177.454		A618	HA	1H	4.135
P613	CA	13C	64.113		A618	N	15N	120.569
P613	CB	13C	32.051		A618	QB	1H	1.349
P613	CD	13C	50.326		A619	C	13C	178.495
P613	CG	13C	27.508		A619	CA	13C	53.301
P613	HA	1H	4.455		A619	CB	13C	19.173

A619	HN	1H	7.711		R624	CD	13C	43.754
A619	HA	1H	4.224		R624	HN	1H	8.401
A619	N	15N	120.946		R624	HA	1H	4.108
A619	QB	1H	1.405		R624	HG3	1H	1.603
L620	C	13C	177.965		R624	N	15N	119.79
L620	CA	13C	56.272		M625	C	13C	177.79
L620	CB	13C	41.964		M625	CA	13C	57.065
L620	CD1	13C	25.259		M625	CB	13C	31.448
L620	CD2	13C	23.651		M625	CE	13C	17.096
L620	CG	13C	27.698		M625	CG	13C	32.449
L620	HN	1H	7.584		M625	HN	1H	8.19
L620	HA	1H	4.126		M625	HA	1H	4.3
L620	HG	1H	1.601		M625	HB2	1H	2.066
L620	N	15N	117.769		M625	HB3	1H	1.962
L620	QB	1H	1.539		M625	HG2	1H	2.456
L620	QD1	1H	0.809		M625	HG3	1H	2.452
L620	QD2	1H	0.83		M625	N	15N	118.759
K621	C	13C	176.556		M625	QE	1H	1.828
K621	CA	13C	56.725		E626	C	13C	179.49
K621	CB	13C	32.801		E626	CA	13C	59.851
K621	CD	13C	29.452		E626	CB	13C	29.762
K621	CE	13C	42.375		E626	CG	13C	36.69
K621	CG	13C	25.004		E626	HN	1H	8.241
K621	HN	1H	7.767		E626	HA	1H	3.921
K621	HA	1H	4.203		E626	HB3	1H	1.981
K621	HB2	1H	1.844		E626	N	15N	119.235
K621	HB3	1H	1.731		N627	C	13C	177.901
K621	HE3	1H	2.919		N627	CA	13C	55.862
K621	HG2	1H	1.363		N627	CB	13C	38.227
K621	HG3	1H	1.351		N627	HN	1H	8.172
K621	N	15N	118.808		N627	HA	1H	4.513
D622	C	13C	176.976		N627	HB2	1H	2.842
D622	CA	13C	54.415		N627	HB3	1H	2.774
D622	CB	13C	41.876		N627	N	15N	117.699
D622	HN	1H	7.824		L628	C	13C	178.755
D622	HA	1H	4.517		L628	CA	13C	58.268
D622	HB2	1H	2.704		L628	CB	13C	41.838
D622	HB3	1H	2.707		L628	CD1	13C	25.305
D622	N	15N	120.185		L628	CD2	13C	24.434
R623	C	13C	177.415		L628	HN	1H	7.85
R623	CA	13C	57.878		L628	HA	1H	4.233
R623	CB	13C	29.725		L628	HB2	1H	1.911
R623	CD	13C	43.604		L628	HB3	1H	1.648
R623	HN	1H	8.33		L628	N	15N	123.195
R623	HA	1H	4.134		L628	QD1	1H	0.831
R623	HB2	1H	1.826		L628	QD2	1H	0.832
R623	HB3	1H	1.813		V629	C	13C	177.765
R623	HG2	1H	1.59		V629	CA	13C	67.08
R623	HG3	1H	1.59		V629	CB	13C	31.839
R623	N	15N	121.185		V629	CG1	13C	21.427
R624	C	13C	178.773		V629	CG2	13C	23.403
R624	CA	13C	58.638		V629	HN	1H	8.331
R624	CB	13C	29.993		V629	HA	1H	3.436

V629	HB	1H	2.037	V635	CG1	13C	22.062
V629	N	15N	119.875	V635	CG2	13C	22.093
V629	QG1	1H	0.85	V635	HN	1H	7.945
V629	QG2	1H	1.015	V635	HA	1H	3.66
A630	C	13C	181.023	V635	HB	1H	1.866
A630	CA	13C	55.635	V635	N	15N	119.053
A630	CB	13C	18.142	V635	QG1	1H	0.772
A630	HN	1H	7.763	V635	QG2	1H	0.546
A630	HA	1H	3.999	E636	C	13C	178.803
A630	N	15N	120.571	E636	CA	13C	61.483
A630	QB	1H	1.484	E636	HN	1H	8.448
Y631	C	13C	176.869	E636	HA	1H	3.84
Y631	CA	13C	61.079	E636	HB2	1H	1.575
Y631	CB	13C	38.227	E636	HB3	1H	1.574
Y631	HN	1H	7.83	E636	HG2	1H	2.288
Y631	HA	1H	4.251	E636	HG3	1H	2.279
Y631	HB2	1H	3.184	E636	N	15N	120.31
Y631	HB3	1H	3.207	G637	C	13C	176.777
Y631	N	15N	120.093	G637	CA	13C	47.602
Y631	QD	1H	7.069	G637	HN	1H	8.086
Y631	QE	1H	6.702	G637	HA1	1H	3.853
Y631	CD*	13C	132.857	G637	HA2	1H	3.528
Y631	CE*	13C	118.232	G637	N	15N	107.009
A632	C	13C	179.227	D638	C	13C	180.175
A632	CA	13C	55.401	D638	CA	13C	57.264
A632	CB	13C	20.496	D638	CB	13C	40.35
A632	HN	1H	8.514	D638	HN	1H	8.111
A632	HA	1H	3.663	D638	HA	1H	4.508
A632	N	15N	122.265	D638	HB2	1H	2.872
A632	QB	1H	1.486	D638	HB3	1H	2.688
K633	C	13C	180.289	D638	N	15N	122.307
K633	CA	13C	59.902	M639	C	13C	177.872
K633	CB	13C	33.012	M639	CA	13C	58.943
K633	HN	1H	8.583	M639	CE	13C	19.08
K633	HA	1H	3.956	M639	HN	1H	8.023
K633	HB2	1H	1.783	M639	N	15N	121.013
K633	HB3	1H	1.807	M639	QE	1H	1.937
K633	N	15N	115.942	Y640	C	13C	178.261
K633	QE	1H	2.879	Y640	CA	13C	62.178
K634	C	13C	178.686	Y640	CB	13C	39.061
K634	CA	13C	59.446	Y640	HN	1H	9.245
K634	CB	13C	32.018	Y640	HA	1H	4.287
K634	HN	1H	7.694	Y640	HB2	1H	3.466
K634	HA	1H	4.012	Y640	HB3	1H	3.031
K634	HB2	1H	1.843	Y640	N	15N	121.092
K634	HB3	1H	2.02	Y640	QD	1H	6.536
K634	HD3	1H	1.38	Y640	QE	1H	5.978
K634	HE2	1H	2.879	Y640	CD*	13C	132.636
K634	HE3	1H	2.876	Y640	CE*	13C	116.927
K634	N	15N	123.235	E641	C	13C	178.227
V635	C	13C	178.781	E641	CA	13C	57.832
V635	CA	13C	66.038	E641	CB	13C	30.062
V635	CB	13C	31.911	E641	CG	13C	35.932

E641	HN	1H	7.984		D647	HA	1H	4.274
E641	HA	1H	4.293		D647	HB2	1H	2.43
E641	HB2	1H	2.083		D647	HB3	1H	2.433
E641	HB3	1H	2.169		D647	N	15N	117.081
E641	HG2	1H	2.486		E648	C	13C	177.322
E641	HG3	1H	2.506		E648	CA	13C	59.614
E641	N	15N	114.771		E648	CB	13C	30.186
S642	C	13C	175.47		E648	CG	13C	37.012
S642	CA	13C	60.418		E648	HN	1H	7.728
S642	CB	13C	64.611		E648	HB2	1H	1.851
S642	HN	1H	7.934		E648	HB3	1H	1.838
S642	HA	1H	4.365		E648	N	15N	121.058
S642	HB2	1H	3.894		Y649	C	13C	176.091
S642	HB3	1H	3.895		Y649	CA	13C	61.087
S642	N	15N	112.752		Y649	CB	13C	39.051
A643	C	13C	178.061		Y649	HN	1H	7.308
A643	CA	13C	53.029		Y649	HA	1H	3.91
A643	CB	13C	19.68		Y649	HB2	1H	2.621
A643	HN	1H	8.099		Y649	HB3	1H	2.783
A643	HA	1H	4.184		Y649	N	15N	121.412
A643	N	15N	123.985		Y649	QD	1H	6.828
A643	QB	1H	1.53		Y649	QE	1H	6.807
N644	C	13C	174.206		Y649	CD*	13C	133.144
N644	CA	13C	53.712		Y650	C	13C	179.367
N644	CB	13C	40.435		Y650	CA	13C	61.048
N644	HN	1H	9.063		Y650	CB	13C	37.91
N644	HA	1H	5.037		Y650	HN	1H	8.118
N644	HB2	1H	2.888		Y650	HA	1H	3.881
N644	HB3	1H	2.699		Y650	HB2	1H	2.992
N644	N	15N	117.019		Y650	HB3	1H	2.998
S645	C	13C	172.121		Y650	N	15N	115.859
S645	CA	13C	56.758		Y650	QD	1H	7.171
S645	CB	13C	65.228		Y650	QE	1H	6.867
S645	HN	1H	6.826		Y650	CD*	13C	132.417
S645	HA	1H	3.637		Y650	CE*	13C	118.079
S645	HB2	1H	3.854		H651	C	13C	177.223
S645	HB3	1H	3.853		H651	CA	13C	59.462
S645	N	15N	111.23		H651	CB	13C	28.624
R646	C	13C	177.307		H651	HN	1H	8.268
R646	CA	13C	59.241		H651	HA	1H	4.31
R646	CB	13C	30.496		H651	HB2	1H	3.311
R646	CD	13C	44.161		H651	HB3	1H	3.309
R646	HN	1H	8.652		H651	N	15N	118.632
R646	HA	1H	3.184		L652	C	13C	180.81
R646	HB2	1H	1.884		L652	CA	13C	58.143
R646	HB3	1H	1.831		L652	CB	13C	42.089
R646	HG2	1H	1.56		L652	CD1	13C	26.146
R646	HG3	1H	1.559		L652	CD2	13C	22.396
R646	N	15N	121.838		L652	CG	13C	31.29
D647	C	13C	178.891		L652	HN	1H	8.975
D647	CA	13C	57.541		L652	HA	1H	3.922
D647	CB	13C	40.52		L652	HB2	1H	1.97
D647	HN	1H	8.125		L652	HB3	1H	2.022

L652	HG	1H	1.52		Y658	HB3	1H	3.084
L652	N	15N	120.78		Y658	N	15N	119.036
L652	QD1	1H	0.942		Y658	QD	1H	7.143
L652	QD2	1H	0.894		Y658	QE	1H	6.804
L653	C	13C	178.278		Y658	CD*	13C	133.266
L653	CA	13C	57.976		Y658	CE*	13C	118.055
L653	CB	13C	41.718		K659	C	13C	179.639
L653	CD1	13C	25.618		K659	CA	13C	59.875
L653	CD2	13C	25.117		K659	CB	13C	32.915
L653	HN	1H	7.724		K659	CE	13C	42.447
L653	HA	1H	3.806		K659	HN	1H	8.096
L653	HB2	1H	1.545		K659	HA	1H	3.831
L653	HB3	1H	1.543		K659	HB3	1H	1.947
L653	HG	1H	1.347		K659	N	15N	119.131
L653	N	15N	120.878		K659	QE	1H	2.957
L653	QD1	1H	0.571		I660	C	13C	178.391
L653	QD2	1H	0.713		I660	CA	13C	65.218
A654	C	13C	180.911		I660	CB	13C	38.424
A654	CA	13C	55.525		I660	CD1	13C	14.427
A654	CB	13C	18.052		I660	CG1	13C	29.228
A654	HN	1H	7.981		I660	CG2	13C	17.878
A654	HA	1H	3.839		I660	HN	1H	8.278
A654	N	15N	120.81		I660	HA	1H	3.735
A654	QB	1H	1.369		I660	HB	1H	1.863
E655	C	13C	178.792		I660	HG12	1H	1.1
E655	CA	13C	59.287		I660	HG13	1H	1.1
E655	CB	13C	29.838		I660	N	15N	120.664
E655	CG	13C	36.809		I660	QD1	1H	0.801
E655	HN	1H	8.173		I660	QG2	1H	0.803
E655	HA	1H	3.965		Q661	C	13C	179.253
E655	N	15N	117.715		Q661	CA	13C	59.688
K656	C	13C	178.518		Q661	CB	13C	28.478
K656	CA	13C	58.16		Q661	CG	13C	34.436
K656	CB	13C	32.13		Q661	HN	1H	8.225
K656	HN	1H	7.817		Q661	HA	1H	3.917
K656	HA	1H	4.224		Q661	HE21	1H	6.641
K656	N	15N	120.275		Q661	HE22	1H	7.336
I657	C	13C	177.344		Q661	HG2	1H	2.549
I657	CA	13C	66.27		Q661	HG3	1H	2.283
I657	CB	13C	37.963		Q661	N	15N	118.94
I657	CD1	13C	13.622		Q661	NE2	15N	110.651
I657	CG2	13C	17.316		Q661	QB	1H	1.972
I657	HN	1H	8.18		K662	C	13C	179.167
I657	HA	1H	3.419		K662	CA	13C	58.697
I657	HB	1H	1.775		K662	CB	13C	32.052
I657	N	15N	119.027		K662	CG	13C	24.617
I657	QD1	1H	0.668		K662	HN	1H	8.07
I657	QG2	1H	0.754		K662	HA	1H	3.936
Y658	C	13C	177.931		K662	N	15N	119.821
Y658	CA	13C	61.15		E663	C	13C	179.476
Y658	CB	13C	38.128		E663	CA	13C	59.382
Y658	HN	1H	7.876		E663	CB	13C	29.487
Y658	HB2	1H	3.081		E663	CG	13C	36.879

E663	HN	1H	8.028		R671	HA	1H	4.31
E663	HB3	1H	2.405		R671	N	15N	122.162
E663	N	15N	120.1		L672	C	13C	182.54
L664	C	13C	179.779		L672	CA	13C	56.811
L664	CA	13C	57.817		L672	CB	13C	43.456
L664	CB	13C	41.786		L672	CD1	13C	25.389
L664	HN	1H	8.051		L672	CD2	13C	23.616
L664	N	15N	119.868		L672	HN	1H	7.709
E665	C	13C	178.909		L672	HA	1H	4.108
E665	CA	13C	59.111		L672	HB2	1H	1.519
E665	CB	13C	29.564		L672	HB3	1H	1.518
E665	CG	13C	36.372		L672	N	15N	128.248
E665	HN	1H	7.924		L672	QD1	1H	0.822
E665	HA	1H	3.996		L672	QD2	1H	0.794
E665	N	15N	120.018					
E666	C	13C	178.932
E666	CA	13C	58.829
E666	CB	13C	29.529
E666	CG	13C	36.582
E666	HN	1H	8.004
E666	HA	1H	4.001
E666	N	15N	119.252
K667	C	13C	178.495
K667	CA	13C	58.182
K667	CB	13C	32.444
K667	HN	1H	7.879
K667	HA	1H	4.098
K667	N	15N	119.182
R668	C	13C	177.69
R668	HN	1H	7.872
R668	N	15N	119.21
R669	C	13C	177.018
R669	CA	13C	57.298
R669	CB	13C	30.808
R669	CD	13C	43.847
R669	CG	13C	27.702
R669	HN	1H	7.851
R669	HA	1H	4.195
R669	HB3	1H	1.827
R669	N	15N	119.138
S670	C	13C	174.372
S670	CA	13C	59.1
S670	CB	13C	63.849
S670	HN	1H	7.958
S670	HA	1H	4.336
S670	N	15N	115.456
S670	QB	1H	3.86
R671	C	13C	175.343
R671	CA	13C	56.281
R671	CB	13C	30.639
R671	CD	13C	43.768
R671	CG	13C	27.379
R671	HN	1H	7.985

Appendix A2

Order Parameter of KIX

Residue	Model	S2s	S2f	te [ps]	Rex [s^{-1}]
588	2	0.363		8.73E+02	
590	4	0.576		9.74E+02	3.159
592	4	0.73		1.22E+03	5.278
593	4	0.727		9.06E+02	4.715
594	4	0.646		9.03E+02	4.663
595	4	0.831		6.71E+02	1.524
596	4	0.71		7.21E+02	0.893
597	4	0.706		8.45E+02	5.245
598	4	0.676		8.36E+02	6.833
599	4	0.905		3.98E+02	3.748
600	4	0.865		7.42E+02	4.812
601	4	0.855		6.25E+02	2.049
603	4	0.817		6.58E+02	4.245
604	4	0.875		5.68E+02	3.779
605	4	0.845		7.71E+02	6.097
607	4	0.865		6.75E+02	5.889
608	4	0.891		5.32E+02	4.584
609	4	0.897		5.59E+02	6.463
610	4	0.899		5.47E+02	5.69
611	4	0.882		4.76E+02	4.86
612	4	0.738		7.55E+02	5.372
614	4	0.677		7.45E+02	1.033
616	2	0.599		7.54E+02	
618	4	0.619		8.51E+02	0.535
620	4	0.613		7.50E+02	2.769
621	4	0.674		8.03E+02	1.131
624	4	0.613		8.60E+02	4.519
625	4	0.749		9.50E+02	5.15
626	4	0.829		6.97E+02	3.444
628	4	0.801		7.91E+02	4.011
629	4	0.794		7.45E+02	4.303
630	4	0.866		7.97E+02	5.216
632	4	0.756		9.28E+02	5.074
633	4	0.816		6.66E+02	5.015
634	4	0.887		6.68E+02	3.985
635	4	0.858		6.87E+02	5.198
636	4	0.76		7.79E+02	6.371
637	2	0.899		6.66E+02	
638	4	0.851		6.34E+02	3.536
640	4	0.874		7.86E+02	4.61
641	4	0.884		6.87E+02	5.214
642	4	0.898		4.97E+02	2.09
643	4	0.821		8.59E+02	2.82
644	4	0.883		4.89E+02	1.868
645	4	0.878		7.27E+02	2.722
646	4	0.815		7.48E+02	6.182

647	4	0.915		1.96E+02	5.53
649	4	0.921		4.69E+02	5.06
650	4	0.935		1.20E+02	4.379
651	4	0.903		5.37E+02	6.27
652	4	0.91		4.93E+02	5.435
654	4	0.929		9.15E+01	4.629
657	4	0.906		4.72E+02	3.926
659	4	0.895		4.91E+02	5.136
660	4	0.829		6.97E+02	6.282
661	4	0.868		6.80E+02	5.043
662	4	0.865		5.66E+02	5.59
663	4	0.838		7.38E+02	3.386
664	4	0.903		4.36E+02	3.515
665	4	0.848		5.14E+02	3.91
670	5	0.483	0.974	8.54E+02	
671	5	0.348	0.941	8.27E+02	

Appendix B1

Chemical Shifts of KIX.MLL

Residue	Atom	Nuclei	Shift [ppm]
G586	C	13C	173.963
G586	CA	13C	45.214
G586	HN	1H	8.472
G586	HA1	1H	4
G586	HA2	1H	3.932
G586	N	15N	110.673
V587	C	13C	176.34
V587	CA	13C	62.229
V587	CB	13C	32.782
V587	CG1	13C	21.171
V587	CG2	13C	20.746
V587	HN	1H	8.027
V587	HA	1H	4.098
V587	HB	1H	2.018
V587	N	15N	119.752
V587	QG1	1H	0.891
V587	QG2	1H	0.904
R588	C	13C	176.109
R588	CA	13C	56.167
R588	CB	13C	30.651
R588	CD	13C	43.404
R588	CG	13C	27.227
R588	HN	1H	8.528
R588	HA	1H	4.322
R588	HB3	1H	1.811
R588	HD3	1H	3.178
R588	HG2	1H	1.56
R588	HG3	1H	1.654
R588	N	15N	125.669
K589	C	13C	177.598
K589	CA	13C	54.923
K589	CB	13C	32.589
K589	CD	13C	29.281
K589	CE	13C	42.559
K589	CG	13C	24.725
K589	HN	1H	8.116
K589	HA	1H	4.186
K589	HB2	1H	0.819
K589	HB3	1H	1.147
K589	N	15N	121.018
G590	C	13C	176.465
G590	CA	13C	47.196
G590	HN	1H	8.669
G590	HA1	1H	3.753
G590	HA2	1H	3.967

Residue	Atom	Nuclei	Shift [ppm]
G590	N	15N	112.531
W591	C	13C	178.177
W591	CA	13C	58.128
W591	CB	13C	27.754
W591	CD1	13C	126.769
W591	CZ2	13C	115.801
W591	HN	1H	8.026
W591	HA	1H	4.505
W591	HB2	1H	3.167
W591	HB3	1H	3.598
W591	HD1	1H	7.073
W591	HE1	1H	9.228
W591	HZ2	1H	7.509
W591	N	15N	119.435
W591	NE1	15N	129.443
H592	C	13C	176.533
H592	CA	13C	56.278
H592	CB	13C	28.484
H592	CD2	13C	119.991
H592	HN	1H	7.165
H592	HA	1H	3.501
H592	HB2	1H	2.929
H592	HB3	1H	2.921
H592	HD1	1H	7.449
H592	HD2	1H	7.177
H592	N	15N	119.34
E593	C	13C	176.675
E593	CA	13C	58.108
E593	CB	13C	29.18
E593	CG	13C	35.666
E593	HN	1H	7.726
E593	HA	1H	3.98
E593	HB2	1H	1.796
E593	HB3	1H	1.798
E593	HG3	1H	2.118
E593	N	15N	116.536
H594	C	13C	173.966
H594	CA	13C	54.264
H594	CB	13C	29.182
H594	CD2	13C	119.965
H594	HN	1H	7.53
H594	HA	1H	4.95
H594	HB2	1H	3.27
H594	HB3	1H	3.716
H594	HD2	1H	7.281
H594	N	15N	112.885
V595	C	13C	174.593
V595	CA	13C	62.043
V595	CB	13C	33.362
V595	CG1	13C	22.368
V595	CG2	13C	21.596
V595	HN	1H	7.492
V595	HA	1H	4.5

V595	HB	1H	2.236
V595	N	15N	120.678
V595	QG1	1H	1.153
V595	QG2	1H	1.241
T596	C	13C	175.419
T596	CA	13C	60.001
T596	CB	13C	71.072
T596	CG2	13C	22.025
T596	HN	1H	7.583
T596	HA	1H	4.494
T596	N	15N	115.525
T596	QG2	1H	1.318
Q597	C	13C	178.079
Q597	CA	13C	58.754
Q597	CB	13C	28.012
Q597	CG	13C	33.667
Q597	HN	1H	8.929
Q597	HA	1H	3.818
Q597	HB2	1H	2.056
Q597	HB3	1H	2.099
Q597	HE21	1H	6.676
Q597	HE22	1H	7.395
Q597	HG3	1H	2.375
Q597	N	15N	120.346
Q597	NE2	15N	112.572
D598	C	13C	178.494
D598	CA	13C	56.893
D598	CB	13C	40.534
D598	HN	1H	8.382
D598	HA	1H	4.34
D598	HB3	1H	2.593
D598	N	15N	117.842
L599	C	13C	179.129
L599	CA	13C	58.443
L599	CB	13C	41.634
L599	CD1	13C	24.054
L599	CD2	13C	25.688
L599	CG	13C	27.599
L599	HN	1H	7.671
L599	HA	1H	4.243
L599	HB2	1H	2.071
L599	HB3	1H	1.851
L599	HG	1H	1.882
L599	N	15N	123.174
L599	QD1	1H	1.232
L599	QD2	1H	1.321
R600	C	13C	179.103
R600	CA	13C	60.396
R600	CB	13C	30.52
R600	HN	1H	7.768
R600	HA	1H	4.322
R600	HB3	1H	1.808
R600	HG3	1H	1.561

R600	N	15N	118.132
S601	C	13C	177.665
S601	CA	13C	61.534
S601	CB	13C	62.758
S601	HN	1H	8.501
S601	HA	1H	4.134
S601	HB2	1H	3.969
S601	HB3	1H	3.94
S601	N	15N	112.865
H602	C	13C	176.286
H602	CA	13C	58.909
H602	CB	13C	28.089
H602	CD2	13C	119.967
H602	HN	1H	8.098
H602	HA	1H	4.493
H602	HB2	1H	3.501
H602	HB3	1H	3.538
H602	HD2	1H	7.166
H602	N	15N	121.543
L603	C	13C	179.275
L603	CA	13C	58.097
L603	CB	13C	40.222
L603	CD1	13C	25.757
L603	CD2	13C	22.64
L603	CG	13C	27.46
L603	HN	1H	8.293
L603	HA	1H	4.028
L603	HB2	1H	2.192
L603	HB3	1H	1.335
L603	HG	1H	1.947
L603	N	15N	122.394
L603	QD1	1H	0.959
L603	QD2	1H	0.802
V604	C	13C	178.026
V604	CA	13C	67.892
V604	CB	13C	31.603
V604	CG1	13C	21.501
V604	CG2	13C	23.929
V604	HN	1H	8.409
V604	HA	1H	3.428
V604	HB	1H	2.218
V604	N	15N	120.325
V604	QG1	1H	0.829
V604	QG2	1H	1.031
H605	C	13C	176.891
H605	CA	13C	59.091
H605	CB	13C	27.88
H605	CD2	13C	119.96
H605	HN	1H	7.908
H605	HA	1H	4.252
H605	HB2	1H	3.411
H605	HB3	1H	3.35
H605	HD2	1H	7.15

H605	N	15N	116.275
K606	C	13C	178.947
K606	CA	13C	58.804
K606	HN	1H	8.092
K606	HA	1H	4.273
K606	N	15N	119.506
L607	C	13C	177.899
L607	CA	13C	58.826
L607	CB	13C	42.523
L607	CD1	13C	25.743
L607	CD2	13C	25.098
L607	HN	1H	7.994
L607	HA	1H	3.958
L607	HB2	1H	1.996
L607	HB3	1H	1.634
L607	N	15N	121.321
L607	QD1	1H	0.884
L607	QD2	1H	0.814
V608	C	13C	177.033
V608	CA	13C	67.943
V608	CB	13C	31.652
V608	CG1	13C	20.956
V608	CG2	13C	24.207
V608	HN	1H	8.036
V608	HA	1H	3.347
V608	HB	1H	2.22
V608	N	15N	118.191
V608	QG1	1H	0.935
V608	QG2	1H	1.027
Q609	C	13C	176.992
Q609	CA	13C	58.108
Q609	CB	13C	29.153
Q609	CG	13C	34.367
Q609	HN	1H	8.108
Q609	HA	1H	3.888
Q609	HB3	1H	1.982
Q609	HE21	1H	7.426
Q609	HE22	1H	6.823
Q609	HG3	1H	2.295
Q609	N	15N	116.772
Q609	NE2	15N	111.483
A610	C	13C	178.498
A610	CA	13C	53.778
A610	CB	13C	19.392
A610	HN	1H	7.756
A610	HA	1H	4.033
A610	N	15N	119.316
A610	QB	1H	1.521
I611	C	13C	174.299
I611	CA	13C	63.725
I611	CB	13C	39.306
I611	CD1	13C	14.122
I611	CG1	13C	28.492

I611	CG2	13C	18.835
I611	HN	1H	7.498
I611	HA	1H	3.675
I611	HB	1H	1.895
I611	HG12	1H	2.161
I611	HG13	1H	2.102
I611	N	15N	115.839
I611	QD1	1H	0.936
I611	QG2	1H	0.896
F612	C	13C	171.61
F612	CA	13C	51.716
F612	CB	13C	39.682
F612	HN	1H	8.235
F612	HA	1H	5.096
F612	HB2	1H	3.385
F612	HB3	1H	3.388
F612	N	15N	116.531
F612	QD	1H	6.831
F612	QE	1H	6.813
F612	CD*	13C	129.396
F612	CE*	13C	131.289
P613	C	13C	178.269
P613	CA	13C	64.778
P613	CB	13C	32.444
P613	CD	13C	50.155
P613	HA	1H	4.573
P613	HB2	1H	2.426
P613	HB3	1H	1.989
P613	HD2	1H	3.732
P613	HD3	1H	3.431
P613	HG2	1H	2.022
P613	HG3	1H	2.049
T614	C	13C	172.048
T614	CA	13C	58.106
T614	CB	13C	69.549
T614	CG2	13C	21.487
T614	HN	1H	8.025
T614	HA	1H	4.47
T614	HB	1H	4.166
T614	N	15N	109.561
T614	QG2	1H	1.074
P615	C	13C	176.462
P615	CA	13C	62.692
P615	CB	13C	31.302
P615	CD	13C	49.847
P615	CG	13C	26.728
P615	HA	1H	3.99
P615	HB2	1H	1.446
P615	HB3	1H	0.869
P615	HD2	1H	3.274
P615	HD3	1H	3.265
P615	HG2	1H	1.218
P615	HG3	1H	1.654

D616	C	13C	174.226	K621	CG	13C	24.835
D616	CA	13C	51.858	K621	HN	1H	7.272
D616	CB	13C	39.93	K621	HA	1H	4.337
D616	HN	1H	8.145	K621	HB2	1H	1.78
D616	HA	1H	4.753	K621	HB3	1H	1.974
D616	HB2	1H	2.805	K621	HG3	1H	1.504
D616	HB3	1H	2.99	K621	N	15N	115.255
D616	N	15N	122.743	D622	C	13C	178.117
P617	C	13C	178.885	D622	CA	13C	53.884
P617	CA	13C	66.015	D622	CB	13C	43.987
P617	CB	13C	31.934	D622	HN	1H	7.454
P617	CD	13C	50.613	D622	HA	1H	4.493
P617	CG	13C	28.001	D622	HB2	1H	3.033
P617	HA	1H	4.11	D622	HB3	1H	2.854
P617	HB2	1H	2.353	D622	N	15N	123.382
P617	HB3	1H	2.243	R623	C	13C	178.321
P617	HD2	1H	3.814	R623	CA	13C	58.789
P617	HD3	1H	3.855	R623	CB	13C	29.511
P617	HG2	1H	2.129	R623	CD	13C	42.932
P617	HG3	1H	1.926	R623	CG	13C	26.876
A618	C	13C	180.518	R623	HN	1H	9.107
A618	CA	13C	54.722	R623	HA	1H	4.087
A618	CB	13C	18.191	R623	HB2	1H	1.851
A618	HN	1H	8.093	R623	HB3	1H	1.862
A618	HA	1H	4.083	R623	HG2	1H	1.659
A618	N	15N	118.548	R623	HG3	1H	1.722
A618	QB	1H	1.455	R623	N	15N	130.356
A619	C	13C	179.318	R624	C	13C	178.521
A619	CA	13C	54.685	R624	CA	13C	58.679
A619	CB	13C	18.655	R624	CB	13C	28.099
A619	HN	1H	8.039	R624	CD	13C	43.715
A619	HA	1H	4.325	R624	HN	1H	9.582
A619	N	15N	122.623	R624	HA	1H	3.834
A619	QB	1H	1.519	R624	HD2	1H	2.832
L620	C	13C	178.288	R624	HD3	1H	3.191
L620	CA	13C	57.139	R624	N	15N	119.125
L620	CB	13C	42.147	M625	C	13C	178.749
L620	CD1	13C	25.254	M625	CA	13C	56.796
L620	CD2	13C	23.282	M625	CB	13C	30.89
L620	CG	13C	27.166	M625	CE	13C	17.392
L620	HN	1H	7.606	M625	HN	1H	7.953
L620	HA	1H	4.047	M625	HA	1H	4.527
L620	HB2	1H	1.786	M625	HB2	1H	2.382
L620	HB3	1H	1.517	M625	HB3	1H	2.39
L620	HG	1H	1.595	M625	HG2	1H	2.686
L620	N	15N	114.041	M625	HG3	1H	2.687
L620	QD1	1H	0.833	M625	N	15N	120.202
L620	QD2	1H	0.849	M625	QE	1H	1.917
K621	C	13C	175.867	E626	C	13C	179.64
K621	CA	13C	55.453	E626	CA	13C	58.98
K621	CB	13C	32.881	E626	CB	13C	28.532
K621	CD	13C	29.004	E626	HN	1H	7.431
K621	CE	13C	42.002	E626	HA	1H	4.06

E626	HB2	1H	2.115		Y631	N	15N	121.083
E626	HB3	1H	2.18		Y631	QD	1H	6.988
E626	N	15N	117.897		Y631	QE	1H	6.613
N627	C	13C	177.54		Y631	CD*	13C	132.511
N627	CA	13C	55.798		Y631	CE*	13C	118.406
N627	CB	13C	37.504		A632	C	13C	179.014
N627	HN	1H	7.442		A632	CA	13C	55.342
N627	HA	1H	4.489		A632	CB	13C	19.824
N627	HB2	1H	2.811		A632	HN	1H	8.292
N627	HB3	1H	2.818		A632	HA	1H	3.682
N627	HD21	1H	6.839		A632	N	15N	122.444
N627	HD22	1H	7.784		A632	QB	1H	1.543
N627	N	15N	117.95		K633	C	13C	180.004
N627	ND2	15N	112.042		K633	CA	13C	59.704
L628	C	13C	177.838		K633	CB	13C	32.667
L628	CA	13C	59.342		K633	CD	13C	29.828
L628	CB	13C	41.701		K633	CE	13C	42.006
L628	CD1	13C	26.42		K633	CG	13C	26.855
L628	CD2	13C	26.555		K633	HN	1H	8.548
L628	CG	13C	28.772		K633	HA	1H	4.01
L628	HN	1H	7.873		K633	HB2	1H	1.862
L628	HA	1H	4.189		K633	HB3	1H	2.009
L628	HB2	1H	2.473		K633	HD3	1H	1.635
L628	HB3	1H	1.817		K633	HE2	1H	2.839
L628	HG	1H	1.818		K633	HE3	1H	2.907
L628	N	15N	124.396		K633	HG3	1H	1.367
L628	QD1	1H	1.201		K633	N	15N	115.912
L628	QD2	1H	1.207		K634	C	13C	178.603
V629	C	13C	177.552		K634	CA	13C	59.102
V629	CA	13C	67.225		K634	CB	13C	31.789
V629	CB	13C	31.687		K634	CD	13C	29.019
V629	CG1	13C	21.184		K634	CE	13C	42.314
V629	CG2	13C	22.716		K634	CG	13C	24.702
V629	HN	1H	8.246		K634	HN	1H	7.943
V629	HA	1H	3.483		K634	HA	1H	4.012
V629	HB	1H	2.118		K634	N	15N	123.87
V629	N	15N	120.503		V635	C	13C	178.574
V629	QG1	1H	0.918		V635	CA	13C	66.1
V629	QG2	1H	1.127		V635	CB	13C	31.611
A630	C	13C	180.849		V635	CG1	13C	22.149
A630	CA	13C	55.414		V635	CG2	13C	22.063
A630	CB	13C	18.092		V635	HN	1H	8.165
A630	HN	1H	8.159		V635	HA	1H	3.676
A630	HA	1H	4.032		V635	HB	1H	1.879
A630	N	15N	120.687		V635	N	15N	119.215
A630	QB	1H	1.542		V635	QG1	1H	0.798
Y631	C	13C	177.591		V635	QG2	1H	0.525
Y631	CA	13C	61.311		E636	C	13C	178.666
Y631	CB	13C	38.219		E636	CA	13C	61.689
Y631	HN	1H	8.102		E636	CB	13C	28.719
Y631	HA	1H	4.239		E636	CG	13C	35.411
Y631	HB2	1H	3.362		E636	HN	1H	8.331
Y631	HB3	1H	3.238		E636	HA	1H	3.862

E636	HB2	1H	1.573	E641	HG3	1H	2.636
E636	HB3	1H	1.576	E641	N	15N	115.098
E636	HG2	1H	2.315	S642	C	13C	175.251
E636	HG3	1H	2.322	S642	CA	13C	60.175
E636	N	15N	120.094	S642	CB	13C	64.388
G637	C	13C	176.614	S642	HN	1H	7.968
G637	CA	13C	47.337	S642	HA	1H	4.394
G637	HN	1H	8.145	S642	HB3	1H	3.923
G637	HA1	1H	3.597	S642	N	15N	112.869
G637	HA2	1H	3.88	A643	C	13C	177.897
G637	N	15N	106.839	A643	CA	13C	52.599
D638	C	13C	180.109	A643	CB	13C	19.692
D638	CA	13C	56.894	A643	HN	1H	8.096
D638	CB	13C	40.088	A643	HA	1H	4.227
D638	HN	1H	8.338	A643	N	15N	123.763
D638	HA	1H	4.543	A643	QB	1H	1.584
D638	HB2	1H	2.747	N644	C	13C	173.978
D638	HB3	1H	2.954	N644	CA	13C	53.354
D638	N	15N	122.731	N644	CB	13C	40.219
M639	C	13C	177.737	N644	HN	1H	9.102
M639	CA	13C	58.675	N644	HA	1H	5.11
M639	CB	13C	32.53	N644	HB2	1H	2.748
M639	CE	13C	19.35	N644	HB3	1H	2.932
M639	CG	13C	33.093	N644	HD21	1H	7.003
M639	HN	1H	8.193	N644	HD22	1H	8.013
M639	HA	1H	4.389	N644	N	15N	117.176
M639	HB2	1H	2.469	N644	ND2	15N	115.923
M639	HB3	1H	2.143	S645	C	13C	171.965
M639	HG2	1H	2.724	S645	CA	13C	56.522
M639	HG3	1H	2.892	S645	CB	13C	64.968
M639	N	15N	121.055	S645	HN	1H	6.865
M639	QE	1H	1.998	S645	HA	1H	3.632
Y640	C	13C	178.311	S645	HB3	1H	3.888
Y640	CA	13C	61.907	S645	N	15N	111.225
Y640	CB	13C	38.95	R646	C	13C	177.709
Y640	HN	1H	9.328	R646	CA	13C	59.031
Y640	HA	1H	4.298	R646	CB	13C	30.253
Y640	HB2	1H	3.538	R646	CD	13C	43.838
Y640	HB3	1H	3.087	R646	CG	13C	27.214
Y640	N	15N	121.235	R646	HN	1H	8.685
Y640	QD	1H	6.512	R646	HA	1H	3.186
Y640	QE	1H	5.957	R646	HB2	1H	1.901
Y640	CD*	13C	132.599	R646	HB3	1H	1.864
Y640	CE*	13C	117.039	R646	HD2	1H	3.364
E641	C	13C	178.006	R646	HD3	1H	3.23
E641	CA	13C	57.446	R646	HG2	1H	1.665
E641	CB	13C	29.702	R646	HG3	1H	1.56
E641	CG	13C	35.237	R646	N	15N	121.944
E641	HN	1H	8.079	D647	C	13C	178.86
E641	HA	1H	4.366	D647	CA	13C	57.125
E641	HB2	1H	2.15	D647	CB	13C	40.289
E641	HB3	1H	2.239	D647	HN	1H	8.119
E641	HG2	1H	2.568	D647	HA	1H	4.295

D647	HB3	1H	2.479	L652	HB2	1H	2.072
D647	N	15N	116.817	L652	HB3	1H	2.043
E648	C	13C	177.064	L652	HG	1H	1.646
E648	CA	13C	59.262	L652	N	15N	121.135
E648	CB	13C	30.138	L652	QD1	1H	1
E648	CG	13C	36.447	L652	QD2	1H	0.956
E648	HN	1H	7.799	L653	C	13C	178.085
E648	HA	1H	3.99	L653	CA	13C	58.338
E648	HB3	1H	1.891	L653	CB	13C	41.886
E648	HG2	1H	2.353	L653	CD1	13C	25.809
E648	HG3	1H	2.214	L653	CD2	13C	24.926
E648	N	15N	121.231	L653	CG	13C	27.21
Y649	C	13C	176.14	L653	HN	1H	7.769
Y649	CA	13C	60.669	L653	HA	1H	3.833
Y649	CB	13C	38.957	L653	HB2	1H	1.336
Y649	HN	1H	7.338	L653	HB3	1H	1.72
Y649	HA	1H	3.999	L653	HG	1H	1.593
Y649	HB2	1H	2.894	L653	N	15N	120.947
Y649	HB3	1H	2.645	L653	QD1	1H	0.54
Y649	N	15N	122.045	L653	QD2	1H	0.753
Y649	QD	1H	6.821	A654	C	13C	180.274
Y649	QE	1H	6.832	A654	CA	13C	55.356
Y649	CD*	13C	133.188	A654	CB	13C	18.19
Y649	CE*	13C	118.222	A654	HN	1H	8.111
Y650	C	13C	179.058	A654	HA	1H	3.884
Y650	CA	13C	60.493	A654	N	15N	120.863
Y650	CB	13C	37.642	A654	QB	1H	1.45
Y650	HN	1H	8.072	E655	C	13C	178.311
Y650	HA	1H	3.999	E655	CA	13C	59.079
Y650	HB2	1H	3.072	E655	CB	13C	29.414
Y650	HB3	1H	3.005	E655	CG	13C	35.832
Y650	N	15N	115.581	E655	HN	1H	8.363
Y650	QD	1H	7.092	E655	HA	1H	4.018
Y650	QE	1H	6.829	E655	HB2	1H	2.064
Y650	CD*	13C	132.118	E655	HB3	1H	2.007
Y650	CE*	13C	118.105	E655	HG2	1H	2.303
H651	C	13C	177.144	E655	HG3	1H	2.186
H651	CA	13C	59.303	E655	N	15N	118.047
H651	CB	13C	28.256	K656	C	13C	178.388
H651	CD2	13C	120.04	K656	CA	13C	58.129
H651	HN	1H	8.311	K656	CB	13C	31.41
H651	HA	1H	4.313	K656	HN	1H	7.852
H651	HB2	1H	3.341	K656	HA	1H	4.05
H651	HB3	1H	3.364	K656	N	15N	120.122
H651	HD2	1H	7.22	I657	C	13C	177.061
H651	N	15N	118.435	I657	CA	13C	66.526
L652	C	13C	180.822	I657	CB	13C	37.9
L652	CA	13C	57.893	I657	CD1	13C	13.396
L652	CB	13C	42.037	I657	CG1	13C	31.101
L652	CD1	13C	26.027	I657	CG2	13C	17.139
L652	CD2	13C	22.199	I657	HN	1H	8.199
L652	HN	1H	9.141	I657	HA	1H	3.391
L652	HA	1H	3.993	I657	HB	1H	1.894

I657	N	15N	118.294	K662	C	13C	178.745
I657	QD1	1H	0.722	K662	CA	13C	58.521
I657	QG2	1H	0.808	K662	CB	13C	31.622
Y658	C	13C	177.869	K662	CD	13C	28.411
Y658	CA	13C	60.869	K662	CE	13C	41.831
Y658	CB	13C	38.205	K662	CG	13C	24.01
Y658	HN	1H	8.066	K662	HN	1H	8.11
Y658	HA	1H	4.303	K662	HA	1H	3.961
Y658	HB2	1H	3.145	K662	N	15N	119.532
Y658	HB3	1H	3.154	E663	C	13C	179.429
Y658	N	15N	119.43	E663	CA	13C	59.493
Y658	QD	1H	7.103	E663	CB	13C	29.164
Y658	QE	1H	6.798	E663	CG	13C	35.709
Y658	CD*	13C	133.322	E663	HN	1H	8.011
Y658	CE*	13C	118.083	E663	HA	1H	4.021
K659	C	13C	180.019	E663	HB2	1H	2.141
K659	CA	13C	59.86	E663	HB3	1H	2.389
K659	CB	13C	32.691	E663	N	15N	121.313
K659	CD	13C	29.48	L664	C	13C	178.785
K659	HN	1H	8.309	L664	CA	13C	58.174
K659	HA	1H	3.814	L664	CB	13C	41.905
K659	HD2	1H	1.731	L664	CD1	13C	26.821
K659	HD3	1H	1.93	L664	CD2	13C	23.801
K659	HE2	1H	2.902	L664	CG	13C	26.767
K659	HE3	1H	2.982	L664	HN	1H	8.342
K659	N	15N	118.321	L664	HA	1H	3.918
I660	C	13C	177.404	L664	HB2	1H	1.417
I660	CA	13C	66.076	L664	HB3	1H	1.942
I660	CB	13C	38.384	L664	HG	1H	1.751
I660	CD1	13C	14.24	L664	N	15N	119.46
I660	CG2	13C	18.011	L664	QD1	1H	0.966
I660	HN	1H	8.546	L664	QD2	1H	0.782
I660	HA	1H	3.586	E665	C	13C	179.161
I660	HB	1H	1.954	E665	CA	13C	58.815
I660	HG12	1H	1.486	E665	CB	13C	29.133
I660	HG13	1H	1.486	E665	CG	13C	35.296
I660	N	15N	121.103	E665	HN	1H	8.018
I660	QD1	1H	0.917	E665	HA	1H	3.973
I660	QG2	1H	0.891	E665	N	15N	118.822
Q661	C	13C	179.682	E666	C	13C	179.536
Q661	CA	13C	59.868	E666	CA	13C	58.91
Q661	CB	13C	28.061	E666	CB	13C	28.881
Q661	CG	13C	34.776	E666	HN	1H	8.014
Q661	HN	1H	8.554	E666	HA	1H	3.972
Q661	HA	1H	3.931	E666	N	15N	118.722
Q661	HB2	1H	2.315	K667	C	13C	179.425
Q661	HB3	1H	1.96	K667	CA	13C	57.383
Q661	HE21	1H	6.689	K667	CB	13C	32.005
Q661	HE22	1H	7.333	K667	CD	13C	28.121
Q661	HG2	1H	2.691	K667	CE	13C	42.129
Q661	HG3	1H	2.31	K667	CG	13C	25.043
Q661	N	15N	118.093	K667	HN	1H	8.056
Q661	NE2	15N	110.241	K667	HA	1H	4.141

K667	HE3	1H	2.931	D2840	HB3	1H	2.676
K667	HG3	1H	1.631	D2840	N	15N	121.043
K667	N	15N	119.177	A2841	C	13C	178.153
R668	C	13C	178.26	A2841	CA	13C	50.805
R668	CA	13C	58.964	A2841	CB	13C	19.284
R668	CB	13C	30.211	A2841	HN	1H	8.242
R668	HN	1H	8.218	A2841	HA	1H	4.588
R668	HA	1H	3.959	A2841	N	15N	124.425
R668	N	15N	119.491	A2841	QB	1H	1.408
R669	C	13C	177.325	G2842	C	13C	173.892
R669	CA	13C	57.551	G2842	CA	13C	43.189
R669	CB	13C	30.109	G2842	HN	1H	8.379
R669	CD	13C	43.377	G2842	HA2	1H	3.923
R669	CG	13C	27.317	G2842	N	15N	107.424
R669	HN	1H	7.793	N2843	C	13C	175.362
R669	HA	1H	4.17	N2843	CA	13C	51.024
R669	HB3	1H	1.888	N2843	CB	13C	39.275
R669	N	15N	117.972	N2843	HN	1H	8.152
S670	C	13C	174.266	N2843	HA	1H	4.754
S670	CA	13C	58.946	N2843	HB2	1H	2.665
S670	CB	13C	63.814	N2843	HB3	1H	2.848
S670	HN	1H	7.794	N2843	HD21	1H	7.596
S670	HA	1H	4.41	N2843	HD22	1H	6.938
S670	HB3	1H	3.942	N2843	N	15N	118.674
S670	N	15N	114.336	N2843	ND2	15N	112.944
R671	C	13C	175.272	I2844	C	13C	176.869
R671	CA	13C	56.121	I2844	CA	13C	60.498
R671	CB	13C	30.507	I2844	CB	13C	38.494
R671	CD	13C	43.442	I2844	CD1	13C	13.548
R671	CG	13C	26.772	I2844	CG1	13C	27.672
R671	HN	1H	7.74	I2844	CG2	13C	18.049
R671	HA	1H	4.347	I2844	HN	1H	9.623
R671	HB3	1H	1.742	I2844	HA	1H	4.05
R671	HD3	1H	3.17	I2844	HB	1H	1.928
R671	N	15N	122.062	I2844	HG12	1H	1.175
L672	C	13C	182.273	I2844	HG13	1H	1.474
L672	CA	13C	56.357	I2844	N	15N	123.402
L672	CB	13C	43.244	I2844	QD1	1H	0.835
L672	CD1	13C	25.309	I2844	QG2	1H	0.855
L672	CD2	13C	23.357	L2845	C	13C	174.427
L672	HN	1H	7.699	L2845	CA	13C	50.279
L672	HA	1H	4.179	L2845	CB	13C	43.207
L672	HB2	1H	1.601	L2845	CD2	13C	24.802
L672	HB3	1H	1.593	L2845	HN	1H	8.858
L672	N	15N	127.973	L2845	HA	1H	4.411
L672	QD1	1H	0.891	L2845	HB3	1H	1.554
L672	QD2	1H	0.852	L2845	HG	1H	1.254
D2840	C	13C	175.967	L2845	N	15N	123.673
D2840	CA	13C	52.225	L2845	QD2	1H	0.772
D2840	CB	13C	41.236	P2846	C	13C	178.181
D2840	HN	1H	8.15	P2846	CA	13C	60.601
D2840	HA	1H	4.545	S2847	C	13C	175.627
D2840	HB2	1H	2.693	S2847	CA	13C	60.038

S2847	HN	1H	8.916		F2852	QE	1H	7.532
S2847	HA	1H	4.402		V2853	C	13C	179.082
S2847	HB2	1H	3.927		V2853	CA	13C	63.476
S2847	HB3	1H	3.927		V2853	CG1	13C	21.891
S2847	N	15N	120.069		V2853	CG2	13C	21.616
D2848	C	13C	178.955		V2853	HN	1H	8.106
D2848	CA	13C	54.393		V2853	HA	1H	3.922
D2848	CB	13C	39.371		V2853	HB	1H	1.843
D2848	HN	1H	8.911		V2853	N	15N	117.171
D2848	HA	1H	4.388		V2853	QG1	1H	0.65
D2848	HB2	1H	2.564		V2853	QG2	1H	0.818
D2848	HB3	1H	2.682		L2854	C	13C	179.214
D2848	N	15N	119.269		L2854	CA	13C	55.035
I2849	C	13C	177.044		L2854	CD1	13C	25.823
I2849	CA	13C	61.864		L2854	CD2	13C	22.973
I2849	CB	13C	37.528		L2854	HN	1H	8.361
I2849	CD1	13C	12.791		L2854	HA	1H	3.954
I2849	CG2	13C	18.335		L2854	HB2	1H	1.771
I2849	HN	1H	7.175		L2854	HB3	1H	1.771
I2849	HA	1H	3.874		L2854	HG	1H	1.43
I2849	HB	1H	1.716		L2854	N	15N	119.806
I2849	HG12	1H	1.058		L2854	QD1	1H	0.8
I2849	HG13	1H	1.49		L2854	QD2	1H	0.758
I2849	N	15N	121.423		K2855	C	13C	176.957
I2849	QD1	1H	0.645		K2855	CA	13C	55.662
I2849	QG2	1H	0.851		K2855	CG	13C	25.318
M2850	C	13C	176.975		K2855	HN	1H	7.739
M2850	CA	13C	57.09		K2855	HA	1H	4.141
M2850	CB	13C	32.221		K2855	HB2	1H	1.874
M2850	CE	13C	17.624		K2855	HB3	1H	1.871
M2850	HN	1H	8.089		K2855	HG2	1H	1.463
M2850	HA	1H	3.909		K2855	HG3	1H	1.457
M2850	HB2	1H	2.088		K2855	N	15N	117.264
M2850	HB3	1H	1.912		K2855	QD	1H	1.683
M2850	HG3	1H	2.415		K2855	QE	1H	2.979
M2850	N	15N	119.407		N2856	C	13C	173.621
M2850	QE	1H	1.988		N2856	CA	13C	51.6
D2851	C	13C	177.653		N2856	HN	1H	7.396
D2851	CA	13C	55.44		N2856	HA	1H	4.805
D2851	CB	13C	41.255		N2856	HB3	1H	2.917
D2851	HN	1H	8.229		N2856	N	15N	115.917
D2851	HA	1H	4.289		T2857	C	13C	171.722
D2851	HB2	1H	2.599		T2857	CA	13C	57.466
D2851	HB3	1H	2.712		T2857	CG2	13C	21.588
D2851	N	15N	116.671		T2857	HN	1H	7.473
F2852	C	13C	176.838		T2857	HA	1H	4.775
F2852	CA	13C	57.243		T2857	HB	1H	4.146
F2852	CB	13C	39.544		T2857	N	15N	115.043
F2852	HN	1H	7.29		T2857	QG2	1H	1.179
F2852	HA	1H	4.32					
F2852	HB3	1H	3.243					
F2852	N	15N	118.549					
F2852	QD	1H	7.072					

Appendix B2

Order Parameters of KIX.MLL

Residue	Model	S2s	S2f	te [ps]	Rex [s⁻¹]
588	5	0.39	0.951	9.31E+02	
590	4	0.619		1.08E+03	3.438
592	4	0.799		1.15E+03	5.106
593	4	0.811		8.12E+02	3.204
594	4	0.739		8.31E+02	0.986
595	4	0.855		6.55E+02	1.551
596	5	0.751	0.957	8.08E+02	
597	4	0.772		8.18E+02	4.73
598	4	0.802		8.15E+02	5.495
599	4	0.904		4.70E+02	3.856
601	4	0.881		6.48E+02	1.749
603	4	0.907		7.03E+02	4.241
604	4	0.884		6.41E+02	3.39
605	4	0.952		1.48E+02	2.548
608	4	0.934		8.26E+01	2.561
610	4	0.948		4.08E+02	2.581
611	4	0.887		6.59E+02	1.594
612	4	0.937		1.29E+02	2.174
614	5	0.806	0.892	7.44E+02	
616	4	0.765		7.19E+02	1.15
618	4	0.828		6.25E+02	0.544
620	5	0.869	0.97	6.01E+02	
621	4	0.847		6.10E+02	1.003
622	2	0.841		7.07E+02	
623	4	0.825		8.73E+02	3.703
624	4	0.943		3.55E+02	2.495
625	4	0.813		9.11E+02	3.923
626	4	0.873		5.64E+02	2.808
627	4	0.932		2.68E+02	2.088
628	4	0.88		7.80E+02	1.885
629	4	0.886		9.41E+02	2.847
630	4	0.926		4.59E+02	3.26
632	4	0.881		9.99E+02	2.967
633	4	0.864		8.57E+02	3.151
634	4	0.95		3.07E+02	2.445
635	4	0.888		6.41E+02	3.512
636	4	0.874		9.18E+02	3.455
637	2	0.894		6.41E+02	
638	4	0.899		6.48E+02	4.773
639	4	0.87		7.67E+02	3.72
640	4	0.953		2.69E+02	3.706
641	4	0.934		4.57E+02	3.04
642	4	0.928		2.61E+02	0.415
643	4	0.847		7.86E+02	2.766
644	4	0.894		5.28E+02	0.99
645	4	0.927		5.39E+02	0.989

646	4	0.803		7.99E+02	7.343
648	4	0.959		4.31E+02	4.723
649	4	0.929		4.86E+02	4.02
650	4	0.922		5.91E+02	3.712
651	4	0.929		5.31E+02	5.53
652	4	0.942		2.57E+02	4.193
653	4	0.945		5.70E+02	3.424
654	4	0.952		1.91E+02	2.747
655	4	0.898		5.12E+02	4.732
656	4	0.952		1.33E+02	3.529
657	4	0.949		1.69E+02	2.388
659	4	0.946		3.18E+02	3.904
660	4	0.896		6.08E+02	3.388
664	4	0.904		5.39E+02	3.754
666	4	0.963		2.16E+02	2.749
667	4	0.94		3.97E+02	2.514
668	4	0.866		7.07E+02	2.99
670	5	0.669	0.964	9.07E+02	
671	5	0.483	0.935	7.87E+02	

Appendix C1

Chemical Shifts of KIX.pKID

Residue	Atom	Nuclei	Shift [ppm]
G586	C	13C	173.951
G586	CA	13C	43.3
G586	HN	1H	8.497
G586	N	15N	110.66
V587	C	13C	176.215
V587	CA	13C	60.232
V587	HN	1H	8.043
V587	N	15N	119.774
R588	C	13C	176.269
R588	CA	13C	54.329
R588	HN	1H	8.569
R588	N	15N	125.777
K589	C	13C	177.571
K589	CA	13C	53.028
G590	CA	13C	45.305
G590	HN	1H	8.726
G590	N	15N	112.507
W591	C	13C	178.145
W591	CA	13C	56.41
W591	HN	1H	8.072
W591	HE1	1H	9.202
W591	N	15N	119.366
W591	NE1	15N	129.324
H592	C	13C	176.703
H592	CA	13C	54.319
H592	HN	1H	7.132
H592	N	15N	119.586
E593	C	13C	176.696
E593	CA	13C	56.334
E593	HN	1H	7.713
E593	N	15N	116.618
H594	C	13C	174.074
H594	CA	13C	52.566
H594	HN	1H	7.49
H594	N	15N	113.002
V595	C	13C	174.495
V595	CA	13C	60.153
V595	HN	1H	7.51
V595	N	15N	120.761
T596	C	13C	175.387
T596	CA	13C	58.165
T596	HN	1H	7.561
T596	N	15N	115.308
Q597	C	13C	178.114
Q597	CA	13C	56.836
Q597	HN	1H	8.951
Q597	N	15N	120.243
D598	C	13C	178.434
D598	CA	13C	55.131
D598	HN	1H	8.372
D598	N	15N	117.976
L599	C	13C	179.053
L599	CA	13C	56.47
L599	HN	1H	7.688
L599	N	15N	123.047
R600	C	13C	178.938
R600	CA	13C	58.657
R600	HN	1H	7.864
R600	N	15N	118.185
S601	C	13C	177.401
S601	CA	13C	59.674
S601	HN	1H	8.468
S601	N	15N	112.918
H602	C	13C	177.465
H602	CA	13C	56.936
H602	HN	1H	8.064
H602	N	15N	122.235
L603	C	13C	179.261
L603	CA	13C	56.223
L603	HN	1H	8.345
L603	N	15N	121.686
V604	C	13C	177.899
V604	CA	13C	65.873
V604	HN	1H	8.488
V604	N	15N	120.154
H605	C	13C	177.304
H605	CA	13C	57.386
H605	HN	1H	7.825
H605	N	15N	116.686
K606	C	13C	179.424
K606	CA	13C	56.84
K606	HN	1H	8.019
K606	N	15N	119.169
L607	C	13C	178.012
L607	CA	13C	56.874
L607	HN	1H	8.167
L607	N	15N	121.864
V608	CA	13C	65.541
V608	HN	1H	8.09
V608	N	15N	118.118
Q609	C	13C	177.126
Q609	CA	13C	55.942
Q609	HN	1H	7.899
Q609	N	15N	115.761
A610	C	13C	178.463
A610	CA	13C	51.809
A610	HN	1H	7.569
A610	N	15N	118.93

I611	C	13C	175.211		A630	C	13C	180.844
I611	CA	13C	175.225		A630	CA	13C	53.461
I611	HN	1H	7.592		A630	HN	1H	7.884
I611	N	15N	114.052		A630	N	15N	120.583
F612	C	13C	171.698		Y631	C	13C	176.541
F612	CA	13C	53.327		Y631	CA	13C	59.217
F612	HN	1H	8.124		Y631	HN	1H	7.932
F612	N	15N	120.157		Y631	N	15N	120.295
P613	C	13C	177.28		A632	C	13C	179.013
P613	CA	13C	61.861		A632	CA	13C	53.244
T614	C	13C	172.799		A632	HN	1H	8.577
T614	CA	13C	56.758		A632	N	15N	122.269
T614	HN	1H	7.963		K633	C	13C	180.126
T614	N	15N	114.594		K633	CA	13C	57.695
D616	C	13C	177.601		K633	HN	1H	8.697
D616	CA	13C	52.895		K633	N	15N	116.225
D616	HN	1H	8.128		K634	C	13C	178.501
D616	N	15N	121.411		K634	CA	13C	57.301
P617	C	13C	178.075		K634	HN	1H	7.766
P617	CA	13C	62.675		K634	N	15N	123.418
A618	C	13C	178.879		V635	C	13C	178.283
A618	CA	13C	51.643		V635	CA	13C	64.003
A618	HN	1H	8.275		V635	HN	1H	8.065
A618	N	15N	120.7		V635	N	15N	119.078
A619	C	13C	178.319		E636	C	13C	178.701
A619	CA	13C	51.266		E636	CA	13C	59.597
A619	HN	1H	7.787		E636	HN	1H	8.55
A619	N	15N	121.019		E636	N	15N	119.97
L620	C	13C	177.698		G637	C	13C	176.607
L620	CA	13C	54.066		G637	CA	13C	45.457
L620	HN	1H	7.644		G637	HN	1H	8.113
L620	N	15N	117.581		G637	N	15N	106.648
K621	C	13C	176.348		D638	C	13C	180.091
K621	CA	13C	54.468		D638	CA	13C	55.071
K621	HN	1H	7.812		D638	HN	1H	8.227
K621	N	15N	118.685		D638	N	15N	122.623
D622	C	13C	176.882		M639	C	13C	177.708
D622	CA	13C	52.283		M639	CA	13C	56.67
D622	HN	1H	7.854		M639	HN	1H	8.233
D622	N	15N	120.345		M639	N	15N	120.885
E626	CA	13C	57.94		Y640	C	13C	178.172
N627	C	13C	177.712		Y640	CA	13C	60.102
N627	CA	13C	53.696		Y640	HN	1H	9.403
N627	HN	1H	8.245		Y640	N	15N	121.503
N627	N	15N	117.785		E641	C	13C	178.087
L628	C	13C	178.403		E641	CA	13C	55.72
L628	CA	13C	56.027		E641	HN	1H	8.026
L628	HN	1H	7.936		E641	N	15N	114.898
L628	N	15N	123.431		S642	C	13C	175.298
V629	C	13C	177.593		S642	CA	13C	58.263
V629	CA	13C	64.948		S642	HN	1H	7.95
V629	HN	1H	8.391		S642	N	15N	112.726
V629	N	15N	119.947		A643	C	13C	178.013

A643	CA	13C	50.759		I657	CA	13C	64.006
A643	HN	1H	8.162		Y658	C	13C	176.838
A643	N	15N	123.829		Y658	CA	13C	60.42
N644	C	13C	173.977		Y658	HN	1H	9.013
N644	CA	13C	51.479		Y658	N	15N	121.066
N644	HN	1H	9.177		K659	C	13C	179.895
N644	N	15N	117.466		K659	CA	13C	57.848
S645	C	13C	171.932		K659	HN	1H	8.367
S645	CA	13C	54.583		K659	N	15N	117.492
S645	HN	1H	6.923		I660	C	13C	178.157
S645	N	15N	111.45		I660	CA	13C	63.278
R646	C	13C	177.159		I660	HN	1H	8.05
R646	CA	13C	57.04		I660	N	15N	120.734
R646	HN	1H	8.738		Q661	C	13C	179.884
R646	N	15N	122.267		Q661	CA	13C	57.756
D647	C	13C	179.07		Q661	HN	1H	8.752
D647	CA	13C	55.476		Q661	N	15N	119.019
D647	HN	1H	8.217		K662	C	13C	179.594
D647	N	15N	116.913		K662	CA	13C	55.484
E648	C	13C	176.967		K662	HN	1H	8.322
E648	CA	13C	57.75		K662	N	15N	118.202
E648	HN	1H	7.922		E663	C	13C	179.309
E648	N	15N	121.553		E663	CA	13C	57.422
Y649	C	13C	176.225		E663	HN	1H	8.088
Y649	CA	13C	58.801		E663	N	15N	121.492
Y649	HN	1H	7.383		L664	C	13C	179.515
Y649	N	15N	121.862		L664	CA	13C	55.742
Y650	C	13C	178.471		L664	HN	1H	8.221
Y650	CA	13C	59.632		L664	N	15N	120.237
Y650	HN	1H	8.051		E665	C	13C	179.562
Y650	N	15N	115.844		E665	HN	1H	7.959
H651	C	13C	178.279		E665	N	15N	119.589
H651	CA	13C	58.056		E666	C	13C	177.478
H651	HN	1H	8.19		E666	CA	13C	56.11
H651	N	15N	116.39		E666	HN	1H	7.986
L652	C	13C	180.737		E666	N	15N	119.45
L652	CA	13C	56.155		K667	C	13C	178.584
L652	HN	1H	9.071		K667	HN	1H	7.943
L652	N	15N	122.391		K667	N	15N	119.466
L653	C	13C	178.324		R668	C	13C	177.551
L653	CA	13C	56.111		R668	CA	13C	55.971
L653	HN	1H	7.882		R668	HN	1H	7.955
L653	N	15N	121.013		R668	N	15N	119.189
A654	CA	13C	63.999		R669	C	13C	176.922
A654	HN	1H	8.092		R669	CA	13C	55.27
A654	N	15N	118.593		R669	HN	1H	7.917
E655	C	13C	177.682		R669	N	15N	119.325
E655	HN	1H	8.728		S670	C	13C	174.211
E655	N	15N	118.221		S670	CA	13C	56.965
K656	CA	13C	178.378		S670	HN	1H	8.031
K656	HN	1H	7.681		S670	N	15N	115.425
K656	N	15N	119.646		R671	C	13C	175.18
I657	C	13C	176.774		R671	CA	13C	54.123

R671	HN	1H	8.035
R671	N	15N	122.326
L672	C	13C	182.358
L672	CA	13C	54.754
L672	HN	1H	7.782
L672	N	15N	128.326

Appendix C2

Order Parameters of KIX.pKID

Residue	Model	S2s	S2f	te [ps]	Rex [s⁻¹]
588	2	0.41		8.65E+02	
590	4	0.736		8.79E+02	3.405
592	4	0.852		7.68E+02	7.651
593	4	0.904		4.28E+02	5.131
594	4	0.809		5.67E+02	2.332
595	4	0.911		1.44E+02	3.153
596	2	0.846		4.94E+02	
597	4	0.815		6.57E+02	6.555
598	4	0.846		7.60E+02	6.405
599	4	0.918		1.05E+02	6.166
600	4	0.913		5.69E+01	6.614
601	4	0.931		1.27E+02	3.607
603	4	0.912		5.08E+02	3.73
604	4	0.939		1.89E+02	4.758
605	4	0.894		4.53E+01	6.144
606	4	0.924		7.25E+01	5.782
607	4	0.913		4.03E+02	3.054
608	4	0.887		3.13E+01	7.994
609	4	0.89		4.67E+01	5.621
610	4	0.911		5.55E+01	5.493
611	4	0.943		1.38E+02	6.639
612	4	0.846		5.91E+02	5.765
614	4	0.751		5.70E+02	0.606
616	4	0.601		7.93E+02	1.534
618	4	0.75		7.68E+02	0.389
619	2	0.749		7.85E+02	
620	4	0.662		6.97E+02	6.127
621	4	0.691		7.59E+02	3.666
622	4	0.797		5.69E+02	1.423
627	4	0.897		5.05E+02	5.114
628	4	0.918		1.90E+02	6.346
629	4	0.915		8.89E+01	5.868
630	4	0.879		3.89E+01	6.901
631	4	0.907		5.79E+01	5.357
632	4	0.919		6.47E+02	5.908
633	4	0.936		1.80E+02	4.734
634	4	0.913		4.32E+01	6.141
636	4	0.88		5.48E+02	6.237
637	2	0.907		5.79E+01	
638	4	0.95		2.47E+02	5.982
639	4	0.953		2.29E+02	5.443
640	4	0.884		5.03E+01	6.293
641	4	0.883		3.66E+01	6.423
642	4	0.894		8.67E+01	3.322
643	4	0.928		4.51E+02	4.907
644	4	0.854		5.00E+01	4.632

645	4	0.942		2.92E+02	3.693
646	4	0.883		6.83E+02	8.432
647	4	0.923		1.06E+02	6.256
648	4	0.888		2.92E+01	9.485
649	4	0.923		1.01E+02	6.892
650	4	0.944		8.22E+01	3.9
651	4	0.862		3.45E+01	8.053
652	4	0.943		3.20E+02	7.12
653	4	0.943		2.11E+02	6.925
654	4	0.857		3.24E+01	7.591
655	4	0.921		2.63E+02	8.711
656	4	0.883		3.31E+01	7.371
658	4	0.921		4.44E+02	8.108
659	4	0.89		4.86E+01	6.939
660	4	0.948		2.35E+02	4.422
661	4	0.925		1.43E+02	8.444
662	4	0.935		8.84E+01	9.91
664	4	0.85		5.25E+02	4.969
666	4	0.756		6.47E+02	1.427
668	4	0.802		5.32E+02	3.521
669	4	0.664		6.69E+02	2.72
670	2	0.541		8.35E+02	
672	5	0.178	0.772	7.55E+02	

Appendix D1

Chemical Shifts of KIX.MLL.pKID

Residues	Atom	Nuclei	Shift [ppm]
G586	C	13C	173.939
G586	CA	13C	45.282
G586	HN	1H	8.459
G586	HA1	1H	3.936
G586	HA2	1H	3.861
G586	N	15N	110.618
V587	C	13C	176.346
V587	CA	13C	62.225
V587	CB	13C	32.865
V587	CG1	13C	21.247
V587	CG2	13C	20.723
V587	HN	1H	8.009
V587	HA	1H	4.064
V587	HB	1H	1.968
V587	N	15N	119.766
V587	QG1	1H	0.861
V587	QG2	1H	0.876
R588	C	13C	176.097
R588	CA	13C	56.352
R588	CB	13C	30.657
R588	CD	13C	43.488
R588	CG	13C	27.29
R588	HN	1H	8.521
R588	HA	1H	4.292
R588	HB3	1H	1.78
R588	HD3	1H	3.147
R588	HG2	1H	1.529
R588	HG3	1H	1.609
R588	N	15N	125.698
K589	C	13C	177.575
K589	CA	13C	55.112
K589	CB	13C	32.733
K589	HN	1H	8.11
K589	HA	1H	4.17
K589	HB2	1H	0.84
K589	HB3	1H	1.169
K589	HE2	1H	2.918
K589	HE3	1H	2.931
K589	HG3	1H	1.169
K589	N	15N	120.982
G590	C	13C	176.53
G590	CA	13C	47.202
G590	HN	1H	8.668
G590	HA1	1H	3.945

Residues	Atom	Nuclei	Shift [ppm]
G590	HA2	1H	3.724
G590	N	15N	112.517
W591	C	13C	178.237
W591	CA	13C	58.5
W591	CB	13C	27.459
W591	CD1	13C	126.759
W591	HN	1H	8.101
W591	HA	1H	4.505
W591	HB3	1H	3.173
W591	HD1	1H	7.045
W591	HE1	1H	9.225
W591	HZ2	1H	7.486
W591	N	15N	119.659
W591	NE1	15N	129.424
H592	C	13C	176.475
H592	CA	13C	56.162
H592	CB	13C	28.413
H592	HN	1H	7.195
H592	HA	1H	3.471
H592	HB2	1H	2.902
H592	HB3	1H	2.909
H592	N	15N	119.211
E593	C	13C	176.639
E593	CA	13C	58.328
E593	CB	13C	29.2
E593	CG	13C	35.551
E593	HN	1H	7.735
E593	HA	1H	3.95
E593	HB2	1H	1.787
E593	HB3	1H	1.777
E593	HG2	1H	2.11
E593	HG3	1H	2.12
E593	N	15N	116.607
H594	C	13C	173.819
H594	CA	13C	54.384
H594	CB	13C	29.146
H594	HN	1H	7.475
H594	HA	1H	4.953
H594	HB2	1H	3.709
H594	HB3	1H	3.251
H594	N	15N	112.61
V595	C	13C	174.522
V595	CA	13C	62.158
V595	CB	13C	33.224
V595	CG1	13C	22.299
V595	CG2	13C	21.497
V595	HN	1H	7.471
V595	HA	1H	4.461
V595	HB	1H	2.172
V595	N	15N	120.754
V595	QG1	1H	1.084
V595	QG2	1H	1.186
T596	C	13C	175.353

T596	CA	13C	60.153		S601	HB2	1H	3.923
T596	CB	13C	71.233		S601	HB3	1H	3.914
T596	CG2	13C	22.006		S601	N	15N	113.024
T596	HN	1H	7.565		H602	CA	13C	58.85
T596	HA	1H	4.558		H602	CB	13C	28.168
T596	N	15N	115.344		H602	HN	1H	8.11
T596	QG2	1H	1.288		H602	HA	1H	4.506
Q597	C	13C	178.081		H602	HB2	1H	3.556
Q597	CA	13C	58.811		H602	HB3	1H	3.452
Q597	CB	13C	28.048		H602	N	15N	121.786
Q597	CG	13C	33.7		L603	C	13C	179.221
Q597	HN	1H	8.901		L603	CA	13C	58.266
Q597	HA	1H	3.776		L603	CB	13C	40.663
Q597	HB2	1H	2.017		L603	CD1	13C	26.109
Q597	HB3	1H	2.035		L603	CD2	13C	23.85
Q597	HE21	1H	6.657		L603	CG	13C	27.425
Q597	HE22	1H	7.375		L603	HN	1H	8.424
Q597	HG3	1H	2.338		L603	HA	1H	3.974
Q597	N	15N	120.234		L603	HB3	1H	2.172
Q597	NE2	15N	112.588		L603	HG	1H	1.93
D598	C	13C	178.409		L603	N	15N	121.956
D598	CA	13C	57.112		L603	QD1	1H	0.945
D598	CB	13C	40.391		L603	QD2	1H	0.899
D598	HN	1H	8.33		V604	C	13C	177.92
D598	HA	1H	4.306		V604	CA	13C	68.053
D598	HB3	1H	2.539		V604	CB	13C	31.415
D598	N	15N	117.85		V604	CG1	13C	21.473
L599	C	13C	179.152		V604	CG2	13C	23.89
L599	CA	13C	58.55		V604	HN	1H	8.413
L599	CB	13C	41.662		V604	HA	1H	3.379
L599	CD1	13C	23.975		V604	HB	1H	2.211
L599	CD2	13C	25.715		V604	N	15N	120.055
L599	CG	13C	27.469		V604	QG1	1H	0.805
L599	HN	1H	7.651		V604	QG2	1H	1.025
L599	HA	1H	4.179		H605	C	13C	177.183
L599	HB2	1H	2.014		H605	CA	13C	59.292
L599	HB3	1H	1.792		H605	CB	13C	27.811
L599	HG	1H	1.819		H605	HN	1H	7.727
L599	N	15N	123.061		H605	HA	1H	4.272
L599	QD1	1H	1.193		H605	N	15N	116.126
L599	QD2	1H	1.272		K606	C	13C	179.326
R600	C	13C	178.901		K606	CA	13C	59.024
R600	CA	13C	60.605		K606	HN	1H	8.106
R600	CB	13C	30.393		K606	HA	1H	3.979
R600	HN	1H	7.783		K606	N	15N	119.075
R600	HB3	1H	1.815		K606	QB	1H	2.034
R600	HG3	1H	1.522		K606	QG	1H	1.592
R600	N	15N	118.247		L607	C	13C	177.926
S601	C	13C	177.665		L607	CA	13C	59.066
S601	CA	13C	61.662		L607	CB	13C	42.294
S601	CB	13C	62.779		L607	CD1	13C	26.011
S601	HN	1H	8.464		L607	CD2	13C	24.829
S601	HA	1H	4.072		L607	CG	13C	27.795

L607	HN	1H	8.296		F612	HA	1H	5.084
L607	HA	1H	3.898		F612	HB2	1H	3.339
L607	HB2	1H	1.582		F612	HB3	1H	3.319
L607	HB3	1H	1.988		F612	N	15N	117.203
L607	HG	1H	1.75		F612	QD	1H	6.807
L607	N	15N	122.132		F612	QE	1H	6.798
L607	QD1	1H	0.838		F612	CD*	13C	129.409
L607	QD2	1H	0.786		F612	CE*	13C	131.236
V608	C	13C	177.75		P613	C	13C	178.086
V608	CA	13C	67.932		P613	CA	13C	64.721
V608	CB	13C	31.674		P613	CB	13C	32.29
V608	CG1	13C	21.046		P613	CD	13C	50.213
V608	CG2	13C	24.343		P613	HA	1H	4.571
V608	HN	1H	7.928		P613	HB2	1H	2.361
V608	HA	1H	3.292		P613	HB3	1H	1.963
V608	HB	1H	2.203		P613	HD2	1H	3.368
V608	N	15N	117.895		P613	HD3	1H	3.664
V608	QG1	1H	0.896		T614	CA	13C	58.36
V608	QG2	1H	1.02		T614	CB	13C	69.597
Q609	C	13C	176.801		T614	CG2	13C	21.366
Q609	CA	13C	58.023		T614	HN	1H	7.951
Q609	CB	13C	29.013		T614	HA	1H	4.332
Q609	CG	13C	34.218		T614	HB	1H	4.113
Q609	HN	1H	7.965		T614	N	15N	109.455
Q609	HA	1H	3.878		T614	QG2	1H	1.01
Q609	HB2	1H	1.916		P615	C	13C	176.506
Q609	HB3	1H	1.922		P615	CA	13C	62.702
Q609	HE21	1H	6.769		P615	CB	13C	31.231
Q609	HE22	1H	7.401		P615	HA	1H	4.002
Q609	HG2	1H	2.253		P615	HB3	1H	0.896
Q609	N	15N	116.709		P615	QD	1H	3.235
Q609	NE2	15N	111.273		D616	CA	13C	52.041
A610	C	13C	179.001		D616	CB	13C	39.743
A610	CA	13C	53.723		D616	HN	1H	8.197
A610	CB	13C	19.376		D616	HA	1H	4.718
A610	HN	1H	7.704		D616	HB2	1H	2.787
A610	HA	1H	4.046		D616	HB3	1H	2.967
A610	N	15N	118.772		D616	N	15N	122.774
A610	QB	1H	1.481		P617	C	13C	178.9
I611	C	13C	174.158		P617	CA	13C	66.019
I611	CA	13C	63.873		P617	HA	1H	4.067
I611	CB	13C	39.265		P617	QB	1H	2.293
I611	CD1	13C	13.861		A618	C	13C	180.531
I611	CG2	13C	18.363		A618	CA	13C	54.762
I611	HN	1H	7.508		A618	CB	13C	18.183
I611	HA	1H	3.691		A618	HN	1H	8.095
I611	HB	1H	1.855		A618	HA	1H	4.06
I611	HG13	1H	2.078		A618	N	15N	118.514
I611	N	15N	116.355		A618	QB	1H	1.42
I611	QD1	1H	0.88		A619	C	13C	179.29
I611	QG2	1H	0.871		A619	CA	13C	54.943
F612	CA	13C	51.675		A619	CB	13C	18.528
F612	HN	1H	8.223		A619	HN	1H	8.047

A619	HA	1H	4.311
A619	N	15N	122.474
A619	QB	1H	1.518
L620	C	13C	178.264
L620	CA	13C	57.111
L620	CB	13C	42.081
L620	CD1	13C	25.29
L620	CD2	13C	23.221
L620	HN	1H	7.588
L620	HA	1H	4.028
L620	HG	1H	1.51
L620	N	15N	113.984
L620	QB	1H	1.767
L620	QD1	1H	0.823
L620	QD2	1H	0.829
K621	C	13C	175.864
K621	CA	13C	55.624
K621	CB	13C	32.846
K621	HN	1H	7.253
K621	HA	1H	4.315
K621	HB2	1H	1.761
K621	HB3	1H	1.939
K621	HG3	1H	1.498
K621	N	15N	115.103
D622	C	13C	178.1
D622	CA	13C	54.094
D622	CB	13C	44.198
D622	HN	1H	7.433
D622	HA	1H	4.477
D622	HB2	1H	2.835
D622	HB3	1H	3.043
D622	N	15N	123.385
R623	C	13C	178.239
R623	CA	13C	58.889
R623	CB	13C	29.365
R623	CD	13C	43.166
R623	HN	1H	9.101
R623	HA	1H	4.081
R623	N	15N	130.438
R623	QB	1H	1.832
R624	C	13C	178.414
R624	CA	13C	58.648
R624	CB	13C	28.348
R624	HN	1H	9.575
R624	HA	1H	3.807
R624	HD2	1H	2.82
R624	HD3	1H	3.168
R624	HG3	1H	1.503
R624	N	15N	119.003
M625	C	13C	178.803
M625	CA	13C	57.155
M625	CB	13C	30.803
M625	CE	13C	17.51
M625	HN	1H	7.895
M625	HA	1H	4.481
M625	HB2	1H	2.362
M625	HB3	1H	2.357
M625	N	15N	120.211
M625	QE	1H	1.89
E626	C	13C	179.587
E626	CA	13C	59.063
E626	CB	13C	28.369
E626	HN	1H	7.396
E626	HA	1H	4.039
E626	N	15N	117.81
E626	QB	1H	2.115
N627	C	13C	177.652
N627	CA	13C	55.903
N627	CB	13C	37.288
N627	HN	1H	7.451
N627	HA	1H	4.474
N627	HD21	1H	6.809
N627	HD22	1H	7.768
N627	N	15N	118.006
N627	ND2	15N	111.634
N627	QB	1H	2.8
L628	C	13C	177.655
L628	CA	13C	59.212
L628	CB	13C	41.35
L628	CD1	13C	24.959
L628	CD2	13C	27.024
L628	CG	13C	28.517
L628	HN	1H	7.906
L628	HA	1H	4.208
L628	HB2	1H	2.496
L628	HB3	1H	1.679
L628	HG	1H	1.767
L628	N	15N	124.319
L628	QD1	1H	1.133
L628	QD2	1H	1.179
V629	C	13C	177.545
V629	CA	13C	67.237
V629	CB	13C	31.652
V629	CG1	13C	21.257
V629	CG2	13C	22.695
V629	HN	1H	8.265
V629	HA	1H	3.468
V629	HB	1H	2.095
V629	N	15N	120.553
V629	QG1	1H	0.886
V629	QG2	1H	1.093
A630	C	13C	180.803
A630	CA	13C	55.422
A630	CB	13C	18.118
A630	HN	1H	8.151
A630	HA	1H	4.004

A630	N	15N	120.598	E636	HB3	1H	1.554
A630	QB	1H	1.52	E636	HG2	1H	2.292
Y631	C	13C	176.361	E636	HG3	1H	2.292
Y631	CA	13C	61.585	E636	N	15N	119.794
Y631	CB	13C	38.274	G637	C	13C	176.641
Y631	HN	1H	8.131	G637	CA	13C	47.502
Y631	HA	1H	4.218	G637	HN	1H	8.089
Y631	N	15N	121.213	G637	HA1	1H	3.595
Y631	QB	1H	3.227	G637	HA2	1H	3.86
Y631	QD	1H	6.949	G637	N	15N	106.417
Y631	QE	1H	6.593	D638	C	13C	180.17
Y631	CD*	13C	132.406	D638	CA	13C	57.006
Y631	CE*	13C	118.411	D638	CB	13C	39.862
A632	C	13C	178.96	D638	HN	1H	8.411
A632	CA	13C	55.307	D638	HA	1H	4.514
A632	CB	13C	19.885	D638	HB2	1H	2.693
A632	HN	1H	8.367	D638	HB3	1H	2.95
A632	HA	1H	3.668	D638	N	15N	122.792
A632	N	15N	122.461	M639	C	13C	177.917
A632	QB	1H	1.521	M639	CA	13C	58.107
K633	C	13C	179.928	M639	CE	13C	19.774
K633	CA	13C	59.727	M639	HN	1H	8.326
K633	CB	13C	32.865	M639	HA	1H	4.46
K633	HN	1H	8.522	M639	HG2	1H	2.423
K633	HA	1H	3.977	M639	HG3	1H	2.425
K633	HD2	1H	1.598	M639	N	15N	120.533
K633	HD3	1H	1.598	M639	QE	1H	2.025
K633	N	15N	116.17	Y640	C	13C	178.394
K633	QB	1H	1.853	Y640	CA	13C	62.253
K634	C	13C	178.514	Y640	CB	13C	38.802
K634	CA	13C	59.23	Y640	HN	1H	9.393
K634	CB	13C	31.916	Y640	HA	1H	4.276
K634	HN	1H	7.914	Y640	HB2	1H	3.052
K634	HA	1H	4.014	Y640	HB3	1H	3.573
K634	N	15N	123.724	Y640	N	15N	121.734
K634	QB	1H	2.049	Y640	QD	1H	6.535
V635	C	13C	178.305	Y640	QE	1H	5.936
V635	CA	13C	66.133	Y640	CD*	13C	132.613
V635	CB	13C	31.641	Y640	CE*	13C	117.079
V635	CG1	13C	21.957	E641	C	13C	177.892
V635	CG2	13C	22.122	E641	CA	13C	57.559
V635	HN	1H	8.153	E641	CB	13C	29.575
V635	HA	1H	3.643	E641	CG	13C	35.164
V635	HB	1H	1.837	E641	HN	1H	8.012
V635	N	15N	119.138	E641	HA	1H	4.327
V635	QG1	1H	0.741	E641	HG2	1H	2.508
V635	QG2	1H	0.504	E641	HG3	1H	2.577
E636	C	13C	178.645	E641	N	15N	114.967
E636	CA	13C	61.868	E641	QB	1H	2.163
E636	CB	13C	28.816	S642	C	13C	175.199
E636	HN	1H	8.347	S642	CA	13C	60.205
E636	HA	1H	3.763	S642	CB	13C	64.606
E636	HB2	1H	1.564	S642	HN	1H	7.9

S642	HA	1H	4.42		E648	QB	1H	1.877
S642	HB2	1H	3.907		E648	QG	1H	2.468
S642	HB3	1H	3.91		Y649	C	13C	176.398
S642	N	15N	112.599		Y649	CA	13C	60.797
A643	C	13C	177.957		Y649	CB	13C	38.706
A643	CA	13C	52.674		Y649	HN	1H	7.421
A643	CB	13C	19.857		Y649	HA	1H	3.963
A643	HN	1H	8.108		Y649	HB2	1H	2.568
A643	HA	1H	4.176		Y649	HB3	1H	2.97
A643	N	15N	123.63		Y649	N	15N	122.127
A643	QB	1H	1.566		Y649	QD	1H	6.744
N644	C	13C	173.946		Y649	QE	1H	6.752
N644	CA	13C	53.486		Y649	CD*	13C	133.172
N644	CB	13C	40.107		Y649	CE*	13C	118.264
N644	HN	1H	9.145		Y650	C	13C	178.543
N644	HA	1H	5.072		Y650	CA	13C	61.904
N644	HB2	1H	2.725		Y650	CB	13C	38.116
N644	HB3	1H	2.911		Y650	HN	1H	8.002
N644	HD21	1H	6.995		Y650	HA	1H	3.878
N644	HD22	1H	7.981		Y650	HB2	1H	2.746
N644	N	15N	117.266		Y650	HB3	1H	3.037
N644	ND2	15N	115.679		Y650	N	15N	115.815
S645	C	13C	171.968		Y650	QD	1H	7.096
S645	CA	13C	56.533		Y650	QE	1H	6.786
S645	CB	13C	64.969		Y650	CD*	13C	132.054
S645	HN	1H	6.869		Y650	CE*	13C	118.244
S645	HA	1H	3.624		H651	C	13C	178.472
S645	HB3	1H	3.877		H651	CA	13C	59.833
S645	N	15N	111.279		H651	CB	13C	28.239
R646	C	13C	177.235		H651	HN	1H	8.234
R646	CA	13C	59.049		H651	HA	1H	4.233
R646	CB	13C	30.334		H651	N	15N	115.975
R646	HN	1H	8.715		H651	QB	1H	3.297
R646	HA	1H	3.165		L652	C	13C	180.801
R646	HB2	1H	1.876		L652	CA	13C	58.096
R646	HB3	1H	1.877		L652	CB	13C	42.224
R646	HD2	1H	3.266		L652	CD1	13C	25.904
R646	HD3	1H	3.356		L652	CD2	13C	22.153
R646	N	15N	122.346		L652	HN	1H	9.206
D647	C	13C	179.432		L652	HA	1H	4.096
D647	CA	13C	57.504		L652	HB3	1H	1.835
D647	CB	13C	41.032		L652	N	15N	122.802
D647	HN	1H	8.238		L652	QD1	1H	0.954
D647	HA	1H	4.447		L652	QD2	1H	0.907
D647	HB2	1H	2.407		L653	C	13C	178.28
D647	HB3	1H	2.557		L653	CA	13C	58.269
D647	N	15N	117.089		L653	CB	13C	42.75
E648	C	13C	176.934		L653	CD1	13C	25.94
E648	CA	13C	59.736		L653	CD2	13C	24.206
E648	CB	13C	29.711		L653	CG	13C	26.629
E648	HN	1H	7.982		L653	HN	1H	7.984
E648	HA	1H	3.923		L653	HA	1H	3.791
E648	N	15N	122.214		L653	HB3	1H	1.747

L653	HG	1H	1.481	K659	HN	1H	8.427
L653	N	15N	120.85	K659	HA	1H	3.918
L653	QD1	1H	0.275	K659	N	15N	117.005
L653	QD2	1H	0.666	K659	QB	1H	1.977
A654	C	13C	178.807	I660	C	13C	177.46
A654	CA	13C	55.018	I660	CA	13C	66.128
A654	CB	13C	17.852	I660	CB	13C	38.408
A654	HN	1H	8.361	I660	CD1	13C	14.364
A654	HA	1H	3.808	I660	CG2	13C	18.03
A654	N	15N	119.709	I660	HN	1H	8.422
A654	QB	1H	1.079	I660	HA	1H	3.591
E655	C	13C	177.455	I660	HB	1H	1.969
E655	CA	13C	60.01	I660	N	15N	121.312
E655	CB	13C	29.662	I660	QD1	1H	0.934
E655	HN	1H	8.459	I660	QG2	1H	0.907
E655	HA	1H	3.991	Q661	C	13C	180.038
E655	HB2	1H	1.821	Q661	CA	13C	60.106
E655	HB3	1H	1.993	Q661	CB	13C	27.762
E655	HG2	1H	2.264	Q661	HN	1H	8.888
E655	HG3	1H	2.267	Q661	HA	1H	3.896
E655	N	15N	118.371	Q661	N	15N	118.553
K656	C	13C	178.423	Q661	QB	1H	2.207
K656	CA	13C	58.376	Q661	QG	1H	2.644
K656	CB	13C	31.274	K662	C	13C	179.364
K656	HN	1H	7.766	K662	CA	13C	57.991
K656	HA	1H	4.12	K662	CB	13C	31.31
K656	HB3	1H	1.974	K662	HN	1H	8.107
K656	N	15N	119.253	K662	N	15N	118.014
I657	C	13C	176.81	E663	C	13C	179.289
I657	CA	13C	65.546	E663	CA	13C	59.553
I657	CB	13C	37.439	E663	CB	13C	28.784
I657	CD1	13C	13.035	E663	HN	1H	8.039
I657	CG2	13C	18.501	E663	HA	1H	4.096
I657	HN	1H	8.121	E663	HG2	1H	2.425
I657	HA	1H	3.442	E663	HG3	1H	2.409
I657	HB	1H	1.916	E663	N	15N	122.154
I657	HG13	1H	1.707	E663	QB	1H	2.168
I657	N	15N	117.639	L664	C	13C	178.863
I657	QD1	1H	0.712	L664	CA	13C	58.401
I657	QG2	1H	0.837	L664	CB	13C	41.721
Y658	C	13C	177.199	L664	CD1	13C	26.702
Y658	CA	13C	62.395	L664	CD2	13C	23.776
Y658	HN	1H	8.879	L664	CG	13C	27.284
Y658	HB2	1H	3.125	L664	HN	1H	8.5
Y658	HB3	1H	3.127	L664	HA	1H	3.869
Y658	N	15N	120.79	L664	HB2	1H	1.377
Y658	QD	1H	6.931	L664	HB3	1H	1.964
Y658	QE	1H	7.137	L664	HG	1H	1.753
Y658	CD*	13C	132.402	L664	N	15N	120.017
Y658	CE*	13C	118.937	L664	QD1	1H	0.9
K659	C	13C	180.195	L664	QD2	1H	0.726
K659	CA	13C	59.89	E665	C	13C	179.049
K659	CB	13C	32.78	E665	CA	13C	59.335

E665	CB	13C	29.108	S670	N	15N	114.264
E665	HN	1H	8.03	R671	C	13C	175.293
E665	HA	1H	3.934	R671	CA	13C	56.326
E665	HB2	1H	2.103	R671	CB	13C	30.677
E665	HB3	1H	2.118	R671	CD	13C	43.792
E665	N	15N	118.34	R671	CG	13C	26.913
E665	QG	1H	2.345	R671	HN	1H	7.734
E666	C	13C	179.357	R671	HA	1H	4.329
E666	CA	13C	59.063	R671	HB2	1H	1.915
E666	CB	13C	28.942	R671	HB3	1H	1.739
E666	CG	13C	35.411	R671	HD2	1H	3.147
E666	HN	1H	7.844	R671	HD3	1H	3.146
E666	HA	1H	4.002	R671	HG2	1H	1.734
E666	HB2	1H	2.124	R671	HG3	1H	1.663
E666	HB3	1H	2.115	R671	N	15N	122.047
E666	HG2	1H	2.302	L672	CA	13C	56.591
E666	HG3	1H	2.387	L672	CB	13C	43.172
E666	N	15N	118.765	L672	CD1	13C	25.291
K667	C	13C	179.419	L672	CD2	13C	23.358
K667	CA	13C	57.599	L672	CG	13C	27.181
K667	CB	13C	32.172	L672	HN	1H	7.698
K667	HN	1H	8.029	L672	HA	1H	4.143
K667	HA	1H	4.074	L672	HB2	1H	1.581
K667	N	15N	118.988	L672	HB3	1H	1.543
K667	QD	1H	1.591	L672	HG	1H	1.59
R668	C	13C	178.177	L672	N	15N	127.942
R668	CA	13C	59.15	L672	QD1	1H	0.862
R668	CB	13C	30.301	L672	QD2	1H	0.834
R668	CD	13C	43.624	D116	C	13C	176.304
R668	HN	1H	8.201	D116	CA	13C	54.783
R668	HA	1H	3.95	D116	CB	13C	41.092
R668	HD2	1H	3.12	D116	HN	1H	8.092
R668	HD3	1H	3.121	D116	HA	1H	4.521
R668	N	15N	119.302	D116	HB2	1H	2.695
R668	QB	1H	1.845	D116	HB3	1H	2.694
R668	QG	1H	1.567	D116	N	15N	120.754
R669	C	13C	177.297	S117	C	13C	174.893
R669	CA	13C	57.802	S117	CA	13C	58.653
R669	CB	13C	30.322	S117	CB	13C	63.748
R669	HN	1H	7.759	S117	HN	1H	8.266
R669	HA	1H	4.16	S117	HA	1H	4.451
R669	HB2	1H	1.877	S117	HB2	1H	3.909
R669	HB3	1H	1.878	S117	HB3	1H	3.893
R669	HG3	1H	1.685	S117	N	15N	115.611
R669	N	15N	118.035	V118	C	13C	176.909
R669	QD	1H	3.159	V118	CA	13C	63.122
S670	C	13C	174.236	V118	CB	13C	32.396
S670	CA	13C	59.101	V118	CG1	13C	20.96
S670	CB	13C	63.809	V118	CG2	13C	21.215
S670	HN	1H	7.785	V118	HN	1H	8.11
S670	HA	1H	4.398	V118	HA	1H	4.148
S670	HB2	1H	3.918	V118	HB	1H	2.122
S670	HB3	1H	3.913	V118	N	15N	122.158

V118	QG1	1H	0.956	R124	HN	1H	8.073
V118	QG2	1H	0.95	R124	HA	1H	3.97
T119	C	13C	175.18	R124	HB2	1H	1.835
T119	CA	13C	62.723	R124	HB3	1H	1.835
T119	CB	13C	69.6	R124	HD2	1H	3.198
T119	CG2	13C	21.842	R124	HD3	1H	3.198
T119	HN	1H	8.175	R124	HG2	1H	1.735
T119	HA	1H	4.288	R124	HG3	1H	1.541
T119	HB	1H	4.167	R124	N	15N	118.721
T119	HG1	1H	1.233	R125	C	13C	178.073
T119	N	15N	116.781	R125	CA	13C	58.887
D120	C	13C	177.546	R125	CB	13C	29.99
D120	CA	13C	55.831	R125	HN	1H	7.881
D120	CB	13C	41.141	R125	HA	1H	3.95
D120	HN	1H	8.319	R125	HB2	1H	1.781
D120	HA	1H	4.545	R125	HB3	1H	1.781
D120	HB2	1H	2.7	R125	N	15N	119.866
D120	HB3	1H	2.702	R125	QD	1H	2.955
D120	N	15N	122.504	R125	QG	1H	1.528
S121	C	13C	176.4	E126	C	13C	178.575
S121	CA	13C	61.002	E126	CA	13C	58.839
S121	CB	13C	63.018	E126	CB	13C	29.455
S121	HN	1H	8.4	E126	CG	13C	36.145
S121	HA	1H	4.14	E126	HN	1H	8.053
S121	HB2	1H	3.933	E126	HA	1H	3.973
S121	HB3	1H	3.916	E126	HB2	1H	2.068
S121	N	15N	116.525	E126	HB3	1H	2.062
Q122	C	13C	178.031	E126	HG2	1H	2.17
Q122	CA	13C	58.429	E126	HG3	1H	2.325
Q122	CB	13C	28.223	E126	N	15N	121.372
Q122	CG	13C	33.841	I127	C	13C	178.873
Q122	HN	1H	8.142	I127	CA	13C	64.189
Q122	HA	1H	4.03	I127	CB	13C	38.408
Q122	HB2	1H	2.128	I127	CD1	13C	13.244
Q122	HB3	1H	2.111	I127	CG1	13C	28.563
Q122	HE21	1H	6.804	I127	CG2	13C	17.408
Q122	HE22	1H	7.59	I127	HN	1H	7.766
Q122	HG2	1H	2.361	I127	HA	1H	3.681
Q122	HG3	1H	2.382	I127	HB	1H	1.817
Q122	N	15N	122.204	I127	HG12	1H	1.62
Q122	NE2	15N	112.089	I127	HG13	1H	1.121
K123	C	13C	178.553	I127	N	15N	119.812
K123	CA	13C	58.438	I127	QD1	1H	0.825
K123	CB	13C	30.059	I127	QG2	1H	0.858
K123	HN	1H	8.104	L128	C	13C	177.961
K123	HA	1H	4.045	L128	CA	13C	57.881
K123	N	15N	120.8	L128	CB	13C	40.412
K123	QB	1H	1.846	L128	CD1	13C	24.277
K123	QG	1H	1.471	L128	CD2	13C	24.106
R124	C	13C	178.235	L128	HN	1H	7.901
R124	CA	13C	58.944	L128	HA	1H	3.895
R124	CB	13C	30.18	L128	N	15N	122.163
R124	CG	13C	27.838	L128	QB	1H	1.802

L128	QD1	1H	0.38		I137	N	15N	123.67
L128	QD2	1H	0.409		I137	QD1	1H	1.106
S129	C	13C	174.397		I137	QG2	1H	0.887
S129	CA	13C	60.842		L138	C	13C	179.372
S129	CB	13C	62.873		L138	CA	13C	58.167
S129	HN	1H	7.666		L138	CD1	13C	25.576
S129	HA	1H	3.888		L138	CD2	13C	23.372
S129	N	15N	109.832		L138	HN	1H	7.914
S129	QB	1H	3.704		L138	HA	1H	3.656
R130	C	13C	177.152		L138	HG	1H	1.544
R130	CA	13C	56.106		L138	N	15N	119.504
R130	CB	13C	27.714		L138	QB	1H	1.9
R130	HN	1H	7.169		L138	QD1	1H	0.642
R130	HA	1H	4.318		L138	QD2	1H	0.529
R130	HB2	1H	1.756		N139	C	13C	177.454
R130	HB3	1H	1.771		N139	CA	13C	56.102
R130	HD2	1H	3.203		N139	HN	1H	8.472
R130	HD3	1H	3.212		N139	HA	1H	4.296
R130	N	15N	117.95		N139	HD21	1H	6.883
R130	QG	1H	2.073		N139	HD22	1H	7.592
R131	CA	13C	52.594		N139	N	15N	118.084
R131	CB	13C	28.102		N139	ND2	15N	112.088
R131	HN	1H	8.2		N139	QB	1H	2.785
R131	HA	1H	4.288		D140	C	13C	178.686
R131	N	15N	121.605		D140	CA	13C	57.094
R131	QD	1H	3.228		D140	HN	1H	8.059
SEP133	N	15N	113.204		D140	N	15N	120.958
Y134	C	13C	178.247		D140	QB	1H	2.819
Y134	CA	13C	64.466		L141	C	13C	177.859
Y134	HN	1H	6.922		L141	CA	13C	57.677
Y134	HA	1H	4.263		L141	CD1	13C	26.407
Y134	N	15N	119.826		L141	CD2	13C	22.86
Y134	QB	1H	3.709		L141	HN	1H	8.085
Y134	QD	1H	6.449		L141	HA	1H	3.945
Y134	QE	1H	6.578		L141	HB2	1H	1.954
Y134	CD*	13C	132.198		L141	HB3	1H	1.952
Y134	CE*	13C	116.864		L141	HG	1H	1.399
R135	C	13C	176.524		L141	N	15N	117.231
R135	CA	13C	59.727		L141	QD1	1H	0.738
R135	HN	1H	8.015		L141	QD2	1H	0.681
R135	HA	1H	4.001		S142	C	13C	174.685
R135	HB3	1H	1.897		S142	CA	13C	59.075
R135	HG2	1H	1.466		S142	CB	13C	63.93
R135	HG3	1H	1.48		S142	HN	1H	7.597
R135	N	15N	118.319		S142	HA	1H	4.32
K136	CA	13C	59.884		S142	HB2	1H	4.06
K136	HN	1H	8.258		S142	HB3	1H	3.742
K136	HA	1H	4.24		S142	N	15N	109.816
K136	N	15N	119.202		S143	C	13C	174.283
K136	QB	1H	1.91		S143	CA	13C	59.259
I137	CD1	13C	15.066		S143	CB	13C	63.801
I137	CG2	13C	18.19		S143	HN	1H	7.613
I137	HN	1H	7.156		S143	HA	1H	4.36

S143	HB3	1H	3.939
S143	N	15N	117.276
D144	C	13C	175.25
D144	CA	13C	54.119
D144	CB	13C	41.092
D144	HN	1H	8.362
D144	HA	1H	4.651
D144	N	15N	122.05
D144	QB	1H	2.692
A145	C	13C	175.294
A145	CA	13C	50.559
A145	CB	13C	18.385
A145	HN	1H	7.963
A145	HA	1H	4.38
A145	N	15N	124.417
A145	QB	1H	1.309
P146	C	13C	176.623
P146	CA	13C	63.334
P146	QD	1H	3.602
G147	C	13C	172.675
G147	CA	13C	45.269
G147	HN	1H	8.461
G147	HA1	1H	3.831
G147	HA2	1H	3.967
G147	N	15N	109.408
V148	C	13C	173.951
V148	CA	13C	58.898
V148	CB	13C	34.446
V148	CG1	13C	21.226
V148	CG2	13C	20.045
V148	HN	1H	7.603
V148	HA	1H	4.396
V148	HB	1H	1.969
V148	N	15N	118.214
V148	QG1	1H	0.855
V148	QG2	1H	0.84

Appendix D2

Order Parameters of KIX.MLL.pKID

Residue	Model	S2s	S2f	te [ps]	Rex [s^{-1}]
587	5	0.299	0.852	8.99E+02	
588	5	0.408	0.986	8.31E+02	
589	4	0.57		7.68E+02	1.452
590	4	0.724		8.92E+02	2.889
592	4	0.831		7.82E+02	7.95
593	4	0.899		4.93E+02	4.494
594	4	0.766		6.43E+02	2.349
595	4	0.885		4.89E+02	3.036
596	2	0.821		5.63E+02	
597	4	0.771		7.42E+02	6.745
598	4	0.862		6.92E+02	5.96
599	4	0.931		2.36E+02	5.743
600	4	0.933		1.24E+02	5.11
601	4	0.936		1.36E+02	2.015
602	4	0.94		9.46E+01	2.95
604	4	0.922		9.12E+01	4.291
605	4	0.938		1.66E+02	4.429
606	4	0.915		7.35E+01	4.9
607	4	0.951		2.45E+02	3.394
608	4	0.915		6.48E+01	3.922
609	4	0.912		5.73E+01	4.637
610	4	0.93		9.43E+01	4.492
611	4	0.918		6.23E+01	2.276
614	5	0.807	0.898	6.19E+02	
616	4	0.818		5.35E+02	1.248
618	4	0.867		4.77E+02	1.42
620	2	0.907		2.85E+02	
621	4	0.903		2.95E+02	0.879
622	4	0.858		5.42E+02	1.229
623	4	0.821		6.85E+02	2.988
624	4	0.943		3.02E+02	3.92
625	4	0.908		4.96E+02	4.405
626	4	0.878		6.57E+01	4.578
627	4	0.925		1.06E+02	3.948
628	4	0.936		1.53E+02	2.794
629	4	0.951		1.80E+02	3.67
630	4	0.941		2.87E+02	4.393
632	4	0.891		4.99E+02	2.633
633	4	0.927		8.47E+01	4.185
634	4	0.902		4.56E+01	5.021
635	4	0.923		1.03E+02	5.042
636	4	0.921		1.04E+02	6.323
637	5	0.932	0.939	5.41E+02	
638	4	0.936		2.03E+02	5.283
640	4	0.911		5.23E+01	6.16
641	4	0.951		9.90E+01	4.141

642	4	0.894		8.37E+01	2.373
643	4	0.901		6.34E+02	4.581
644	4	0.907		9.00E+01	2.568
645	4	0.927		3.92E+02	2.561
646	4	0.908		5.50E+02	6.823
649	4	0.943		1.17E+02	5.638
650	4	0.945		9.28E+01	4.199
651	4	0.921		7.11E+01	6.334
652	4	0.954		1.88E+02	7.263
653	4	0.951		1.43E+02	5.182
654	4	0.935		2.93E+02	5.097
655	4	0.907		5.39E+02	6.438
656	4	0.957		1.16E+02	4.714
657	4	0.941		1.85E+02	4.179
658	4	0.911		4.96E+02	7.565
659	4	0.942		2.71E+02	5.2
660	4	0.95		9.79E+01	6.193
661	4	0.936		2.84E+02	5.241
662	4	0.933		1.82E+02	6.874
663	4	0.95		1.61E+02	6.977
664	4	0.899		4.24E+02	4.122
665	4	0.9		3.29E+01	5.005
666	4	0.899		7.69E+01	5.132
667	4	0.918		7.07E+01	4.686
668	4	0.927		2.77E+02	3.558
669	4	0.859		5.92E+02	2.057
670	5	0.72	0.953	7.84E+02	
671	5	0.48	0.968	7.80E+02	

Sven Brüschweiler

University of Vienna, Max F. Perutz Laboratories
Department of Structural and Computational Biology
Campus-Vienna-Biocenter 5, 1030 Vienna, Austria
Email: sven.brueschweiler@univie.ac.at

Education

1/2008 - present	**PhD Thesis, University of Vienna** *"The structural and dynamic basis for co-operative ligand binding in the KIX domain of CBP"* Supervisor: Prof. Robert Konrat
12/2007	**M.Sc., Chemistry, University of Vienna, with honors**
12/2006 – 12/2007	**M.Sc. Thesis, University of Vienna** *„Stereospecific Random Coil Chemical Shifts of Diastereotopic Methyl Groups under Native Conditions"* Supervisor: Prof. Robert Konrat
10/2002 – 12/2007	**Studies of Chemistry, University of Vienna** Focus: Theoretical Chemistry, Organic Chemistry, Biochemistry, Physical Chemistry
10/2001 – 10/2002	**Studies of Molecular Biology, University of Vienna**

Research experience

Cloning, recombinant expression, site-directed mutagenesis and purification of proteins and peptides.

Biophysical, dynamics and structural studies of proteins and protein complexes by NMR spectroscopy, ITC, CD spectroscopy and Mass spectrometry.

Courses

2010	EMBO Practical Course: *Biomolecular Simulation,* Institute Pasteur, Paris, France
2009	EMBO Practical Course: *Structure, Dynamics and Function of Biomacromolecules by Solution NMR,* TU München, Garching, Germany
2008	EMBO Practical Course: *Multidimensional NMR in Structural Biology,* IlCiocco, Italy

Publications

Breuker K., **Brüschweiler S.**, Tollinger M. (2011) Electrostatic Stabilization of a Native Protein Structure in the Gas Phase. *Angew. Chem. Int. Ed. Engl.* 50, 873-877. (Inside Cover of the Week; Reviewed in: Barran P.E. (2011) (Re)Solution of a Protein Fold Without Solution. *Angew. Chem. Int. Ed. Engl.* 50, 3120-3122.)

Brüschweiler S., Schanda P., Kloiber K., Brutscher B., Kontaxis G., Konrat R., Tollinger M. (2009) Direct Observation of the Dynamic Process Underlying Allosteric Signal Transmission. *J. Am. Chem. Soc.* 131, 3063-3068. (Reviewed in: Tzeng S.R. and Kalodimos C.G. (2011) Protein dynamics and allostery: an NMR view. *Curr. Opin. Struct. Biol.* 21, 62-67. del Sol A. *et al.* (2009) The Origin of Allosteric Functional Modulation: Multiple Pre-existing Pathways. *Structure* 17, 1042-1050.)

Publications in preparation

Brüschweiler S., Ribarics R., Konrat R., Tollinger M. (2011) Allosteric communication in the KIX domain proceeds through re-packing of the hydrophobic core. To be submitted to *EMBO J.*

Talks

Insights into the Allosteric Communication of the KIX Domain of CBP. March 15th 2011, Seminar at Albert Einstein College of Medicine, NYC, NY, USA

Teaching experience

Tutor in the "Practical Course in Structural Biology", University of Vienna

Tutor in the "Chemical Laboratory Course for Biologists", University of Vienna